Criteria Based Evaluation of Stopping Trajectories in Serial Manipulators

by

Bryan Christopher Steinfeld, B.S.M.E.

Thesis

Presented to the Faculty of the Graduate School of

The University of Texas at Austin

in Partial Fulfillment

of the Requirements

for the Degree of

Master of Science in Engineering

The University of Texas at Austin

December 2009

The Thesis committee for Bryan Christopher Steinfeld

Certifies that this is the approved version of the following thesis:

Criteria Based Evaluation of Stopping Criteria in Serial Manipulators

APPROVED BY

SUPERVISING COMMITTEE:

Supervisor: _____

Delbert Tesar

_____

Mitch Pryor

Dedication

To my parents, Peter and Janis Steinfeld, my brother and sister, Michael and Alyson Steinfeld, and my grandparents, Edward and Majorie Steinfeld, and Dick and Katherine Tymeson.

Acknowledgements

I would like to thank Drs. Chetan Kapoor, Delbert Tesar, and Mitch Pryor for their guidance and advice throughout the writing process. I would additionally like to thank my co-workers at RRG for their assistance, in particular Peter March and Andrew Spencer. Finally, I wish to thank Troy Harden at Los Alamos National Lab for his support and patience.

This work was funded by the Department of Energy under Grant # DE-FG52-04NA25591

Abstract

Criteria Based Evaluation of Stopping Trajectories in Serial Manipulators

Bryan Christopher Steinfeld, MSE

The University of Texas at Austin, 2009

Supervisor: Delbert Tesar

In the past few years, there has been a large push towards adapting traditional industrial manipulators to other, more consumer-centric applications [1]. These include not only house and elderly care, but also towards medical applications that manipulators may be especially suited for, such as rehabilitation of patients who have suffered neurological trauma [2]. Impeding this push are the strict safety requirements necessary to certify a manipulator for use. These requirements include low speed operation and preventing humans from entering the manipulator workspace [3]. These restrictions effectively prevent a manipulator from being used in many of these applications.

Previous work done in manipulator safety research has focused on improving the system's knowledge of its environment and controlling the manipulator's motion to keep

away from potential hazards. These methods are extremely important in terms of avoiding potential collisions but provide little insight into the situation that occurs once a hazard occurs and the manipulator is forced to react.

In order to improve upon the ability to evaluate a manipulator's overall safety, this report establishes a framework to evaluate the capacity of a manipulator to safely "halt" itself. Two sets of criteria are presented in this report. The first set seeks to quantify both the potential of the manipulator to avoid a collision during the stopping motion and the potential severity of the collision. The second set of criteria quantifies the effect of the stopping motion at the actuator level, allowing the operator to identify potential hardware faults and the capacity to which the actuators are performing. A framework for mapping the manipulator's actuator parameters for the gear reduction ratio and the motor torque to the potential safety criteria performance is formulated to allow the manipulator designer to match task requirements to the manipulator design.

Finally, an examination of the effects on operating parameters such as manipulator configuration, end-effector load, and operating speed is presented with a 6DOF industrial manipulator. This analysis showed that the operating speed of the manipulator is the most important determinant of the safety performance, with the distance traveled by the manipulator increasing by a factor of 15 for all configurations when the speed is increased only by a factor of four. Recommendations for the application of these criteria are presented to the reader as well.

Table of Contents

List of Tables

List of Figures

CHAPTER 1

Introduction

In the past few years, a large push in robotics and robotic manipulators has been to expand their uses beyond the traditional industrial, assembly-line usage into areas such as household assistance for the elderly, consumer services [1] and rehabilitation for medical patients who have suffered neurological trauma [2]. As these systems move closer towards humans, a greater emphasis on providing safe systems is necessary to certify these for use by American safety standards. Currently, ANSI/RIA safety standards require that any humans be located either outside the manipulator's workspace, or onerous restrictions are placed upon manipulator operations when a human is located inside the workspace including slow speed operation, use of a teach pendant, presence of only one person inside the manipulator's workspace, safeguarding circuits, and extensive training of the person present inside the manipulator's workspace. Additional requirements include completely avoiding the manipulator's path while in the workspace. [3] This effectively precludes the use of manipulators from being used in the home or in medical applications in the US since the training and infrastructure required to certify a manipulator is infeasible to support their use in these potential new applications.

In order to begin to relax these restrictions, a better framework to evaluate the capacity of serial manipulators to "halt" themselves is needed. While there are many aspects to the overall safety of the system, including hazard detection and hazard response time, this report focuses on providing a method for assessing the safety of a manipulator's motion once the command to respond to a hazard is received by the manipulator and stopping torques are applied to the system.

This chapter first gives an overview of the problem and proceeds to outline the modeling geometry of serial manipulators and the basic concepts of joint space path planning. A short discussion of the dynamics of serial manipulators is also presented. The final section provides a summary of the work presented throughout the rest of the report.

1.1 PROBLEM OVERVIEW

While there have been previous attempts to quantify the safety of a manipulator, these often focus solely on measuring the effects of impacts with humans, with human-care manipulators [4], or on the overall reliability of the system due to various faults [5, 6]. Very little work has been done to either develop a generic measure of the safety of the system, or to quantify the degree to which the system is performing to its capacity during a stopping trajectory. In order to establish this framework, two separate conditions must be satisfied.

1.1.1 Physical Meaning

Any criteria developed must be useful to an operator without requiring a large amount of additional analysis. Without a clear understanding of what each criterion means with respect to the physical reality of the system, adoption and use of the criteria will naturally be limited. Particularly within the internal workings of the manipulator model, there are easily derivable analytical measurements to quantify the performance of the manipulator, but many of these analytics are unable to be easily explained as observable quantities to the operator. Thus, a slightly more complicated analytic calculation that is more easily translatable to a physical phenomenon may be of more use to the operator than one easily derived from the manipulator's equations of motion. This

principle is loosely based on the work of Mark Tisius explaining the physical meaning of manipulator performance criteria. [7]

Particularly as robots move outside of not just highly controlled industrial environments and into more uncontrolled consumer environments, this will become more of an issue. An expansion of the robotic market will result in more manipulators operating outside of the purview of highly skilled and educated robotic technicians, so the available metrics need to be easily accessible to operators with limited robotic experience. While a metric based simply on the determinant of the Jacobian may be easily understood by an operator with experience in manipulator analysis, it will be essentially meaningless to the target market. Given that the end users are the individuals most affected by the safety of the manipulator in terms of their capacity for either economic loss or personal injury due to hazards, their capacity to quickly grasp the risks associated with a system is of paramount importance.

1.1.2 Safety-Capacity Criteria Conflicts

With two metrics at odds with each other, conflicts will naturally occur. A set of system level criteria defined to maximize safety performance of the system will oppose criteria defined to measure the degree to which the manipulator is performing to its capacity. The operator and designer will seek to extract the maximum performance from the manipulator in order to provide the safest stopping motion possible. At the same time, it is desired to operate the actuators at the lowest percentage of capacity as possible in order to prevent internal faults and excessive loading of the system. A system operating at peak performance will necessarily be operating at the capacity of its individual components, so the operator will have to balance these competing desires according to the individual task and safety requirements of the manipulator.

1.2 MANIPULATOR MODELING

In order to develop a meaningful understanding of the stopping motion of serial manipulators, it is important to start with a framework for the geometric analysis of manipulators. Most of the internal capacity criteria are developed somewhat based on these modeling concepts. These modeling techniques are laid out more thoroughly in Thomas and Tesar. [8] The compliance and stiffness models are described as in Hernandez and Tesar. [9]

1.2.1 Kinematics Model

The robot kinematics model is based upon a mapping of input parameters to output parameters. This is done through a set of generalized influence coefficients. Through the use of this generalization, the model can be extended to include all manipulators of varying complexity, from simple planar, overconstrained systems to complex, manipulators with a high degree of redundancy.

These influence components map a set of input parameters to output parameters, so the input and output space must be defined. In theory, joints can be either rotational or prismatic, but to maintain a degree of simplicity in the equations of motion, the input parameters are all described in terms of a rotational value, as most manipulators comprise primarily rotational joints. However, this is easily adapted to account for prismatic joints as well, with only the notation being different. This makes the input vector for a manipulator containing n joints an nx1 vector.

$$\varphi = \varphi(t) = \{\varphi_1(t), \varphi_2(t), \dots, \varphi_n(t)\}^T \tag{1.1}$$

This vector is a function of time, so the input joint velocities and accelerations are defined as the first and second time derivatives respectively.

$$\dot{\varphi} = \dot{\varphi}(t) = \{\dot{\varphi}_1(t), \dot{\varphi}_2(t), \dots, \dot{\varphi}_n(t)\}^T \tag{1.2}$$

$$\ddot{\varphi} = \ddot{\varphi}(t) = \{\ddot{\varphi}_1(t), \ddot{\varphi}_2(t), \dots, \ddot{\varphi}_n(t)\}^T \tag{1.3}$$

The output parameters are the Cartesian location and orientation of the end-effector. While many different representations of the end-effector orientation exist, for the concern of this report, the orientation will be represented as the rotation about each of the three principle axes, denoted by the subscripts following the angle. The variables *x*, *y,* and *z* represent the Cartesian location, and the rotations ψ_x, ψ_y, and ψ_z represent the three orientation parameters.

$$u = \{u_1, u_2, u_3, u_4, u_5, u_6\}^T = \{x, y, z, \psi_x, \psi_y, \psi_z\}^T \tag{1.4}$$

Due to the high degree of coupling in serial manipulators, each of the output parameters is a function of the input parameters, therefore, *u* is a function of the input parameters as follows.

$$\begin{gathered} x = f(\varphi_1, \varphi_2, \dots, \varphi_n) \\ y = f(\varphi_1, \varphi_2, \dots, \varphi_n) \\ z = f(\varphi_1, \varphi_2, \dots, \varphi_n) \\ \psi_x = f(\varphi_1, \varphi_2, \dots, \varphi_n) \\ \psi_y = f(\varphi_1, \varphi_2, \dots, \varphi_n) \\ \psi_z = f(\varphi_1, \varphi_2, \dots, \varphi_n) \end{gathered} \tag{1.5}$$

1.2.1.2 First Order Influence Coefficients

As developed in Thomas and Tesar [8], the first order influence coefficients, or *G* functions, allows the mapping of the time derivatives of the input parameters to the output parameters. These coefficients are defined in such a way that they are functions of the current geometry of the system only. Letting *u* represent the output position of the manipulator, the derivation can be seen in equation 1.6.

$$\dot{u} = \frac{du}{dt} = \frac{\delta u}{\delta \varphi}\frac{\delta \varphi}{\delta t} = [G_{\varphi}^{p}]\dot{\varphi} \tag{1.6}$$

Here, $[G_{\varphi}^{p}]$ represents the matrix containing the first order influence equations, and as can be clearly seen, is entirely a function of the input parameters. Each individual G-function relates a single input joint velocity to a single output velocity. The full matrix of G-functions can be seen as in equation 1.7.

$$[G_{\varphi}^{p}] = \begin{bmatrix} \frac{\delta x}{\delta \varphi_1} & \frac{\delta x}{\delta \varphi_2} & \cdots & \frac{\delta x}{\delta \varphi_n} \\ \frac{\delta y}{\delta \varphi_1} & \frac{\delta y}{\delta \varphi_2} & \cdots & \frac{\delta y}{\delta \varphi_n} \\ \vdots & \vdots & & \vdots \\ \frac{\delta \psi_z}{\delta \varphi_1} & \frac{\delta \psi_z}{\delta \varphi_2} & \cdots & \frac{\delta \psi_z}{\delta \varphi_n} \end{bmatrix} \tag{1.7}$$

While the most general set of G-functions will map the input parameters to the end-effector position, this is not a requirement. G-functions can be used to map the location of any fixed point on the manipulator to the input parameters. This is often useful in dynamics calculations to account for the weight and gravity shift of the links. For the special case of the G-functions mapping to the end-effector location, however, the matrix of G-functions is referred to as the Jacobian.

1.2.1.3 Second Order Influence Coefficients

Mapping input accelerations to output accelerations is also important not only in dynamic analysis, but especially in terms of stopping analysis where the ability to quickly decelerate is of paramount importance to the safety of the manipulator. This mapping is found by taking the second time derivative of the position vector.

$$\ddot{u} = \frac{d^2u}{d^2t} = \frac{\delta u}{\delta \varphi}\frac{\delta^2 \varphi}{\delta^2 t} + \frac{\delta^2 u}{\delta^2 \varphi}\left[\frac{\delta \varphi}{\delta t}\right]^2 = [G_{\varphi}^{p}]\ddot{\varphi} + \dot{\varphi}^T[H_{\varphi\varphi}^{p}]\dot{\varphi} \tag{1.8}$$

Each of these terms represent distinct components of the acceleration. The G-functions are still present to map the joint accelerations to the output accelerations, representing the "tangential" components of the output acceleration. The term, $\left[H_{\varphi\varphi}^{p}\right]$, refers to the second order influence coefficients, and, similar to the G-functions, is solely a function of the geometry of the system. These are grouped into a tensor here commonly known as the Hessian. The Hessian contains both the contributions of the centripetal accelerations, represented by the diagonal terms in the Hessian, and the coriolis acceleration, represented by the off-diagonal terms. The Hessian is an nx6xn tensor for a spatial manipulator with n joints, with 6 referring to the number of output parameters.

1.2.2 Dynamics Model

The entire dynamics model is thoroughly defined in Thomas and Tesar [8] but is briefly described here. First, in order to determine the dynamic torques required to accelerate the manipulator, the effective inertia matrix is defined based upon the mass, M_{jk}, and effective inertia, Π^{jk}, for each link jk in the manipulator.

$$\left[I_{\varphi\varphi}^{*}\right] = \sum_{j=1}^{n}\left\{M_{jk}\left[{}^{j}G_{\varphi}^{c}\right]^{T}\left[{}^{j}G_{\varphi}^{c}\right] + \left[G_{\varphi}^{jk}\right]^{T}\left[\Pi^{\mathrm{jk}}\right]\left[G_{\varphi}^{jk}\right]\right\} \qquad (1.9)$$

The matrix $\left[{}^{j}G_{\varphi}^{c}\right]$ is the matrix of G-functions for the location of the center of gravity of the j-th joint and is a result of the parallel-axis theorem transforming the inertia of the link to a location other than its center of gravity. $\left[G_{\varphi}^{jk}\right]$ represents the simple G-function mapping to the location of the axis origin.

Next, the inertial power matrix must be calculated to determine the total dynamic torques required. This incorporates the centripetal and Coriolis inertial loads by incorporating the Hessian.

$$\left[P^*_{\varphi\varphi\varphi}\right] = \sum_{j=1}^{n} \begin{Bmatrix} M_{jk}\left(\left[\,{}^{j}G^{c}_{\varphi}\right] \circ \left[\,{}^{j}H^{c}_{\varphi\varphi}\right]\right) + \left(\left(\left[\,{}^{j}G^{c}_{\varphi}\right] \circ \left[\Pi^{jk}\right]\right) \circ \left[\,{}^{j}H^{jk}_{\varphi\varphi}\right]\right) \\ +\left[G^{jk}_{\varphi}\right]^{T}\left(\left[\;\; G^{jk}_{\varphi}\right]^{T} \circ \left[\mathrm{P}^{jk}\right]\right)\left[G^{jk}_{\varphi}\right] \end{Bmatrix} \quad (1.10)$$

The variable $\left[\mathrm{P}^{jk}\right]$ is the inertia tensor for each link, and the $\circ$ operator represents the generalized dot product.

With these two matrices calculated, the dynamic torque can be calculated using Eq. 1.11 below.

$$\tau = \left[I^*_{\varphi\varphi}\right]\ddot{\varphi} + \dot{\varphi}^{T}\left[P^*_{\varphi\varphi\varphi}\right]\dot{\varphi} + \sum_{j=1}^{n}\left[\,{}^{j}G^{cg}_{\varphi}\right] L_{g,j} + \left[\,{}^{j}G^{e}_{\varphi}\right]L_e \quad (1.11)$$

The last two terms in the summation refer to the static gravity and end-effector loads. $\left[\,{}^{j}G^{cg}_{\varphi}\right]$ is the set of G-functions mapping the input parameters to the center of gravity of link j, and $\left[\,{}^{j}G^{e}_{\varphi}\right]$ is the set of G-functions mapping to the end-effector for the jth-link. The two *L* terms refer to the gravity loads for each link and the end-effector load, respectively.

1.2.3 Compliance Model

Stiffness is a concern on two levels for safety applications, albeit in two opposing ways. First, a stiffer system is a more precise system, allowing the operator to have a greater confidence in the location of the end-effector. However, a stiffer system will tend to transfer a greater amount of energy to the source of a collision in the case of a safety hazard than a more compliant system will since some of the energy in the collision will be elastically absorbed by the deflection in the manipulator.

This makes an accurate compliance model important to the designer and operator. The compliance model used in this report is developed in Hernandez and Tesar [8], but is briefly summarized here. First, a few assumptions are made in the model:

- Small deformations
- Rotational displacements treated as vectors
- Superposition is valid
- Elasticity is linear
- Small deflections so that geometry is not altered

First, deflections at the node are described by the following vector 1.12.

$$\Delta_i = \{\Delta_{x,i}, \Delta_{y,i}, \Delta_{z,i}, \Delta_{\psi_x,i}, \Delta_{\psi_y,i}, \Delta_{\psi_z,i}\} \tag{1.12}$$

The small deflection assumption means that the rotational displaces can be treated as a single vector, so most of these terms can be ignored. The loading at each node can be defined as in Eq. 1.13.

$$L_i = \{F_{x,i}, F_{y,i}, F_{z,i}, M_{\psi_x,i}, M_{\psi_y,i}, M_{\psi_z,i}\} \tag{1.13}$$

The stiffness matrix forms the basis for the model and allows these quantities to be mapped to each other as in Eq. 1.14.

$$\begin{bmatrix} L_1 \\ L_2 \\ \vdots \\ L_n \end{bmatrix} = \begin{bmatrix} K_{11} & K_{12} & \dots & K_{1n} \\ K_{21} & K_{22} & \dots & K_{2n} \\ \vdots & \vdots & & \vdots \\ K_{n1} & K_{n2} & \dots & K_{nn} \end{bmatrix} \begin{bmatrix} \Delta_1 \\ \Delta_2 \\ \vdots \\ \Delta_n \end{bmatrix} \tag{1.14}$$

The stiffness matrix relates the displacements at one axis to the force at another. This can also be transformed using G-functions to another coordinate system.

Because most deflection occurs at the joint axes due to the weight of the manipulator and end-effector loads, which would be the effective result in a collision, this model can be greatly simplified. Compliance for each axis can be transformed from the end-effector as in Eq. 1.15.

$$[K_{eef}] = \left([G_{\varphi}^{e}][\mathrm{C}_{\varphi}][G_{\varphi}^{e}]^{T}\right)^{-1} \tag{1.15}$$

Here, $[\mathrm{C}_{\varphi}]$ is the deflection per unit torque of the joint in the rotational direction of the axis, and the model is simplified to assume that deflection in other directions at the joint is negligible. This simplified model results in $[\mathrm{C}_{\varphi}]$ being represented as a diagonal matrix. While other terms can be included at the discretion of the operator, there is a quick increase in complexity from the addition of deflections in other axis directions.

1.2.4 Other Gain Functions

1.2.4.1 Actuator Gain Functions

In actual robotic systems, the actuators used often operate at a torque/speed ratio not ideal for use in serial manipulators. This is rectified in mechanical systems through use of a gear ratio. Since G-functions are defined as any mapping of an input to an output, this is a special case of G-functions for a 1-DOF system, and is defined in this case as the inverse of the gear reduction ratio. This is simply the ratio of the output joint speed to the input actuator speed. Because of the simplicity of a 1-DOF transmission speed, this is easily determined. For a gear train reduction of 50:1, the G-function, $\bar{g}$, is equal to 0.02. This G-function is also defined as the inverse of the mechanical advantage of the joint.

Gear ratios also have the advantage of improving torque capacity and stiffness of the system. An improved torque capacity leads to increased responsiveness and acceleration capacity in the system since torque is nearly linearly related to acceleration. Improved stiffness allows for a greater accuracy in system operation because any position error due to low stiffness of the rotor (the main source of compliance as described

previously in Section 1.2.3) being scaled down by the mechanical advantage. This total effect of gear trains upon joint parameters is described in Benedict and Tesar [10]

While there is no absolute requirement that gear trains used in robotic manipulators be speed reducers, in practice this is almost always the case. This refers to the case $\bar{g} \in (0,1]$, with $\bar{g} = 0$ representing an infinite mechanical gain which is impossible to achieve given real world mechanical limits. The case, $\bar{g} = 1$, refers to a direct-drive (non-geared) joint where prime movers are connected directly to the links without transmission through a gear train.

An additional assumption used in this work, although not necessarily required, is that all actuators are 1-DOF and the gear trains transmit motion purely through rotary means. While multiple DOF actuators such as ball joints may be used in manipulators, the analysis framework is established such that these may be modeled as separate 1-DOF joints located at the same axis.

Figure 1.1: Transformations the actuator parameters undergo between motor space and task space [Rios, 2008]

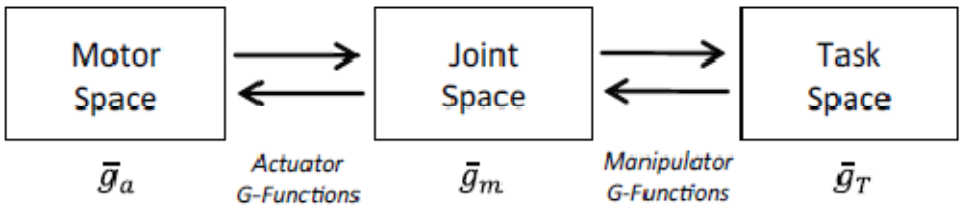

Because of the common traits of g-functions, they are easily combined to create the complete transformation from actuator space to Cartesian, or task space, as in Eq. 1.16.

$$\bar{g}_T = \bar{g}_a \times \bar{g}_m \tag{1.16}$$

The set of manipulator G-functions, $\bar{g}_m$, are the system parameters mapping the joint space to the output space and $\bar{g}_a$ is the set of all actuator transformations. This simple product allows for transformation of the actuator parameters into a useful form for the designer and operator.

1.2.4.2 Effective Distance

Another useful metric used to describe the manipulator G-functions is the effective distance, L_i, This represents the equivalent distance from the end-effector of the manipulator to joint i. It represents the equivalent analogue to the moment arm between a load and the driving actuator in a 1-DOF system. A derivation is included in Rios [11], but is shown here to illustrate the concept as well.

Figure 1.3: Description of serial manipulator geometry [Rios, 2008]

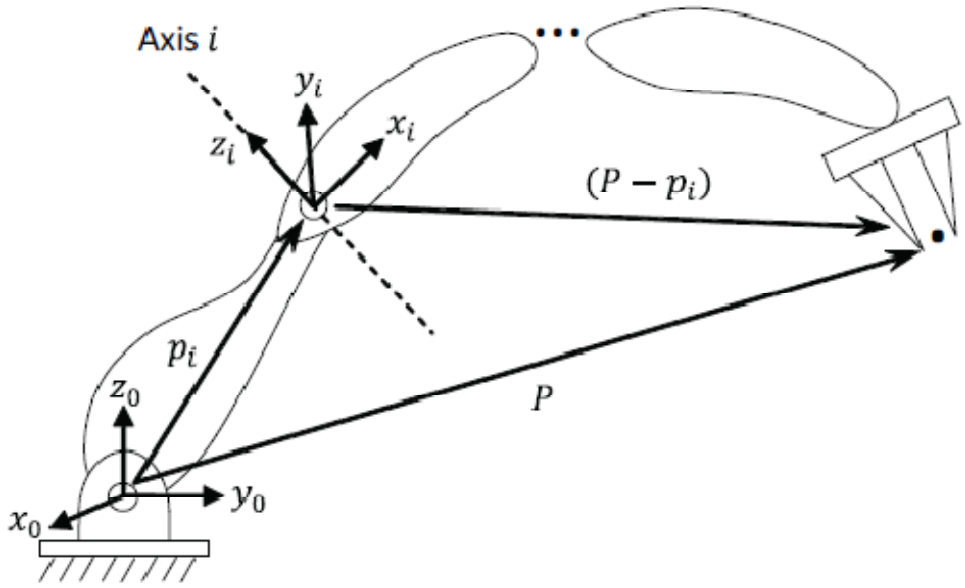

The Jacobian, as previously described, relates the input parameters to the output position and orientation of the manipulator. Because this matrix contains both position and orientation parameters, it can be deconstructed into these two components, that is, the a 3xn matrix containing the mapping of input parameters to the end-effector position, and a 3xn matrix containing the mapping of input parameters to the end-effector orientation. This decomposition is shown in Eq. 1.17.

$$J(\varphi) = \begin{bmatrix} J_T(\varphi) \\ --- \\ J_\psi(\varphi) \end{bmatrix} \tag{1.17}$$

Here, $J \epsilon \mathbb{R}^{6xn}$, $J_T \epsilon \mathbb{R}^{3xn}$ and $J_\psi \epsilon \mathbb{R}^{3xn}$. φ represents the input joint positions. This eliminates the unit discrepancy that inherently exists in a manipulator comprising entirely rotary joints. Since the joint velocities have dimensions of rad/sec, the elements of J_T must have units of length in order for dimensional requirements to be satisfied and the elements of J_ψ must be dimensionless.

As a further simplification, it has been shown in Thomas and Tesar [8] that the columns of J_T can be determined simply through Eq. 1.18.

$$(J_T)_i = s_i \times (P - p_i) \tag{1.18}$$

Here, s_i represents a unit vector pointing along the axis of motion for joint *i*, or along the z-axis of joint *i* in traditional manipulator modeling, p_i is a 3x1 vector representing the location of the origin of the *i*-th axis with respect to the base frame, and *P* is a 3x1 vector representing the location of the end-effector with respect to the base frame. This geometry can be seen in Figure 1.3 as well. The result is that $(P - p_i)$ is the location of the origin of the *i*-th axis with respect to the end-effector and the effective distance, L_i, is defined as in Eq. 1.19.

$$L_i = \|(J_T)_i\| \tag{1.19}$$

The norm, $\|\cdot\|$, denotes the standard Euclidean or 2-norm. In the most basic form, this represents the manipulator gain between the i-th joint and the end-effector, which will then combine in a product with the mechanical gain from the actuator's gear train. For planar manipulators as shown in Figure 1.3, the axis s_i will always be perpendicular to the vector $(P - p_i)$, so the effective distance will always be equal to the simple, measurable distance between the joint and the end-effector.

1.3 TRAJECTORY PLANNING

There is a large body of work done solely on the work of optimizing trajectories for 1-DOF. This work is thoroughly summarized in Rajan [12] although a short examination of different trajectory generation strategies is presented here.

Joint space planning involves ignoring the end-effector motion during path planning and instead treating the joints as independent 1-DOF systems and computing a smooth trajectory to satisfy initial and final conditions. This typically involves a slow ramp up to a maximum velocity or acceleration, followed by a ramp down to a zero velocity at the end of the trajectory.

This type of motion planning is typically used in active stops due its simplicity of calculation and the inherent importance of slowing the entire system as quickly as possible during the trajectory. Since a stopping trajectory will not be complete until each joint is motionless (hazards could still occur even during self-motion of the manipulator), this allows the stopping motion to be completed as quickly as possible.

Also, by generating smooth trajectories for each of the actuators' paths, motion planning in joint space allows for the minimal possibility of errors within the hardware or joint faults. During the stopping trajectory, the actuators will already be operating near or above their operating limits, so by mitigating the potential for large changes in

commanded torque with a smooth trajectory, there will be fewer mechanical faults and required repairs in the manipulator.

The disadvantage from using joint space motion planning is the lack of control over motion of the end-effector. This is a large concern during regular control of the manipulator because the end-effector's path is undetermined between the initial and final positions. Since these concerns are not present during stopping motions, and because of the advantages described above, joint space motion planning will be used to demonstrate the stopping motion and evaluate the stopping criteria in this work.

Three separate joint space motion planning schemes will be discussed briefly here: polynomial, sinusoidal, and trapezoidal. These are some of the more popular joint space motion planning methods, and the methodology and relative advantages and disadvantages of each are shown here.

1.3.1 Cosine Trajectory

Cosine, or sinusoidal, motion planning involves the generation of trajectories based on trigonometric functions. Since all trigonometric functions are differentiable and integral, these functions will lead to an inherently smooth trajectory. However, there are still non-zero initial and final accelerations in the system, which will introduce undesirable shocks to the system, which have the potential to damage actuators and/or gear trains.

The equations that define the total motion for a cosine trajectory are described in Eq. 1.20, and example plots of the trajectory can be seen in Figure 1.4.

$$\begin{aligned} \varphi(t) &= 0.5\{1 - \cos(\pi t)\} \\ \dot{\varphi}(t) &= 0.5\pi \sin(\pi t) \\ \ddot{\varphi}(t) &= 0.5\pi^2 \cos(\pi t) \end{aligned} \tag{1.20}$$

Figure 1.4: Plots of sample cosine trajectories. [March, 2004]

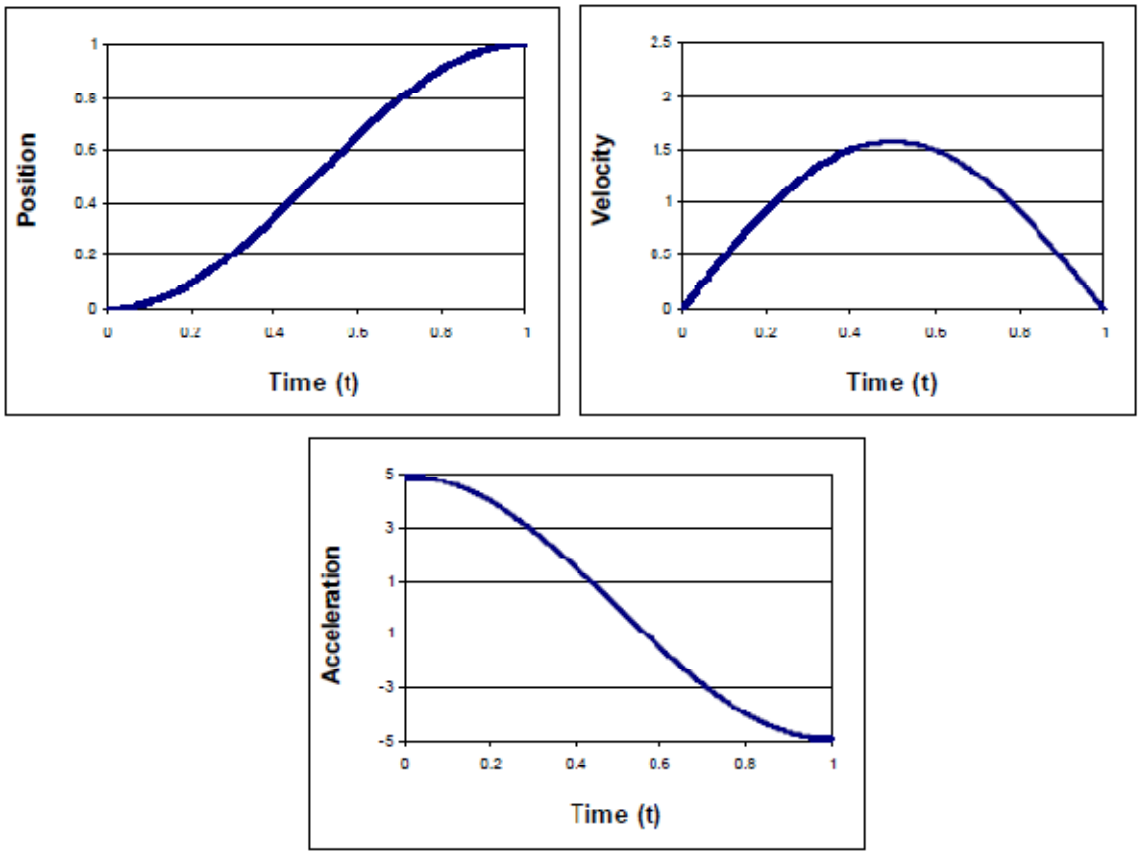

1.3.2 Polynomial Trajectory

Polynomial motion planning is a more general methodology than cosine motion planning because it encompasses more possibilities. In general, however, a polynomial motion plan is one that consists of the output parameter being represented as a polynomial using time as the independent variable. This can allow for the elimination of non-zero initial acceleration shocks simply by using a 3-4-5 polynomial. The name derives from the final exponents of the position vector. Any degree of complexity can be added by expanding the polynomial or increasing it to higher orders. However, as higher orders get added, it becomes more difficult to physically execute the trajectory in

practice, even if the trajectory may be of equal difficulty to compute in theory. The equations of motion for this trajectory are shown in Eq. 1.21.

$$\begin{aligned} \varphi(t) &= 6t^5 - 15t^4 + 10t^3 \\ \dot{\varphi}(t) &= 30t^4 - 60t^3 + 30t^2 \\ \ddot{\varphi}(t) &= 120t^3 - 180t^2 + 60t \end{aligned} \tag{1.21}$$

The trajectories calculated by these equations are shown below in figure 1.5.

Figure 1.5: Plots of sample polynomial trajectories [March, 2004]

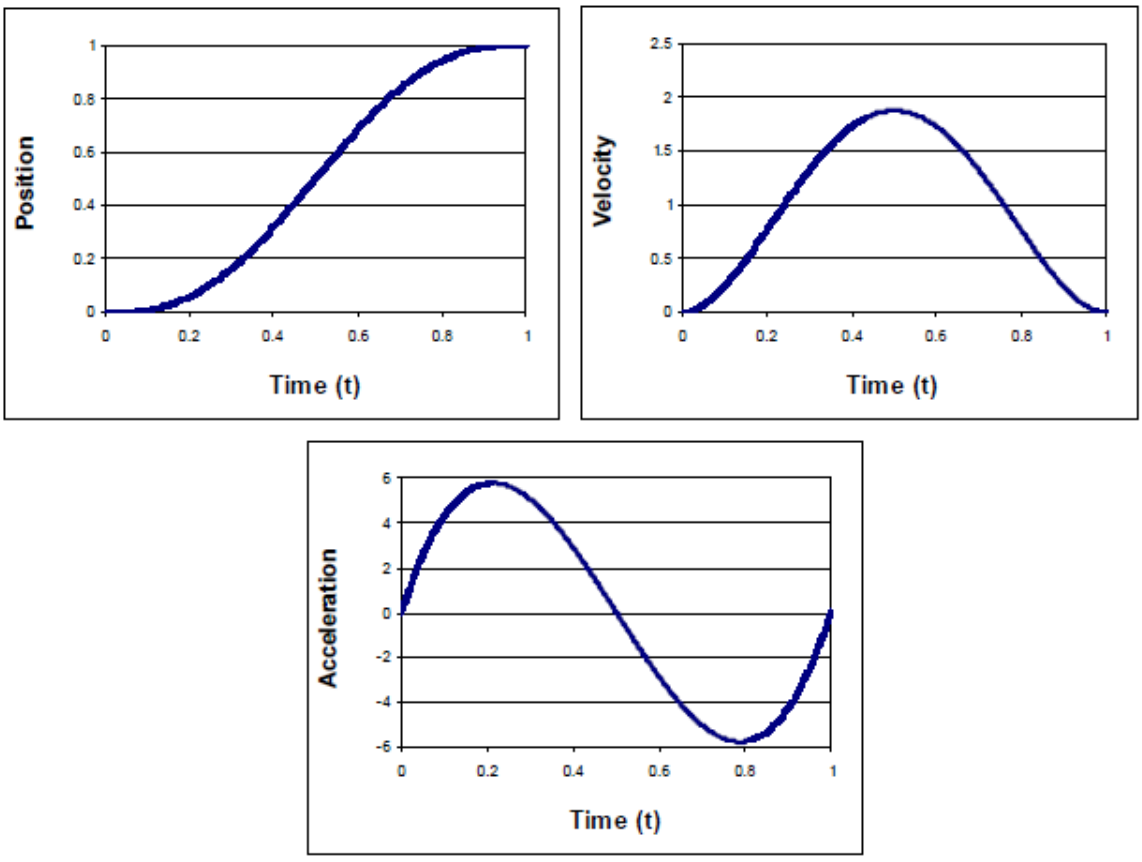

As can be seen, this trajectory has the advantage of beginning and ending accelerations of zero, minimizing the initial and final shocks present in the trajectories.

While 3-4-5 polynomials demonstrate one form of polynomial motion planning, different methods such as the cubic polynomials used in Bazaz and Tondu [15] can also be used, demonstrating the different approaches that can be used.

1.3.3 Trapezoidal Trajectory

Trapezoidal motion planning is the final motion planning algorithm here and is extremely useful in generating smooth trajectories. This method defines one of the derivatives of the output parameters as a trapezoidal curve using piece-wise linear singularity functions. This is done by defining the break points for the trapezoids in the motion plan. This is shown in figure 1.6, where $\{x_0, x_1, \dots, x_5\}$ are the breakpoints in the trajectory. The location of the break points creates the linear functions for the trapezoidal trajectory.

Figure 1.6: Example trapezoidal trajectory [March, 2004]

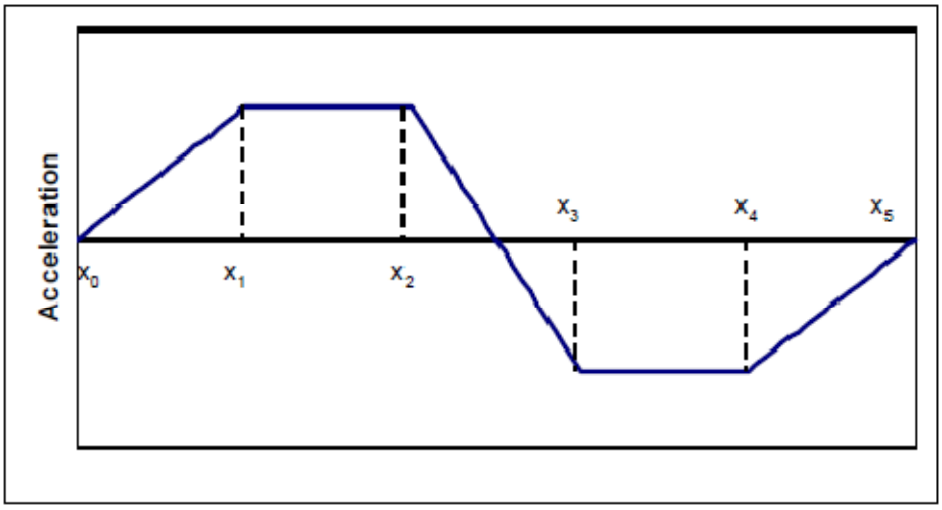

The derivative that the trapezoidal trajectory is located in is known as the order of the motion plan. For example, a trapezoidal trajectory in the acceleration space would be a 2nd order motion plan and a trapezoid in the jerk space would be considered a 3rd order

motion plan. Because the trajectory is a set of linear functions, it is integral despite being piece-wise, so the lower order outputs are then determined through integration of the original trajectory. Higher order motion plans will result in smoother trajectories, but will introduce more unpredictable higher order effects similar to the polynomial or sinusoidal motion plans.

A complete methodology for determining the necessary breakpoints and trapezoid amplitudes given a set of initial and final conditions was defined in Tesar and Matthew [15]. This methodology allows the operator to easily adjust the trapezoidal amplitude and overall motion plan by adjusting the break points, $\{x_0, x_1, \ldots, x_n\}$, for a given trajectory.

Figure 1.7: Plots of sample trapezoidal trajectory [March, 2004]

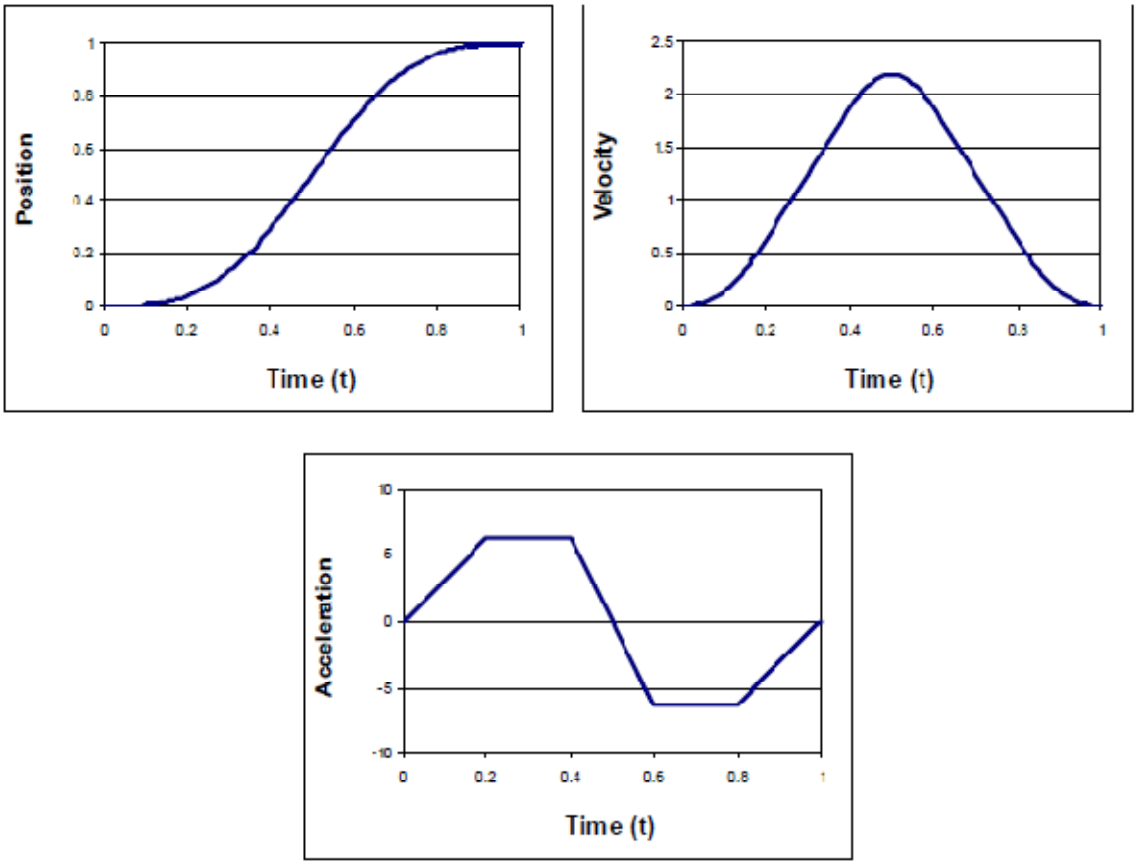

Figure 1.7 shows an example of a 2nd order trapezoidal motion plan. The algorithm has the requirements of an initial and final acceleration built in to minimize shocks, and smooth trajectories are generated in both the velocity and position space. While the discontinuities in the acceleration motion profile will still result in small shocks to the system, these can be smoothed out at the cost of generating some higher order effects by creating the trapezoidal plan in a 3rd or higher order.

The equations used to generate the above plots are shown below in Eq. 1.22 and 1.23. Eq. 1.22 is the equation for the actual equation for the *i*-th derivative of an *n*-th order motion plan. Eq. 1.23 defines the term, $\bar{\vartheta}_{ij}$, from the previous equation.

$$\bar{y}^{n-1} = \sum_{k=1}^{i} \frac{y_0^{n-k} \bar{x}^{i-k}}{(i-k)!} + \sum_{j=1}^{n} \frac{A_j}{(i+1)!} \bar{\partial}_{ij} \tag{1.22}$$

$$\bar{\partial}_{ij} = \left[\frac{\langle x - x_{4j-4} \rangle^{i+1} - \langle x - x_{4j-3} \rangle^{i+1}}{x_{4j-3} - x_{4j-4}} - \frac{\langle x - x_{4j-2} \rangle^{i+1} - \langle x - x_{4j-1} \rangle^{i+1}}{x_{4j-1} - x_{4j-2}} \right] \tag{1.23}$$

1.3.4 Trajectory Comparison

Tesar and Mathew [15] developed a set of five criteria to evaluate the desirability of single DOF motion curves as shown above. This analysis will not be repeated here, but the analysis showed that the trapezoidal motion plan contains a set of desirable properties, including a being completely general up to the *n*-th order and the easy shaping and modification of the motion plan by simply moving the break points.

Due to the conclusions presented in that report, a trapezoidal motion plan is used to generate the sample stopping trajectories in this work, to optimize the trajectory according to legacy work.

1.4 DOCUMENT OUTLINE

The rest of this report is divided as follows. Chapter 2 presents a review of previous work done in the field of manipulator safety. This includes not only attempts to evaluate the safety of a manipulator during operation, but also the work done in order to integrate safety into the system and ensure early detection of hazards. A brief review of the work done to estimate manipulator capabilities given actuator parameters is included here as well.

Chapter 3 presents the formulation and explanation of the safety criteria in this report, including descriptions of their physical and analytical meanings. Criteria to measure both the safety performance of the manipulator and the degree to which the manipulator is performing at its capacity are both included here. Finally, a simple case study is presented to the reader to demonstrate the use of the criteria and how to interpret the results.

Chapter 4 provides an analysis of how the designer can satisfy different task safety requirements given the actuator parameters. This allows the designer to map actuator parameters to potential safety performance of the manipulator and ensure that proper choices are made so that the final system will meet the task requirements.

Chapter 5 presents a 6DOF case study applying the safety criteria developed in previous chapters to a common industrial system that should be familiar to the reader. Chapter 6 will then present conclusions and a summary of future work to be potentially done.

CHAPTER 2

Literature Review

This section is meant to provide an overview of research that has been done in the general field of safety. These include assessing the potential injuries resulting from collisions, incorporating different environmental monitoring systems to prevent collisions, and assessing the safety state of the manipulator during operation. In addition, section on capability estimation is included to provide a framework for the estimation of the stopping performance based upon actuator parameters.

2.1 SAFETY RESEARCH

Since robots were first conceived, they're capacity to harm humans has been a concern. This was originally conceptualized with Isaac Asimov's three laws of robotics first written in 1942. Specifically, human safety is addressed in the first law which states "A robot may not injure a human being, or through inaction, cause a human being to come to harm". [16] While this considered largely the case of autonomous humanoid robots, it illustrates the primary requirement for safety that has driven and constrained all robotic systems, including industrial and mobile systems.

Research into developing safe systems has been conducted in four separate areas. First, researchers have worked on developing an improved awareness of the environment through greater sensor or camera fusion in order to improve safety. As computing power has increased rapidly over the past two decades, the ability of manipulator controllers (PC or embedded) to process data has increased similarly. This has led to more systems utilizing real-time data to gauge the state of their environments rather than the standard

industrial system of maintaining a strictly constant manipulator workspace and operating the manipulator under the assumption of a static environment.

Second, work has been done to develop mechanical solutions to minimize the impact of collisions. These include developing selectively compliant joints [17], using soft materials to lessen the impact [4], and the use of hybrid actuators [18]. This allows for the creation of an inherently safer system under any control strategy due to the lessened potential in the case of collision with a human.

Third, researchers have attempted to map the system parameters and state of the manipulator at the moment of impact to the potential for injury in a human [19, 20]. This is vitally important work to be done in order to reassess safety standards allowing use of robots in physical Human-Robot Interaction (pHRI) applications. In order to certify a manipulator for use in an environment, the maximum potential injury must be known. With a standard methodology for mapping the manipulator's operating specifications to injury potential, an operator can easily determine the safety of a manipulator in a task simply from the manipulator's data sheet.

Finally, work has been done to establish criteria to measure the "safeness" of a manipulator during standard operation and control strategies to optimize the manipulator's motion according to these criteria in order to prevent collisions. These include designing optimal braking strategies [21] in addition to more standard feedback control strategies [22, 23]. These studies tend to focus on establishing a single criterion evaluating the overall safety of the manipulator and application of that criterion rather than developing an overall framework for evaluation. Additionally, they should be considered distinct from this work because the emphasis is largely on evaluating the safety of the manipulator during normal operation before a collision is detected or a stop

command is received while this report focuses on evaluating the safety of a manipulator by its ability to stop itself after the command has been received by the system.

Improving the overall safety of manipulators and advancing towards a situation where manipulators are considered safe enough to incorporate pHRI tasks will incorporate all four of these approaches. A short summary of the work being done in each follows.

2.1.1 Environment Monitoring

The most intuitive form of environmental monitoring is done with integrated camera systems feeding back vision information to the manipulator controller. This technology has progressed to the point of being commercially available in systems like Pilz Automation's SafetyEye [24]. This system, though, is limited largely to the replacement of traditional robot safeguards meant to keep unexpected hazards out of the manipulator workspace such as light curtains, guard gates and other barriers. This makes it of limited use to improving manipulator safety since the net effect is to swap one set of controls for a less invasive control system that has the exact same functionality.

Alternatively, the use of fisheye cameras to track humans and other objects throughout the manipulator workspace has been investigated by Cervera et al. [25]. This improves upon the system by allowing for real-time tracking of motion within the manipulator's space. By covering the entirety of the manipulator's workspace with visual input from several cameras, the operator can ensure that all potential motion is detected. Cervera was able to demonstrate the vision system's ability to not only detect a human entering the work space, but also to have a manipulator react to said human, in the demonstration, moving towards the human. This obstacle data could then be applied to

any obstacle avoidance or collision detection strategy such as the models developed by Harden [26] in order to improve the overall safety of the system.

Figure 2.1: Sample fisheye camera image under different illuminations [Cervera et al, 2008]

Another form of improved environment detection involves the work done by Jeong and Takahashi [21] in the development of a flexible Air Pressure Collision Detection System (APCS). This is a flexible sensor allowing a collision to be detected before a rigid body is impacted by the manipulator in order to improve the response time of the manipulator. A schematic is shown below.

Figure 2.2: a) Basic structure of an APCS, b) Tube type APCS [Jeong and Takahashi, 2009]

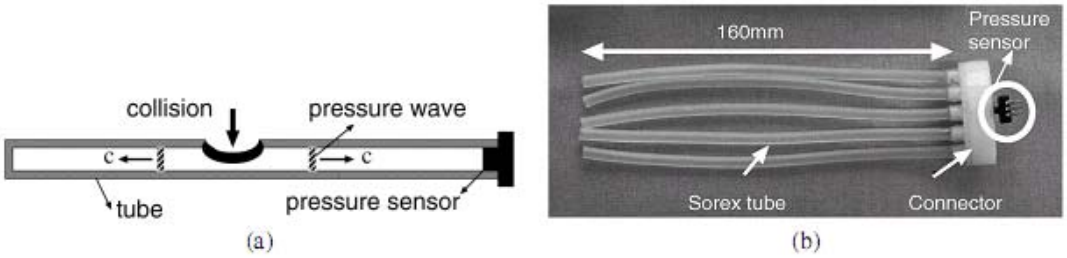

While this does not provide real time information about the environment to the manipulator, it improves the manipulator's early detection of objects in its environment in a non-destructive manner. Initial tests done show that the sensor has an extremely fast response time, on the order of a single millisecond, allowing the manipulator to detect a collision early and implement a stopping strategy before any serious damage is done to either the collision source (which may be a human) or the manipulator itself. As with any

local sensor, however, this will be limited to detecting impacts at the sensor itself, and so implementation of these on a large scale manipulator may add a higher degree of complexity than a camera system which is independent of the manipulator chosen.

2.1.2 Mechanically Safe Joints

This approach to safe manipulators involves replacing the typically highly rigid, stiff joints and links, with softer, more compliant joint technology in order to minimize the damage that the manipulator can cause by transferring energy into the collision hazard. Because stiffness is highly desirable in manipulators in order to improve the precision and responsiveness of the system, this often involves the use of selectively compliant actuators, such as in the work done by Shin et al. [18]. Here, the work done incorporates both pneumatic and electrical actuators in order to take advantage of the natural compressibility of air in the pneumatic actuators to make the system more compliant. In order to provide precise motion, the more accurate, stiffer, electrical actuators are used for small-scale motion.

Figure 2.3: Block Diagram of hybrid pneumatic-electric joint. The macro is a large-scale pneumatic actuator while the mini is a smaller electric actuator [Shinn et. al, 2008]

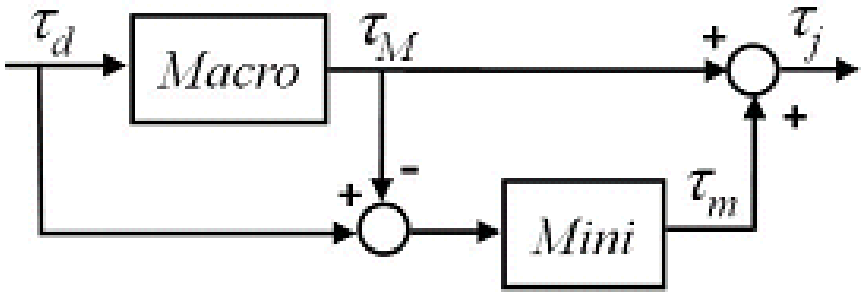

In Ikuta et al. [4], the effects of covering a manipulator with soft materials is examined. A sample diagram of this is shown in fig 2.4.

Figure 2.4: Manipulator covered in soft material [Ikuta et al, 2003]

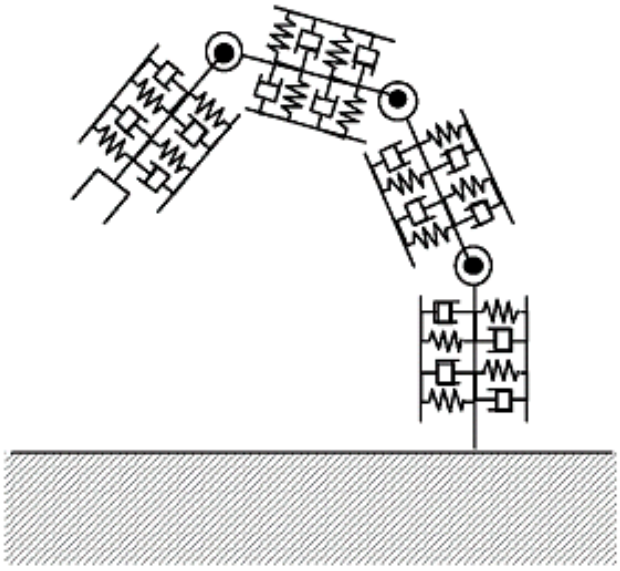

This effectively increases the safety by removing some of the energy in the collision through absorption on the material coating. This effect is represented by the spring-damper model used to model the soft material. The amount of energy transferred from the manipulator to the environment can then be determined through the equations of damped oscillation, which have been thoroughly investigated. Preliminary investigations done in that work show that simply covering a manipulator with a 10mm thick layer of rubber can significantly increase the safety, according to some metrics.

A third hybrid actuation approach involves the work done by Rabindran [17]. Rather than use inherently compliant actuators such as pneumatics or hydraulics, a multi-stage gear train is used to dissipate energy from the system in the case of a sudden shock, allowing the joint to become fully compliant, effectively. This work, while still fairly new, has the potential to greatly improve manipulator safety, simply by allowing for this degree of compliance while still maintaining a stiff system to allow for the manipulator to still be used in applications requiring a degree of precision. The trade-off for the designer

is an added complexity that leads to more potential failure points, and an increased cost. This is mitigated by the simpler control strategy required than for pneumatic-electric hybrid systems, which require both actuators to be in the control loop to complete any motion.

2.1.3 Injury Potential

In order to determine level of potential injury manipulators can cause in a collision, Haddadin et. al did some empirical tests of collisions [19, 20]. A standardized measure of injury potential needed to be included, however, in order to standardize the measurements and convert from measurements of impact upon a dummy into meaningful assessment of the effect upon humans. Used in their work is Head Impact Criterion (HIC), a metric first used in automobile crash tests [14]. HIC is defined in Eq. 2.1 below.

$$HIC_{36} = \max_{\Delta t} \left\{ \Delta t \left(\frac{1}{\Delta t} \int_{t_1}^{t_2} \|\ddot{x}_H\|_2 dt \right)^{5/2} \right\} \leq 1000 \tag{2.1}$$

Here, $\ddot{x}_H$ refers to the resulting acceleration of the subject's head after impact. An HIC value below 650 represents a very low risk of injury as a point of reference. While this criterion is useful for offline determination of the injury risk during certification, the fact that it requires measurement of the subject's resulting motion makes it completely infeasible to be used as an evaluation of manipulator motion.

Through a set of empirical tests using dummies, Haddadin et. al was able to show that the primary factor in determining the HIC of a resultant impact was the impact velocity. As manipulator mass increased, the HIC quickly saturated for a given velocity. Since the impact velocity is a controllable trajectory variable, this bodes well for the potential to greatly improve the potential for injury, at the very least according to HIC.

In order to fully determine the safety of the system, Haddadin also measured the impact force relative to the fracture force for head collisions. This involved a more complicated model of the human head, including differences in the fracture forces for the various bone sections of the cranium. Shown below in figure 2.5 is the head model used, with the variable fracture forces shown in table 2.1.

Figure 2.5: Anatomy of the Human Skull [Haddadin et al, 2008]

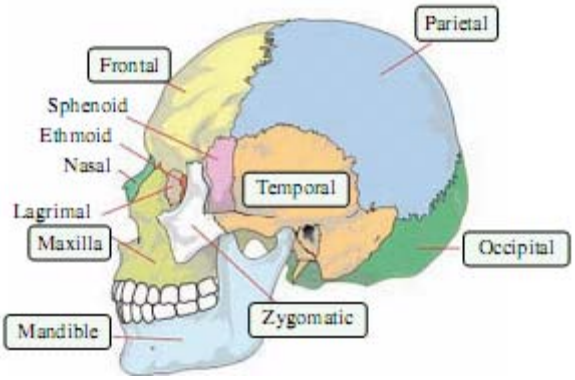

Table 2.1: Facial Impact tolerance of cadaver heads [Haddadin et al, 2008]

Facial Bone	Fracture Force (kN)
Mandible (A-P)	1.78
Mandible (lateral)	0.89
Maxilla	0.66
Zygoma	0.89
Cranial Bone	**Fracture Force (kN)**
Frontal	4.0
Temporo-Parietal	3.12
Occipital	6.41

The described tests seem to imply that manipulators are effectively safe as long as the operating velocity is kept below maximum speed below which an impact forces and HIC injury potential would be below injury threshold. However, a study conducted at the

same time by Haddadin et al [20] involving constrained impacts showed a much higher potential for injury. A constrained, or "clamped" impact refers to an impact where the subject's resulting motion is limited, usually by a wall, but potentially by any fixed object. This is compared to the unconstrained impacts described in their first work where the subject is free to move after impact.

For the case of constrained impact, it was shown that, contrary to the unconstrained situation, the manipulator's weight had a large impact on the potential for injury in the subject. Table 2.2 shows their calculated impact forces for clamped collisions to demonstrate how great the forces generated in clamped collisions are. It should be noted that 2 m/s was shown to be a safe operating speed during the analysis of unconstrained collisions.

Table 2.2: Impact Forces with clamping at 2 m/s for different manipulators

Robot	Contact Force (kN)	Maxilla Fracture?
LWRIII	0.6 @ 1 m/s	No
LWRIII	1.2 @ 2 m/s	Yes
KR3	2.2 @ 2 m/s	Yes
KR6 (Cat0 & 1)	5.1 @ 2 m/s	Yes
KR500 (Cat0 & 1)	23.6 @ 2m/s	Yes
Robot	Contact Force (kN)	Frontal Fracture?
LWRIII	3.5 @ 2 m/s	No
KR3	6.9 @ 2 m/s	Yes
KR6 (Cat0 & 1)	16.3 @ 2 m/s	Yes
KR500 (Cat0 & 1)	86.3 @ 2 m/s	Yes

2.1.4 Safety Evaluation and Control

There has been previous work done in both controlling the manipulator and evaluating its safety during operation. Kulic and Croft [22] established a Danger Criterion (DC), based upon end-effector position and inertia factors. The inertia factor is shown in Eq. 2.2.

$$f_I(I_S) = \frac{I_S}{I_{max}} \tag{2.2}$$

Here, I_S is the current inertia of the manipulator and I_{max} is the maximum allowable safe inertia in the manipulator. The distance factor is computed with the distance between the centers of mass of the manipulator and the human/potential hazard. This factor is shown in Eq. 2.3.

$$f_{CM}(D_{CM}) = \begin{cases} k(\frac{1}{D_{CM}} - \frac{1}{D_{max}})^2 : D_{CM} \leq D_{max} \\ 0 \qquad\qquad\qquad\quad : D_{CM} > D_{max} \end{cases} \tag{2.3}$$

D_{CM} represents the current distance between the centers of mass of the manipulator and the hazard, and D_{max} represents a radius beyond which the manipulator is deemed to be safely unable to reach the hazard. k is a simple scaling factor chosen by the operator to scale the potential function to one when the distance between the hazard and the manipulator is less than a minimum allowable distance.

These two factors are then combined in a product to form the final danger criterion, as in Eq. 2.4.

$$DC = f_I(I_S) \cdot f_{CM}(D_{CM}) \tag{2.4}$$

Since both criteria are scaled to be between zero and one, the DC will also be necessarily be between zero and one, with a value of one indicating a high amount of danger and a value of zero indicating no danger of a collision is present in the system.

This can then be combined into an objective function to control the manipulator during standard operation and using any sort of control optimization scheme.

In situations where a collision is more imminent, the authors modify this approach to include a velocity factor as well. This factor is calculated as in Eq. 2.5.

$$f_v(v) = \begin{cases} k_v(v - V_{min})^2 : v \geq V_{min} \\ 0 \qquad\qquad\quad : v \leq V_{min} \end{cases} \tag{2.5}$$

Also, rather than use simple end-effector information, this is modified to use the critical point for metrics. This refers to the closest point on the manipulator to the hazard. In Eq. 2.5, *v* is defined as being positive when the manipulator is moving towards the person, as well. Because the critical point is being used, the distance factor calculation changes to that shown in Eq. 2.6.

$$f_D(s) = \begin{cases} k_D(\frac{1}{s} - \frac{1}{D_{max}})^2 : s \leq D_{max} \\ 0 \qquad\qquad\quad : s > D_{max} \end{cases} \tag{2.6}$$

In this equation, *s* refers to the distance from the hazard to the critical point on the manipulator rather than the distance between the two centers of mass. With these factors calculated, the Danger Index (DI) is calculated by multiplying the DC by the velocity factor as in Eq. 2.7.

$$DI = f_I(I_S) \cdot f_D(s) \cdot f_v(v) \tag{2.7}$$

With the DI calculated, the authors then use it in a control scheme to generate a virtual force, pushing the manipulator away from collisions when a collision appears to be imminent, rather than relying on the more macro-scale DC described previously. Also to be noted is the use of piece-wise functions in the criteria, which allow for the criteria to be ignored when the manipulator is not currently in a safety-critical state. This allows the operator to implement these criteria into control optimization at all times with a minimal

impact on the overall performance of the manipulator. This type of non-invasive integration of safety controls into the system makes integration into existing controllers easier and will hopefully lead to more wide-spread adoption of safety techniques.

Another framework for safety evaluation is laid out by Ikuta et al [4]. This approach is much more comprehensive, including factors to account for the weight of the manipulator, absorption of covering material, compliance of the joints, physical shape of the links, and surface friction of the impact as passive inputs to the system based on the manipulator design. Active factors input into the model include distance, magnitude of approaching velocity, and moment of inertia of the manipulator. Each of these inputs is combined into an overall measurement of the danger of the manipulator. This can be represented either as a single number, usually represented as the product of all danger indices, or as a node chart, with each node corresponding to one of the separate danger indices. An example of the latter is shown in figure 2.6.

Figure 2.6: Danger-Index Chart [Ikuta et al, 2003]

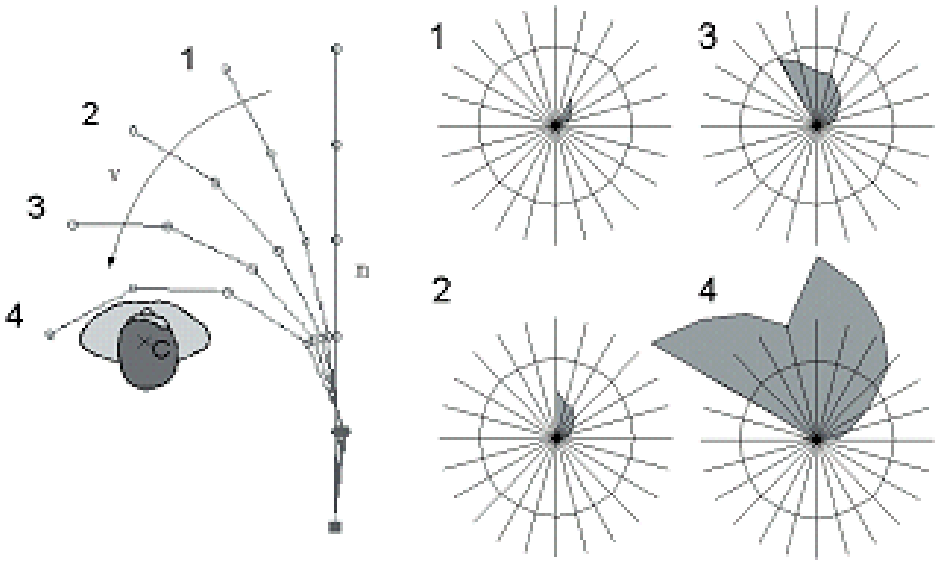

In the demonstrated charts, the nodes in the lower half represent the manipulator-dependent factors such as the manipulator mass and the link compliance. These will be constant for the manipulator regardless of its location and speed. However, the robot control based criteria such as the distance and approaching velocity are shown to increase until they are outside of acceptable limits as the manipulator moves closer and closer to the human inside the workspace.

In order to allow for simple combination of the danger-indices from various factors, this work also scales every factor to between one and zero. The calculation is additionally scalable to allow for as many or as few different defined safety strategies to be included, as shown in Eq. 2.8.

$$\alpha_{dI} = \prod_{i=1}^{n} \alpha_i \tag{2.8}$$

In this equation, α refers to each individual safety strategy while n is the total number of safety strategies utilized. As before, the smaller the value of the danger index, the safer the manipulator is. By combining the factors with a product, it additionally allows for the full effect of an extensive safety strategy. An example given by the authors is that if the manipulator is covered in a perfect shock absorption material the safety factor due to the material absorption will be zero and so the manipulator will pose no danger to a human. No matter what the forces are due to the other factors, this one safety factor will completely mitigate them, and this formulation reflects that.

This work shows a more comprehensive examination of safety than most operators or designers need or are exposed to. Often, the compliance of the joints or the shape of the links will be pre-defined before control strategies are implemented, so including them in an analysis may only serve to muddle said analysis. The overall picture presented by Ikuta is useful on a very large scale, but often the tasks described

(link design compared to robot control) will be implemented by two completely separate sets of designers and operators, and so it may represent too broad an approach to the safety problem.

Alternatively, Jeong and Takahashi [21] developed a more comprehensive torque-based braking strategy in order to optimize safety of the system. This control strategy, referred to as Dynamic Acceleration Polytope Braking (DAPB), is a torque-based control intended to achieve maximum deceleration in order to reduce the impact force in the event of a collision. This braking algorithm seeks to decelerate the manipulator within the manipulator's torque bounds while minimizing the changes in the initial direction vector of the velocity.

The algorithm works by starting with the standard dynamic equation for robotic manipulators, Eq. 2.9.

$$M(\theta)\ddot{\theta} + C\left(\theta, \dot{\theta}\right) + G(\theta) = \tau \tag{2.9}$$

Then, through differentiation of the standard mapping from joint space to Cartesian space, two new vectors are defined in Eq. 2.10 and 2.11.

$$\tilde{\tau} = \tau - C\left(\theta, \dot{\theta}\right) - G(\theta) \tag{2.10}$$

$$\tilde{x}_p = \ddot{x}_p + \dot{J}_P\dot{\theta} \tag{2.11}$$

Using these equations, the following relation is determined in Eq. 2.12.

$$\tilde{x}_p = J_P M^{-1}\tilde{\tau} \tag{2.12}$$

In general, however, the joints will not operate under equal joint bounds, so in order to keep each joint torque within the accepted torque limits, it's necessary to scale the individual joint torques based on the limits. This is done by applying Eq. 2.13 to the operational torque.

$$\hat{\tau} = T_\tau^{-1}\tilde{\tau} \tag{2.13}$$

Where $T_\tau = diag[\tilde{\tau}_{i,max}]$ and $\tilde{\tau}_{i,max}$ refers to the maximum adjusted torque of the *i*-th joint, defined in Eq. 2.14.

$$\tilde{\tau}_{i,max} = \tau_{i,max} - C(\theta, \dot{\theta}) - G(\theta) \tag{2.14}$$

Here, it is shown that this $\tilde{\tau}_{i,max}$ is the maximum applicable torque given the current state of the manipulator. This means that the set of realizable accelerations for the manipulator is defined as Eq. 2.15.

$$\tilde{x}_p = J_P[T_\tau^{-1}M]^{-1}\hat{\tau} \tag{2.15}$$

Eq. 2.15 defines a mapping of the hypercube,$\hat{\tau}$, to a polytope in end-effector acceleration space. This polytope is the Dynamic Acceleration Polytope (DAP) referred to by the title. This mapping can be seen in figure 2.7.

Figure 2.7: Mapping of hypercube in joint torque space to DAP in end-effector acceleration space [Jeong and Takahashi, 2009]

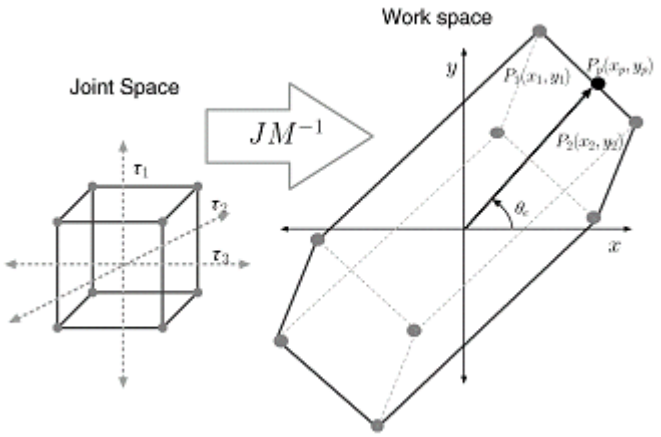

The braking torque is then found by calculating the intersection of the braking direction with the DAP in end-effector acceleration space. This braking acceleration, $\tilde{x}_{b,max}$, can then be used to find the appropriate joint torques by substituting into Eq. 2.15 and solving the inverse problem. In the case of redundant manipulators, special care

must be taken to ensure that the choice of inverse doesn't result in calculation of joint torques that exceed the torque boundaries of the hypercube. Because of these concerns, it is infeasible to use a simple pseudo-inverse for this calculation, and a more complicated inverse may be required.

Simulation results for this control scheme shown promise in their ability to improve on standard braking methods. This includes a vastly improved ability to maintain a constant end-effector velocity direction during the stopping of the manipulator.

Haddadin et al [23] proposed yet another method of collision response in their work involving using an observer to detect torque disturbances and maintaining the manipulator's path while making the manipulator extremely compliant in end-effector space. This is designed to be useful in a case where there are expected external forces applied to the system but unexpected forces still need to be accounted for. If the force exceeds an acceptable amount, it is still possible to revert to another stopping strategy.

The entirety of the control algorithm is omitted from this report, but the authors calculate the expected external torques throughout the manipulator's motion, in order to distinguish between forces which oppose the motion of the manipulator that will generated a reactive response, and forces that are part of the standard execution of the manipulator's trajectory. A general block diagram and sample path of a manipulator using this reactive strategy is shown in figure 2.8.

Figure 2.8: Compliant reactive strategy and sample path [Haddadin et al, 2009]

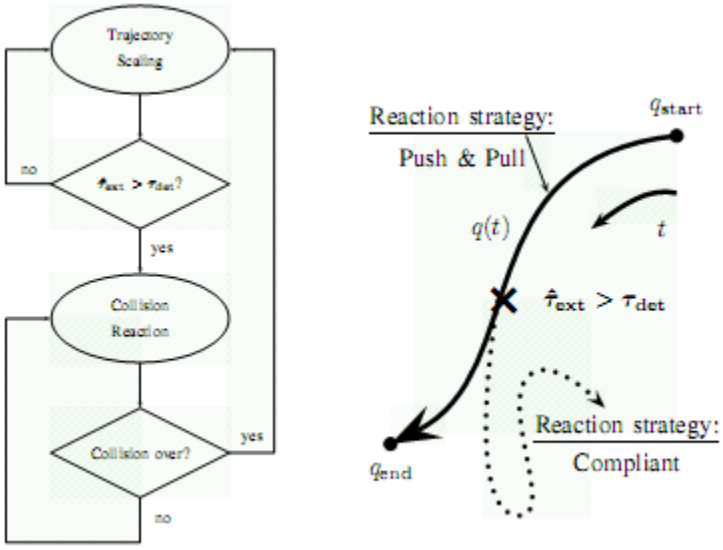

2.2 CAPABILITY ESTIMATION

In order to determine the capabilities of the manipulator to fulfill any set of performance criteria, it is important to know how the actuator's capabilities affect the performance in task space. This was extensively examined in Rios [11], who developed a framework to estimate manipulator performance capabilities based on the actuator transmission gains (gear trains), and the actuator parameters (torque capacity and rotor inertia).

Table 2.2 shows a simple overview of how the actuator level parameters affect various system level parameters. Given that safety is the main concern of this work, the mappings to system level acceleration and effective mass, or inertia, are of greatest interest here.

Table 2.2: Correlation between actuator level and system level parameters [Rios, 2008]

Actuator	System Parameter				
Parameter	Speed	Force	Eff. Mass	Accel.	Accuracy
Gear Ratio	x	x	x	x	x
Speed	x				
Torque		x		x	
Encoder Resolution					x
Stiffness		x			x
Efficiency	x	x		x	
Mass		x	x	x	
Inertia		x	x	x	

As can be seen in table 2.2, the gear ratio between the actuator and the joint is the single greatest determinant of mappings between actuator space and the system-level measurements. As such, it will inform most of the designer's decisions and will be the primary independent variable when providing the operator with a design decision to be made to optimize according to a specific task requirement.

Because the two primary drivers in safety analysis are inertia and acceleration, the mapping of actuator parameters to these system outputs in included.

2.2.1 Inertia Estimation

The effective inertia of an actuator at the system level will comprise only part of the total inertia of the system, since the links will necessarily have inertia as well as long

as they are not massless, which is physically impossible. Therefore the total inertia of all links *i* to N can be represented by Eq. 2.16.

$$I_{ii}^{*} = \sum_{j=i}^{N}\{ {}^{a}I_{ij}^{*} + {}^{l}I_{ij}^{*}\} \tag{2.16}$$

In Eq. 2.16, ${}^{a}I_{ij}^{*}$, and ${}^{l}I_{ij}^{*}$ represent the inertia of actuator and link *j* about axis *i,* respectively and are given as in Eq. 2.17 and 2.18.

$${}^{a}I_{ij}^{*} = m_j^a({}^{a}J_T^{c_j})_i^T({}^{a}J_T^{c_j})_i + ({}^{a}J_R^{c_j})_i^T \Pi_j^a ({}^{a}J_R^{c_j})_i \tag{2.17}$$

$${}^{l}I_{ij}^{*} = m_j^l({}^{l}J_T^{c_j})_i^T({}^{l}J_T^{c_j})_i + ({}^{l}J_R^{c_j})_i^T \Pi_j^l ({}^{l}J_R^{c_j})_i \tag{2.18}$$

Where m_j^a, m_j^l are the masses of the actuators and links respectively and Π_j^a, Π_j^l are the local inertia matrices of the actuators and links respectively. The Jacobian terms are the *i*-th columns of the translational and rotational components of the first-order influence coefficients associated with the centers of mass of the actuator and link *j*. Substituting Eq. 2,18 and 2.17 into Eq. 2.16 gives an equivalent inertia matrix including the inertias of both the actuators and the links. However, this does not take into account the effects of the actuator gear train upon the motor inertia. This relationship is through the square of the mechanical gain, that is, ${}^{a}I_j^{*} = \bar{g}_j{}^2 I_j^M$, so Eq. 2.17 can be re-written as Eq. 2.19.

$${}^{a}I_{ij}^{*} = m_j^a({}^{a}J_T^{c_j})_i^T({}^{a}J_T^{c_j})_i + \bar{g}_j{}^2 I_j^M ({}^{a}J_R^{c_j})_{z,i}{}^2 \tag{2.19}$$

Here, the x- and y- components of the motor inertia are assumed to be negligible compared to z-component and so are excluded. After substituting this final equation, Eq. 2.19, into Eq. 2.16, the designer is able to determine exactly how the individual actuator inertia and gear trains affect the total inertia of the system. The inertia will have an extremely large effect on the total energy in the system, which is considered a key issue in the overall safety.

2.2.2 Acceleration Estimation

Once the inertial parameters have been determined, Rios demonstrates that it is possible to estimate the acceleration capacity of the manipulator. The acceleration is directly related to the torque through the inertia, so solving this in terms of the torque and then substituting into the standard Jacobian mapping ($\ddot{x}_T = J_T\ddot{\varphi}$) yields the Eq. 2.20.

$$\ddot{x}_T = J_T(I^*)^{-1}\tau \tag{2.20}$$

By assigning an arbitrary direction $\hat{t}$ to be the direction of the acceleration and a_i to be the magnitude of the acceleration, Eq. 2.20 can be transformed into Eq. 2.21.

$$a_i\hat{t} = \sum_{i=1}^{N} \frac{\tau_i(J_T)i}{I_{ii}^*} \tag{2.21}$$

This additionally involves the decomposition of the inertia into its individual components in order to separate the joint torques. Finally, after substitution of the motor torque and gear ratio relationship for the torque in equation joint 1 and taking the 2-norm, a final relationship can be attained in Eq. 2.22.

$$a_i \leq \sum_{i=1}^{N} \frac{{\tau_i}^M L_i}{\bar{g}_i \sum_{j=i}^{N} \left\{ {}^a I_{ij}^* + {}^l I_{ij}^* \right\}} \tag{2.22}$$

This means that the minimum end effector acceleration can be defined in terms of the gear ratio and motor torques and inertias, allowing for a relatively straightforward mapping of the parameter. Additionally, since it is a simple sum over every joint, the choices are largely decoupled, so the designer is able to make actuator design decisions largely independent of one another. There will remain a small amount of coupling between the gear ratios within the inertial terms, but this effect should be negligible compared to the straight, inverse relationship that the effective acceleration has with the mechanical advantage. As can be seen clearly, as the mechanical advantage will decrease

(corresponding to an increase in the gear reduction ratio), the manipulator's acceleration capacity will increase. This is directly in contrast with the desired effects of the gear train upon the manipulator inertia, but the designer will have to optimize these opposing forces depending upon his their discretion and the task which the manipulator will perform.

2.3 CONCLUSIONS

In this chapter, an overview of the safety research being done was presented. First, work with sensor systems focused on identifying hazards within the work space and improving the manipulator's environmental awareness was presented. These included simple sensors and elaborate camera systems.

Next, research being done to make manipulators more mechanically safe was shown as a method to improve safety. Selectively compliant actuators, shock absorbent coatings, and hybrid actuators all fall under this category. These represent much more of a front-end design problem than any of the other safety methods presented in this report.

After this, the work being done to quantify the injury potential for manipulators was present. This work is vital in particular to allow for the relaxation of standards for the use of manipulators in pHRI applications. Until it can be demonstrated that the injury potential for manipulator operation is within an acceptable tolerance, it will not be possible to certify manipulators for use in human environments. This requires the mapping of manipulator operating standards to injury severity metrics that already exist within more established safety injuries.

Finally, research about control strategies and safety metrics was presented. This included the all encompassing work of Ikuta et al, which included many manipulator

design factors in addition to control strategies. Additionally the work of Kulic and Croft showed a methodology to constantly assess the level of danger within a manipulator system and optimize the manipulator path according to that level of danger. Optimal strategies for reacting to collisions included not only the DAPB by Jeong and Takahashi, which sought to maintain a constant trajectory while mapping braking performance to end-effector acceleration space, but also the selectively compliant work done by Haddadin et al, which attempted to adjust for expected and unexpected system torques in the system.

Next, the mapping of actuator parameters to system performance was briefly presented. A methodology to map both the system inertia and acceleration capability as functions of the motor torque and gear ratio was presented in order to demonstrate a framework for performance capability of more complex metrics.

There are many aspects to safety in manipulators, and the improvement of safety for manipulators will encompass all four areas presented in this chapter. Each problem can be addressed largely independently, as this report seeks to address one small niche in defining a framework for the evaluation of the actual stopping trajectory generated by a manipulator's braking performance.

CHAPTER 3

Safety Criteria Development

In formulating and choosing criteria to evaluate the safety of a stopping trajectory, an emphasis was placed upon criteria with a clear physical meaning. Simplicity was also a key factor in choosing the criteria. It is desirable for an operator to be able to easily and intuitively understand how each criterion will affect the safety of the manipulator's stopping motion, and the applicability for different tasks. While no single criterion can completely measure the safety of the manipulator, the combination of criteria presented below provides a useful cross-section.

Because the importance of each criterion to the overall safety of the manipulator varies from task to task, it makes it even more important for the operator to be able to understand the physical meanings of the criteria. Particularly as robotics moves into a greater degree of reconfigurability, this ability to determine the safety of the manipulator quickly and intuitively will become important. Rather than requiring a complete re-analysis of the manipulator's safety given a new task, a simple overview of select criteria can let the operator determine whether the safety performance is still acceptable.

After presenting the criteria in the first two sections of this chapter, a simple 2 DOF case study is examined in order to demonstrate the applicability of the criteria. This also provides an example interpretation of the results with the physical meaning explained for the manipulator in the case study.

3.1 System Level Safety Criteria

The criteria that fall under this category comprise the criteria that the operator should use to evaluate the safety of the manipulator's interaction with its environment.

These criteria are largely the calculated as a result of the motion of the end-effector after the stopping command is received and the system begins to decelerate the joints to zero by whatever control scheme the operator has chosen to implement. In terms of evaluating the overall safety of the system, however, the criteria listed here are the pertinent ones for the operator. Some combination of these criteria should be sufficient to determine the general safety of nearly all robotic tasks.

It should be noted, though, that these by no means represent a complete set of safety criteria. The criteria presented here are chosen because of the combination of an understandable physical meaning, and a direct relation to the safety of the end-effector. This list may be expanded upon in the future, as later research or work demands.

3.1.1 Total Distance Traveled

$$\boldsymbol{TDT} = \|\bar{\boldsymbol{x}} - \bar{\boldsymbol{x}}_{\boldsymbol{i}}\| \tag{3.1}$$

Table 3.1: Physical meaning of total distance criterion

Criteria Values	Physical Meaning
TDT→0	Manipulator End-Effector does not move from location that stop command is received at
TDT→∞	Manipulator end-effector moves a large distance from location that stop command is received at

This is the most generic criterion related to stopping trajectories. The primary goal in stopping a manipulator is to prevent further motion of the manipulator. This criterion measures the total distance traveled from the moment that the stopping command is received (x_i). Since there is no linear mapping that occurs between motion in joint space and Cartesian space, this is a non-trivial matter. Motion at joints closer to

the manipulator base will tend to have a greater effect on motion than motion at joints closer to the EEF, as well.

Since safety hazards will occur only if there is a collision between the manipulator and another object, without any directional information it is possible using solely the distance to construct a sphere of safety representing the sum total of possible locations that the manipulator could have entered during the stopping trajectory. As long as no object enters this sphere, no safety hazards will occur without catastrophic failure of one or more of the underlining mechanical elements of the manipulator (gear train, actuators, link damage).

The total distance traveled is also important due to the fact that safety studies have shown that distance is a critical component in determining the potential injury that could be suffered by a clamped impact. In this situation, an individual is trapped between the manipulator and a rigid surface. This causes additional fracture and organ damage as the manipulator moves towards the rigid surface through the individual's person. By minimizing this distance, it is possible to minimize the potential damage that can occur if the manipulator were to clamp an individual in the worst case scenario that the manipulator motion is perpendicular to the clamping surface. As has been shown in the Haddadin et al [19], the robot's weight has almost no correlation to the potential damaged caused by the manipulator in a clamping situation. As long as this criterion is minimized, the total damage that can be inflicted will be minimized as well.

3.1.2 Directional Distance Traveled

$$\boldsymbol{dDST} = \|[\bar{\boldsymbol{x}} - \bar{\boldsymbol{x}}_{\boldsymbol{i}}] \cdot \hat{\boldsymbol{u}}\| \quad \textbf{(3.2)}$$

Table 3.2: Physical meaning of directional distance criterion

Criteria Values	Physical Meaning
dDST→0	Manipulator End-Effector does not move in direction *u* from that stop command is received at
dDST→∞	Manipulator end-effector moves a large distance in direction *u* from location that stop command is received at

This criterion expands upon the previous one by adding in directional information. In general, the total distance traveled may not be a critical safety issue since it is unlikely that the manipulator will be surrounded on all sides by potential safety hazards. Far more likely is that the manipulator will only have possible safety hazards located in certain directions from the EEF, such as a wall, or a human working alongside the manipulator in a cooperative environment. In this case, it is far more critical to minimize motion towards the wall or human than it is to prevent motion in general. It is far safer to allow the EEF to move five cm away from the human than it is to allow the manipulator to move one cm towards the human, since any degree of contact between manipulator and human will result in a safety violation. This is especially important in pHRI (physical Human-Robot Interaction) applications, because by controlling the allowable areas within the robot workspace for humans to be located in, it is possible to further improve safety over a simple stopping procedure by a control scheme that optimizes according to this criterion. If the critical value of this criteria can be determined for a manipulator over its entire workspace, proper safety controls can be

effectively implemented to prevent any safety hazards from occurring in the manipulator's operation.

This is especially important considering the injury potential due to clamping that was discussed with regards to the previous criterion. Injuries can be minimized by preventing motion in the direction of the clamping surface. Simply preventing motion in a direction normal to the clamping surface during the stopping trajectory will improve upon the gains possible with the previous criteria, while also providing a greater degree of certainty to the data.

The *u* vector in this equation should be a unit vector in order to allow for a point of comparison with the previous criterion. A non-unit vector will introduce additional scaling to the criterion, making it difficult to measure the difference between the two. Because of this issue, it is recommended that the operator ensure that the vector used is always normalized.

3.1.3 End-Effector Kinetic Energy

$$\boldsymbol{EKE} = \frac{1}{2}\dot{x}^T[I_{uu}^*]\dot{x} \qquad \textbf{(3.3)}$$

Table 3.3: Physical meaning of end-effector kinetic energy criterion

Criteria Values	Physical Meaning
EKE→0	Energy stored in the manipulator quickly dissipates to a safe amount
EKE→*Manipulator Dependent Maximum*	Energy stored in the manipulator takes a long time to be lowered to a safe amount

Due to the laws of conservation of energy, the amount of energy transferred to an individual or object by the manipulator is inherently limited by the amount of energy stored in the manipulator at the moment of contact. Therefore, it is desired to minimize the kinetic energy stored within the manipulator at all points in the stopping trajectory. This criterion seeks to address the issue. By measuring the kinetic energy in Cartesian space, the mass effects of the links are accounted for in the model rather than simply addressing the inertia of the actuators. With the link mass information accounted for, the criterion can differentiate between critical and non-critical states of energy storage within the system.

In general, this criterion along with the following two criteria can be seen as measurements of the potential severity of a collision, rather than determining the potential for a collision itself. For many applications where the operator may consider collisions to be inevitable within the operation of the system, including systems with a large amount of obstacles moving in unpredictable patterns, or systems which operate closely in tandem with humans where contact with the manipulator may be assumed.

3.1.4 Link Stiffness

$$\boldsymbol{STF} = \|[K^e]\|_f = \sum_{i=1}^{m}\sum_{j=1}^{n}[K^e]_{i,j}^2 \qquad \textbf{(3.4)}$$

Table 3.4: Physical meaning of link stiffness criterion

Criteria Values	Physical Meaning
STF→0	Manipulator is in a configuration such that impact forces will cause deflection of the end-effector
STF→*Manipulator Dependent Maximum*	Manipulator is in a configuration such that impact forces will be transferred to the environment

Similar to the EEF Kinetic Energy criterion, minimizing this criterion does not affect the possibility of a collision, but simply the severity of a collision, should one occur. The link stiffness is a measure of the resistance of the EEF to movement upon application of a force at the EEF. It is desired to be minimized in situations where damage to the manipulator is more preferable than damage to the potential sources for collision, since a manipulator in a "softer" configuration will be more likely to absorb impact in the form of deflection by the EEF, rather than simply continuing through the collision point. This will result in a situation in which the gear train and links of the manipulator are more likely to sustain damage from the unnecessary motion in the opposite direction of the actuator motion. Still, in the event that it is of greater importance to protect the potential collision hazards than it is to prevent damage to the manipulator, this is a valid criterion to optimize. Although the operator should note that, similar to the previous criterion discussed, this should be considered a secondary criterion to optimize since the primary goal of all safety procedures should be to prevent collisions rather than to minimize damage in the event of a collision. In the end, this criterion will not in general minimize the total damage caused by a collision, but will instead transfer the damage done to the manipulator rather than the part of the environment with which the collision occurs.

3.1.5 End-Effector Velocity

$$\boldsymbol{VEL} = \|\dot{\boldsymbol{x}}\| \tag{3.5}$$

Table 3.5: Physical meaning of end-effector velocity criterion

Criteria Values	Physical Meaning
VEL→0	Manipulator end-effector quickly decelerates to a safe speed
VEL→∞	Manipulator end-effector slowly decelerates to a safe speed

This criterion goes along with the minimum total distance criteria. The importance behind differentiating between the two is that studies have shown [19] that in an unclamped impact, the velocity of the manipulator at impact has the greatest correlation with the degree of injury, or Head-Impact Criteria (HIC), a common method of measuring potential head trauma. Since velocity is more important in this situation than the weight or acceleration of the manipulator, it is included here as a potential criterion to be minimized. In general, this will always be important since the stopping procedure itself is a minimization of the velocity norm, and so it may not be necessary to monitor this criterion explicitly. However, as separate optimizations are applied for distance traveled, it may be desirable to combine the optimization with this criterion as well, to both ensure that the manipulator is stopping in the minimum time possible and to minimize potential damage in an unclamped collision. However, as shown by Haddadin et al [19], the latter point may be of less importance since the likelihood of an unclamped

collision resulting in serious injury to a human is very low, regardless of the speed or size of the manipulator.

This criterion can alternately be framed in as a "time to safe velocity" criterion. As described previously by Haddadin et al, there is some velocity beneath which the end-effector will no longer cause lethal or catastrophic injury. By defining this "safe" velocity, and measuring the time it takes the end-effector to slow down to less than this velocity, this may prove to be more useful to the operator in terms of evaluating the safety of the manipulator. An example of this methodology is shown in the case study in section 3.2 of this work for both this and the following criterion.

3.1.6 Directional End-Effector Velocity

$$\boldsymbol{dVEL = \dot{x} \cdot \hat{u}} \tag{3.6}$$

Table 3.6: Physical meaning of directional end-effector velocity criterion

Criteria Values	Physical Meaning
dVEL→0	Manipulator end-effector quickly decelerates to a safe speed in the direction *u*
dVEL→∞	Manipulator end-effector slowly decelerates to a safe speed in the direction *u*

Similar to the directed distance criterion, this criterion expands upon the simple velocity criterion by adding directional information. Again, *u* represents a 6x1 unit vector containing the directional information that is important to the operator. Optionally, this can be floored at zero, such that

$$dVEL = \begin{cases} 0, if\ dVEL \leq 0 \\ dVEL, if\ dVEL > 0 \end{cases}$$

Since the directional vector should indicate a specific direction in which motion will be hazardous, it is usually the case that motion in the opposite direction poses no safety issue, and so can be safely ignored by the operator or control scheme in calculating an optimized path.

However, there may be some issues with this criterion depending on the task being executed. If the potential safety hazard to be avoided is contact with a human, motion that isn't normal to the subject could be considered just as dangerous. For example, with a cutting tool, normal motion may result in a deeper puncture wound while motion transverse to the subject results in a longer slicing wound. In this case, it would be important to monitor not only the velocity normal to the direction that the subject lies in, but also non-normal velocities, and so the operator would be wise to include the total velocity data in their calculations as well.

3.1.7 Distance From Given Trajectory

Table 3.7: Physical meaning of distance from given trajectory criterion

Criteria Values	Physical Meaning
$TRJ \rightarrow 0$	Manipulator end-effector stays close to given trajectory during stopping motion
$TRJ \rightarrow \infty$	Manipulator end-effector moves a large distance from given trajectory during stopping motion

This criterion seeks to measure the distance between the end-effector and a set trajectory (usually the trajectory at the time the stop command is issued. In order to provide for ease of calculation, this trajectory is assumed to be a straight line. The

distance between a point in space and a straight line was calculated in Perry and Tesar, although the derivation is included as follows.

Figure 3.1: Derivation of distance between a point and a line [Perry and Tesar, 1995]

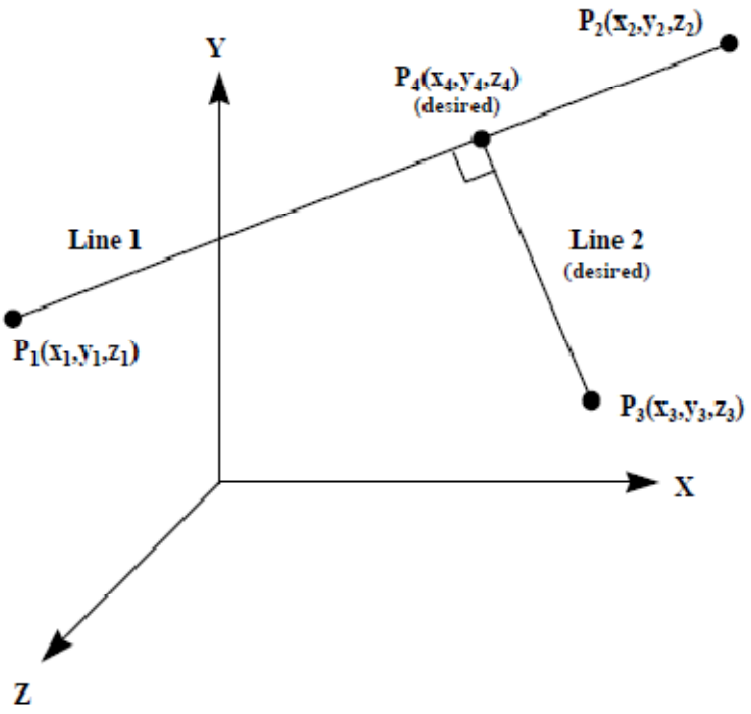

In this derivation, the line denoted by P_1 and P_2 is considered to be some initial trajectory. This can either be specified by the operator or else determined automatically by using the initial position and velocity of the manipulator's end-effector. P_3 represents the current position of the end-effector, which will obviously vary over the course of the trajectory.

First, line 1 can be represented parametrically by Eq. 3.7.

$$\begin{bmatrix} x \\ y \\ z \end{bmatrix} = \begin{bmatrix} x_1 + (x_2 - x_1)t_1 \\ y_1 + (y_2 - y_1)t_1 \\ z_1 + (z_2 - z_1)t_1 \end{bmatrix} \tag{3.7}$$

Similarly, a point on line 2 can be represented parametrically by Eq. 3.8.

$$\begin{bmatrix} x \\ y \\ z \end{bmatrix} = \begin{bmatrix} x_3 + (x_4 - x_3)t_2 \\ y_3 + (y_4 - y_3)t_2 \\ z_3 + (z_4 - z_3)t_2 \end{bmatrix} \tag{3.8}$$

Because Point 4 is located on both lines 1 and 2, Eq. 3.8 can be re-written as Eq. 3.9.

$$\begin{bmatrix} x \\ y \\ z \end{bmatrix} = \begin{bmatrix} x_3 + (x_1 + (x_2 - x_1)t_1 - x_3)t_2 \\ y_3 + (y_1 + (y_2 - y_1)t_1 - y_3)t_2 \\ z_3 + (z_1 + (z_2 - z_1)t_1 - z_3)t_2 \end{bmatrix} \tag{3.9}$$

Since lines 1 and 2 are perpendicular, it should follow that the dot product of the parameter coefficients is equal to zero, so Eq. 3.10 holds true.

$$\begin{bmatrix} (x_2 - x_1) \\ (y_2 - y_1) \\ (z_2 - z_1) \end{bmatrix} \cdot \begin{bmatrix} x_1 + (x_2 - x_1)t_1 - x_3 \\ y_1 + (y_2 - y_1)t_1 - y_3 \\ z_1 + (z_2 - z_1)t_1 - z_3 \end{bmatrix} = 0 \tag{3.10}$$

Solving this equation for t_1 gives Eq. 3.11 as the solution.

$$t_1 = \frac{-(x_2 - x_1)(x_1 - x_3) - (y_2 - y_1)(y_1 - y_3) - (z_2 - z_1)(z_1 - z_3)}{(x_2 - x_1)^2 + (y_2 - y_1)^2 + (z_2 - z_1)^2} \tag{3.11}$$

With t_1 calculated, P_4 can be determined as Eq. 3.12.

$$P_4 = \begin{bmatrix} x_4 \\ y_4 \\ z_4 \end{bmatrix} = \begin{bmatrix} x_1 + (x_2 - x_1)t_1 \\ y_1 + (y_2 - y_1)t_1 \\ z_1 + (z_2 - z_1)t_1 \end{bmatrix} \tag{3.12}$$

And the minimum distance between the end-effector and the original trajectory can be determined in Eq. 3.13.

$$\min distance = \sqrt{(x_3 - x_4)^2 + (y_3 - y_4)^2 + (z_3 - z_4)^2} \tag{3.13}$$

This criterion is especially useful for tasks where the specific path of the end-effector is of importance. This includes applications such as seam welding, where moving away from a specified path can cause damage to the objects being welded to each other, or in rehab applications, where a manipulator moves in a set path in order to exercise a joint. Deviation from this path could cause harm or injury by twisting the rehab subject's appendage in an unnatural way or moving out of a designated "safe" path predefined by the operator. This medical rehab work as described is not currently certifiable by U.S. safety standards, but the principles remain the same.

3.2 JOINT LEVEL CAPABILITY CRITERIA

The joint level criteria presented here are wholly different than the system level criteria. The system level criteria should be optimized to judge the overall safety of the manipulator during a stopping procedure. However, for the joint level criteria, the emphasis is placed on the optimal operation of the system internally. These criteria give the operator a way to evaluate the manipulator's performance during the stopping procedures.

As a rule, by examining these criteria, the manipulator operator or designer can gain insight into potential areas for improvement, either by adjusting the mechanical gains of the actuators, or changing the actuators themselves in the case of the designer.

Additionally, monitoring these criteria can help the operator decide whether it is possible to make further performance gains in the system level criteria. As long as there remains leeway in the joint level criteria between the measured values and the acceptable maximums, the manipulator is not performing at maximum capacity with regards to the system level criteria that are important to the prevention of collisions and the overall safety of the stopping procedures. This will also give the designer or operator insight into the overall balance of the system. If one or two actuators are performing a disproportionate amount of the work in stopping the system, these criteria will indicate the problem and allow the designer to adjust the system either by selecting more powerful actuators or adjusting the gear ratios for these joints. By singling out these bottle necks in the system, it is also possible for large performance gains to be realized by changing the actuator parameters for only one or two joints that are limiting system performance rather than changing parameters at each joint to attempt to achieve performance gains.

3.2.1 Torque Ratio

$$\boldsymbol{TRT} = \left[\frac{\tau_k}{\alpha\tau_{k,nom}}\right]_{max/average} \quad \textbf{(3.13)}$$

Table 3.8: Physical meaning of torque ratio criterion

Criteria Values	Physical Meaning
TRT→0	No actuators operate near the specified torque limits
TRT→1	One or more actuators are operating near the specified torque limits
TRT>1	One or more actuators are operating in an unsafe manner outside the torque limits specified by the operator

In standard operation, an actuator's torque is limited to the nominal torque value to prevent damage to the actuator. However, during stopping procedures, it is desirable to utilize the maximum capacities of the actuator. This is allowable due to the short and infrequent nature of stopping procedures. In general, the maximum allowable torque is between three and five times the nominal torque. This uncertainty is represented by the α-constant, hereby known as the stopping coefficient, which can be chosen by the operator to be anything greater than one and less than five, although in general, should chosen to be between three and five to maximize performance. Lower values for the stopping coefficient will represent a more conservative view with a lower performance capability, while higher values will allow for greater performance. A value of one for the coefficient corresponds to a stopping procedure which does not utilize the added torque capabilities beyond the nominal torque of the actuators.

While the values of three to five represent an enhanced performance relative to that provided by the nominal operating torque, these still represent torque values that the actuators should be able to provide with little risk of damage to themselves or the system. However, it is often the case that damage to the system or a component may be more desirable than the consequences of a collision, which could include serious or fatal injury to an operator within the manipulator workspace. In these cases, the value of the stopping coefficient may be chosen to be as high as ten. For values above five, however, it may be necessary to replace or perform maintenance on the actuator that crosses this torque limit in order to ensure that future safe operation of the system.

A great deal of attention should be paid to this criterion, though, in order to ensure optimal performance of the system level criteria. While it is desirable in general to

minimize this criterion to whatever extent possible, larger values will be indicative of better overall performance in stopping trajectories. As this criterion increases, it indicates that the manipulator is performing closer to the peak of its abilities in terms of being able to decelerate the joints, thereby slowing the EEF as quickly as possible. As values drift farther and farther from one, it indicates that there is a performance gap between where the joints are actually performing at, and the performance capability of the joints. In this sense, it is desirable to maximize the maximum value of this criterion, even though it is listed as a minimization criterion.

The reason it is desirable to keep this criterion minimized is that operating actuators at above their nominal torques for extended periods of time can lead to actuator damage or failure. There, the operator must make a trade off. If a faster stop is more desirable without regard to actuator condition, minimizing this criterion should be considered less important. For applications where it is necessary to prevent actuator damage, however, this criterion should be closely monitored.

This can be monitored either nonlinearly, as a maximum of all the actuators, which is important to provide the operator with the current performance of the actuator operating most closely to its threshold, or else as the average over all actuators, to provide a continuous criterion and display the overall degree to which the system is performing to its capabilities. This additionally allows for the use of optimization strategies which require differentiable objective functions and constraints, a common requirement in modern control strategies.

3.2.2 Kinetic Energy Distribution

$$\boldsymbol{KED} = \left[\frac{\dot{\varphi}^T I_k \dot{\varphi}}{\dot{\varphi}^T I \dot{\varphi}}\right]_{max} \quad \textbf{(3.14)}$$

Table 3.9: Physical meaning of kinetic energy distribution criterion

Criteria Values	Physical Meaning
KED → *Manipulator Dependent Minimum*	Kinetic energy is evenly distributed throughout the links, resulting in no large energy concentrations
KED→1	Kinetic energy is concentrated in one or more joints

For a manipulator to be performing at max efficiency, it is desirable for the energy to be evenly distributed throughout the system to prevent one actuator from doing the majority of the work over the stopping trajectory. By monitoring the looking at the maximum of each link's percentage of the total kinetic energy, this situation can be targeted and addressed. This criterion will necessarily vary from a maximum of one (a single link contains all of the kinetic energy in the system) to 1/n, for an n-DOF manipulator, which would correspond to the kinetic energy being evenly distributed throughout the system.

The maximum of these values is monitored because, as a percentage of kinetic energy, this is by necessity a zero-sum criterion over the entirety of the actuators. The sum of each actuator's value will always be equal to one, so an average is impractical and not useful as a measurement method.

This criterion has one key weakness that is addressed in the following criterion, however, and that is that for the vast majority of manipulators, actuators near the base of the manipulator tend to be larger and have a greater torque capacity than actuators

towards the EEF, where precision and smaller sizes are more important. Therefore, it may not be necessarily desirous to distribute energy completely equally throughout the system, but rather to distribute energy proportionally so each actuator is performing at the same percentage of its capacity in order to remove kinetic energy from the system in the most efficient way possible. Blindly seeking to minimize this criterion in a manipulator with different sizes of actuators can lead to worsened performance and undue fatigue and damage being sustained by the lower capacity actuators in the manipulator. The operator should therefore always use discretion when examining this criterion.

3.2.3 Weighted Kinetic Energy Distribution

$$\boldsymbol{wKED} = \left[\frac{\dot{\varphi}^T I_k \dot{\varphi}}{\dot{\varphi}^T I \dot{\varphi}} \Big/ \gamma_k \right]_{max} \tag{3.15}$$

Table 3.10: Physical meaning of weighted kinetic energy distribution criterion

Criteria Values	Physical Meaning
wKED → *Manipulator Dependent Minimum*	Energy in each joint is much less than the maximum possible concentration for that joint
wKED→∞	Energy in one or more joints is near the maximum possible concentration for the manipulator configuration

In order to address the problems of the previous criterion, a weighted version of the kinetic energy distribution criterion was developed. This criterion adds computational complexity, but allows for easy scaling of the values to eliminate the previously described issues of the generic Kinetic Energy Distribution criterion. To calculate this, first the KE partition values are calculated as described in Tesar and Rios

[28] These numbers represent the maximum percentage of the kinetic energy that could potentially be distributed to each link. Using this value as a scaling factor allows the operator to estimate each actuator's relative energy capacity in its current configuration. Scaling to these values lets the operator judge better whether the energy distribution is acceptable given the differences in actuators than with the previous criterion. A value of one will represent an acceptable state, regardless of which joint it occurs at, since it represents that actuator performing at the maximum acceptable capacity in terms of system energy distribution rather than absorbing the entirety of the system energy. Therefore, the operator should interpret values near one as evidence that there are not many performance gains available given the manipulator configuration, while smaller values will indicate that gains are potentially possible since no individual actuator is operating at or near its capacity.

Calculating this criterion adds a degree of computational complexity, however, since it requires the solution of an eigenvalue problem to determine the KEPV's. When examined off-line in an evaluation sense, this is may not be an issue, but if it is desired to monitor these values in real time, this makes this criterion less useful due to the computing power required.

3.2.4 Joint Kinetic Energy

$$\boldsymbol{JKE} = \dot{\varphi}^T I^* \dot{\varphi} \tag{3.16}$$

Table 3.11: Physical meaning of joint kinetic energy criterion

Criteria Values	Physical Meaning
JKE→0	Manipulator end-effector stays close to given trajectory during stopping motion
JKE → *Manipulator Dependent Maximum*	Manipulator end-effector moves a large distance from given trajectory during stopping motion

The other main issue with the stopping procedures that isn't properly captured by monitoring partition values is the total kinetic energy present in the system. Since partition values are scaled by the total kinetic energy present in the system, the KEPVs may show an undesirable distribution of energy even though the total energy distributed through the system is insufficient to cause any actuator to operate outside of its performance limits. Thus, it becomes necessary to monitor the total energy present to ensure that no false flags are noted from a partition value analysis. This can also be determined by analyzing the torque ratio criterion and checking that the offending joint as determined by partition value analysis is well within the torque limits at the time of the offense.

This criterion is closely coupled with the EEF-kinetic energy criterion, differing in the use of the Jacobian and its pseudo-inverse to transform the energy into Cartesian space. This is done since the kinetic energy as related to the potential damage inflicted by the system, whereas when monitoring the energy in joint space, it is more desirable to monitor the effect of energy on the joints and actuators themselves. Therefore, even

though these two criteria are highly coupled, it is important to monitor both, since the separate transformations display two major different situations, both of which are important to be monitored.

3.2.5 Joint Potential Energy

$$\boldsymbol{JPE} = \frac{1}{2}[L_{ee}^{T}[G_{\varphi}^{e}][C_{\varphi}][G_{\varphi}^{e}]^{T}L_{ee} + {}^{j}L_{g}^{T}[\,{}^{j}G_{\varphi}^{cg}][C_{\varphi}][\,{}^{j}G_{\varphi}^{cg}]^{T}\,{}^{j}L_{g} + \tau_{\varphi}^{T}[C_{\varphi}]\tau_{\varphi}] \quad \textbf{(3.17)}$$

Table 3.12: Physical meaning of joint potential energy criterion

Criteria Values	Physical Meaning
JPE→0	No potential energy is stored within the manipulator joints
JPE → *Manipulator Dependent Maximum*	A large amount of potential energy is stored within the manipulator joints

During the operation of the manipulator, a rigid interface is often assumed, and in most cases, this is a valid assumption. For high loading tasks, however, it is possible for this assumption to no longer be valid, so the operator may want to monitor the potential energy being stored in the joints due to loading of the system. This can lead to errors from two sources. First, a lot of potential energy stored in the system indicates that individual actuators may be close to mechanical failure, either in the form of a catastrophic break, or a less catastrophic, but also dangerous plastic deformation of the actuator, which will lead to permanent systemic errors.

Second, a large amount of potential energy stored in the manipulator indicates that there will be danger at some point when the energy is inevitably released from the manipulator. Thus, while the manipulator may have less kinetic energy, as shown by the

previous criteria, this may not be entirely indicative of the true safety state of the manipulator, which is best represented by the total energy present within the manipulator. This may be neglected for low impact tasks with a lesser load, but as the loading and weight of the manipulator increases, it will be far more important to monitor this criterion to ensure safe operation of the system.

3.3 2 DOF CASE STUDY

In order to demonstrate the use of these criteria, they were calculated for a 2-DOF system with both joints moving at maximum joint velocities from a set position. These joints are decelerated by using a trapezoidal path plan with a set maximum acceleration to generate the plan. This plan was generated in accordance with the work done by Peter March in 2004. This was done to demonstrate both the safety metrics and how the operator should interpret them to improve safety in the system. The system is as shown below in figure 3.2.

Figure 3.2: 2 DOF system represented by case study

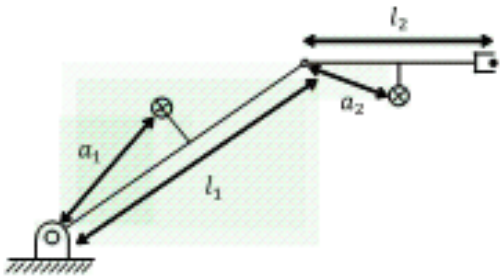

Table 3.13: Actuator parameters for system in case study

	Parameter	Axis 1	Axis 2
Link	Mass (kg)	20	10
	Inertia (kg-m^2)	9	4
	CG Location (m)	0.4	0.3
	Length (m)	0.8	0.5
Actuator	Mass (kg)	10	5
	Rotor Inertia (kg-m^2)	2.5e-3	2.5e-4

3.3.1 Model Description

In order to determine the total energy contained in both the links and actuators, it is necessary to define the effective inertia matrix as follows in Eq. 3.18.

$$I^* = {}^{A}I^* + {}^{L}I^* \tag{3.18}$$

Where ${}^{A}I^*$ is the effective inertia associated with the energy stored in the actuators and ${}^{L}I^*$ is the effective inertia associated with energy stored in the links. In this 2DOF manipulator, the effective inertia matrices are shown in Eq. 3.19 and 3.20.

$${}^{L}I_1^* = \begin{bmatrix} {}^{L}I_1 + {}^{L}m_1 a_1^2 & 0 \\ 0 & 0 \end{bmatrix} \tag{3.19}$$

$${}^{L}I_2^* = \begin{bmatrix} \left({}^{L}I_2^*\right)_{11} & \left({}^{L}I_2^*\right)_{12} \\ \left({}^{L}I_2^*\right)_{21} & \left({}^{L}I_2^*\right)_{22} \end{bmatrix} \tag{3.20}$$

Where a_1 and a_2 are the locations of the center of gravity of each link in the local frame and l_1 and l_2 are the link lengths. The Eqs. for the ${}^{L}I_2^*$ matrix are Eq. 3.21:

$$\begin{aligned}
\left({}^{L}I_2^*\right)_{11} &= {}^{L}I_2 + {}^{L}m_2(l_1^2 + a_2^2 + 2l_1a_2\cos(\varphi_2)) \\
\left({}^{L}I_2^*\right)_{12} = \left({}^{L}I_2^*\right)_{21} &= {}^{L}I_2 + {}^{L}m_2l_1a_2\cos(\varphi_2) + {}^{L}m_2a_2^2 \\
\left({}^{L}I_2^*\right)_{22} &= {}^{L}I_2 + {}^{L}m_2a_2^2
\end{aligned} \tag{3.21}$$

The effective inertia matrices for the actuators are Eqs. 3.22 and 3.23.

$${}^{A}I_1^* = \begin{bmatrix} {}^{A}I_1 & 0 \\ 0 & 0 \end{bmatrix} \tag{3.22}$$

$${}^{A}I_2^* = \begin{bmatrix} {}^{A}I_2 + {}^{A}m_2l_1^2 & {}^{A}I_2 \\ {}^{A}I_2 & {}^{A}I_2 \end{bmatrix} \tag{3.23}$$

The additional assumption is that the actuators are centered about the joint axes of motion. Also, in order to transform the inertias into the proper space, let

$${}^{A}I_1 = {}^{A}I_1^M G_1^2 \tag{3.24}$$

$${}^{A}I_2 = {}^{A}I_2^M G_2^2 \tag{3.25}$$

Where ${}^{A}I_k^M$ and G_k are the rotary inertia of the actuator and the gear train reduction ratio, respectively of actuator *k*. As the reduction ratio increases, this value will tend to dominate the inertia of the link. The manipulator's starting configuration is assumed to be $\varphi_1 = \frac{\pi}{4}$, and $\varphi_2 = \frac{\pi}{4}$ rad, and the initial speed of the manipulators is $\dot{\varphi}_1 = -1.4\,{}^{rad}/_{s}$ and $\dot{\varphi}_2 = -2.25\,{}^{rad}/_{s}$. Simulations were run assuming that the acceleration limits for motion planning of the manipulator were unchanged from normal operation, and also again with more aggressive acceleration limits to illustrate the performance gains possible by using more of the torque capacity of the manipulator.

For this simulation, a standard set of gear ratios of 50:1 for the first joint and 10:1 for the second joint were used. The nominal torques for the actuators at joints 1 and 2 were assumed to be 20 Nm and 10 Nm, respectively.

3.3.2 Joint Level Criteria

3.3.2.1 Torque Ratios

First, the stopping trajectory was simulated assuming that the maximum allowable torque is equal to the nominal torque allowed during normal operation of the manipulator. This uses the standard manipulator's operating accelerations, corresponding to the standard operation of the manipulator. A standard stop in this context refers to the situation of the operator simply telling the manipulator to decelerate to zero speed with no Cartesian interpolation restrictions. This path, shown in Figure 3.3, was generated using a trapezoidal motion plan, hence the square shape.

Figure 3.3: Joint accelerations during standard stopping scheme

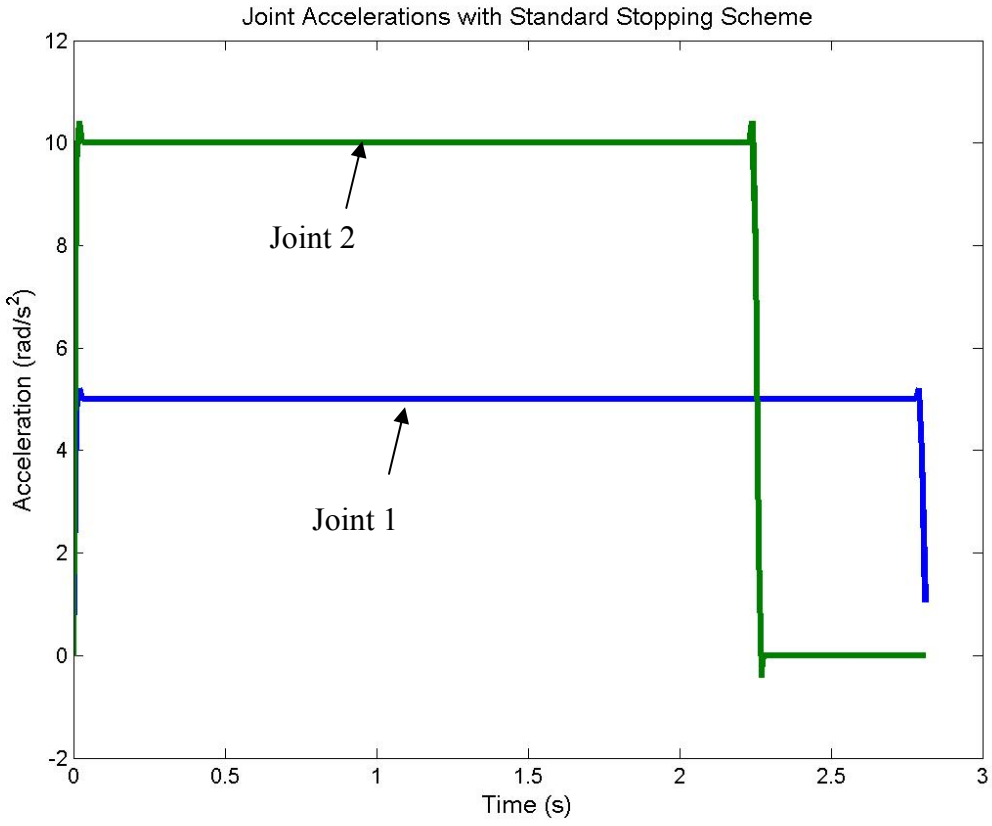

Figure 3.4: Plot of joint torque ratios for standard stop

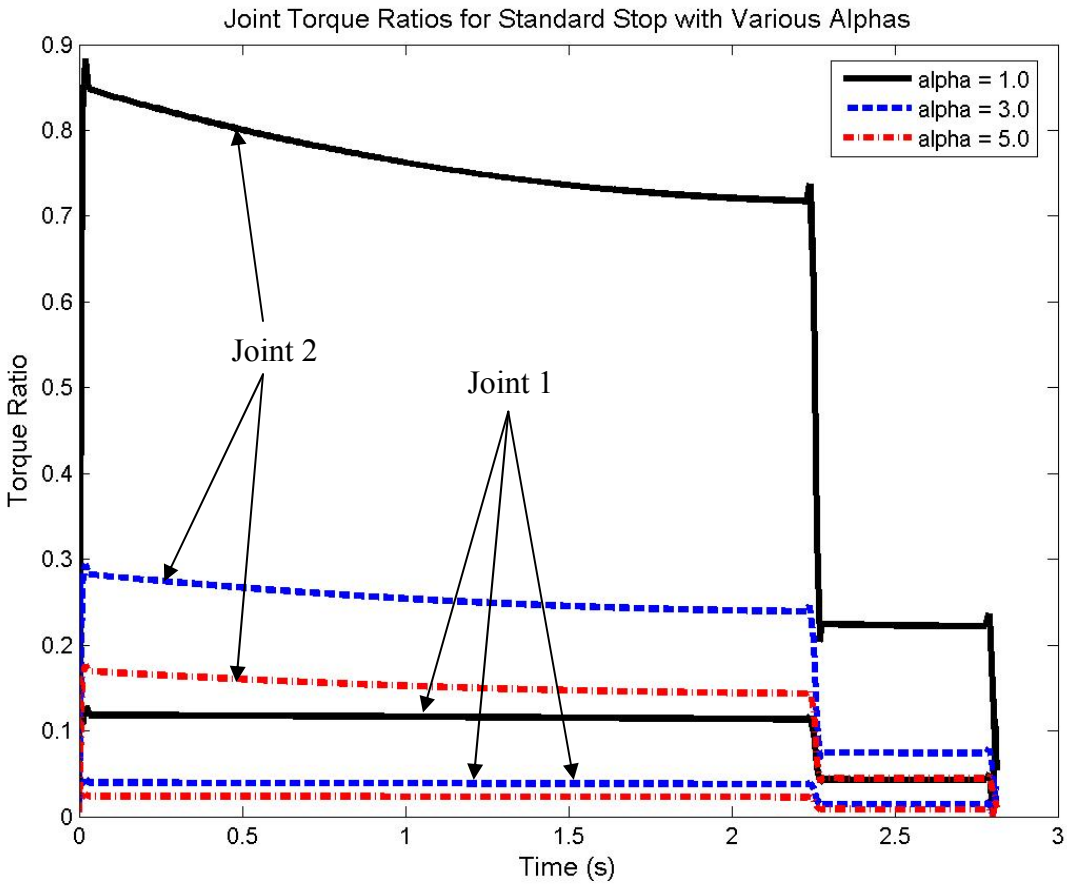

Table 3.14: Table of maximum torque ratio values for standard stop

Alpha	Joint	Maximum Torque Ratio Value
1.0	1	0.13
	2	0.8834
3.0	1	0.0433
	2	0.2945
5.0	1	0.026
	2	0.1767

This motion plan corresponds to optimizing with an alpha of 1 for the nominal torque limits criterion. In fig. 3.4, the torque ratios of each joint are calculated assuming the three standard values of alpha (1.0, 3.0, 5.0) and plotted over the length of the stopping trajectory. As can be seen from the graph, at no point in the trajectory does the criterion's value exceed 1 for either joint, indicating that each axis of the manipulator stays within acceptable torque limits at all times. As long as this continues to be the case, no torque errors should occur within any individual joint.

The other key point to note from this chart is that the criterion's values for each alpha value stays below 1, with the criteria values calculated with $\alpha = 3.0$ and $\alpha = 5.0$ significantly below one at all points in the trajectory. If it is possible to operate the joint actuators at a higher torque than the nominal value for a short period of time, this should indicate to the operator that there are significant gains to be made in the performance of the manipulator by increasing the acceptable torque limits of the control system that generates the torque input for the actuators. For a strictly kinematic control scheme, this would be accomplished by increasing the maximum acceleration limits of the joints, In any torque control scheme, this could be addressed by simply increasing the maximum allowable torque by a factor of three of five, respectively. The impact on this criterion by making such an adjustment is illustrated below in figure 3.5.

Figure 3.5: Joint accelerations for active stopping scheme

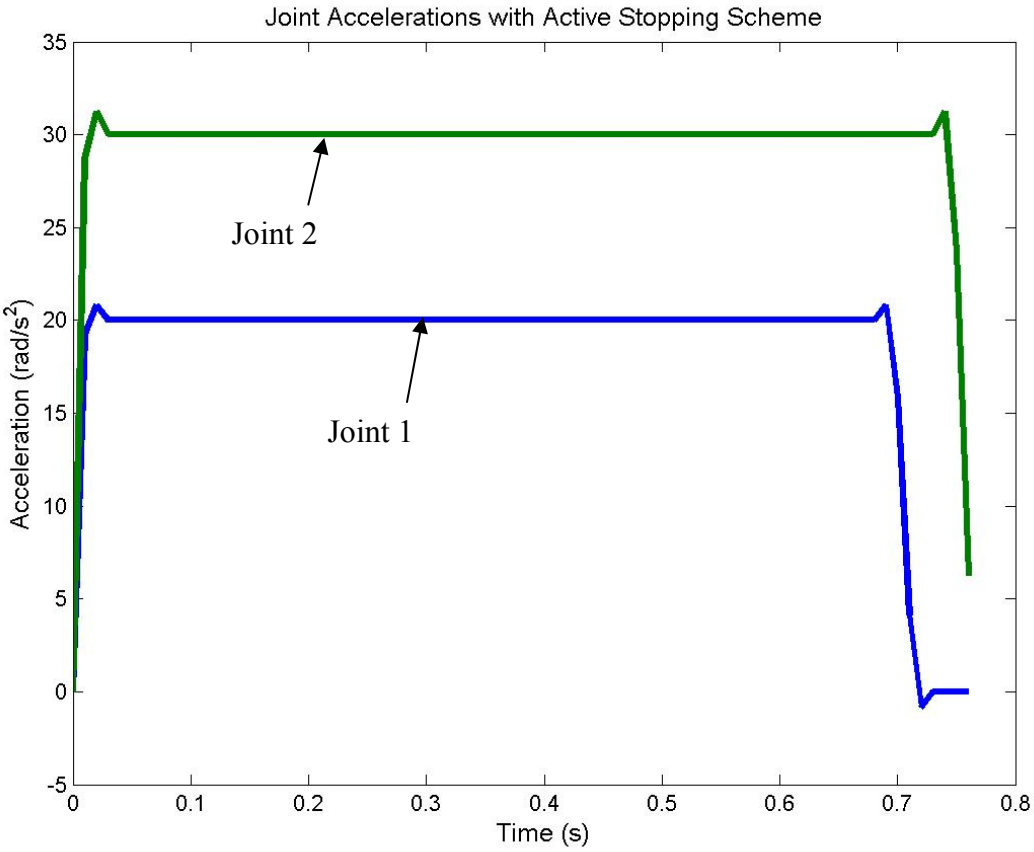

Figure 3.6: Torque ratios during active stopping scheme

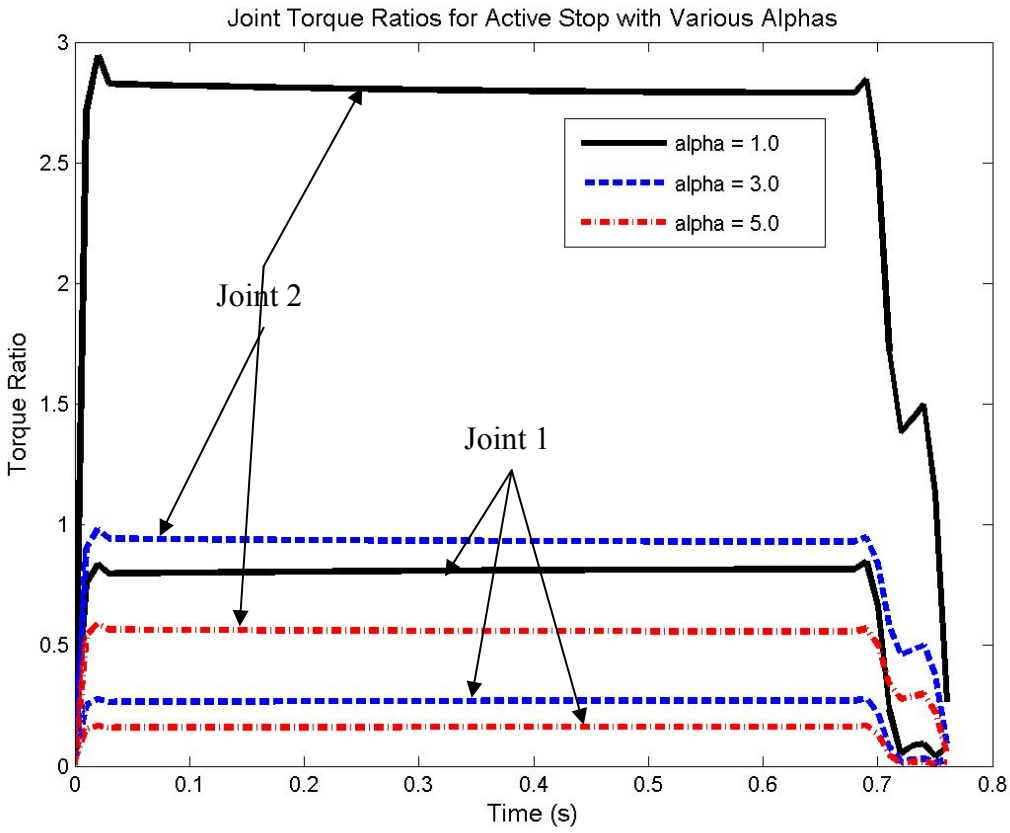

Table 3.15: Maximum torque ratios during active stopping scheme

Alpha	Joint	Maximum Torque Ratio Value
1.0	1	0.8458
	2	2.9441
3.0	1	0.2819
	2	0.9814
5.0	1	0.1692
	2	0.5888

For the purposes of this paper, an "Active Stop" is defined as a stopping trajectory which allows for torques up to three times the nominal actuator torque during the short time span of the stopping motion, corresponding to a stopping coefficient value of three. As stated earlier, this is generally acceptable due to the short duration and extremely low duty cycle of this load upon the individual actuators. In general, however, it is up to the discretion of the operator to decide on the acceptable limits for the system. It can be clearly seen, however, that this control scheme would put unacceptable loads on joint 2 of the manipulator if it was unacceptable to exceed the nominal torque value, with values of the criterion approaching three. Since any value greater than one indicates a potential failure, this would constitute an unacceptable situation for the operator.

Figure 3.7: Joint accelerations during aggressive stopping scheme

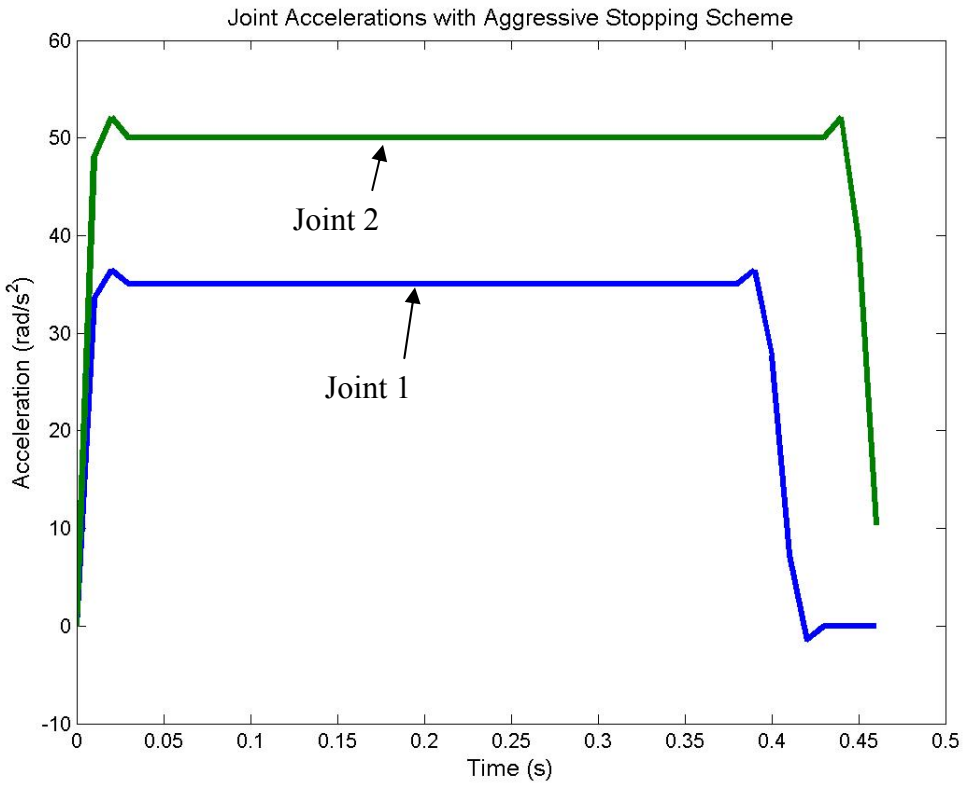

Figure 3.8: Maximum torque ratios during aggressive stopping scheme

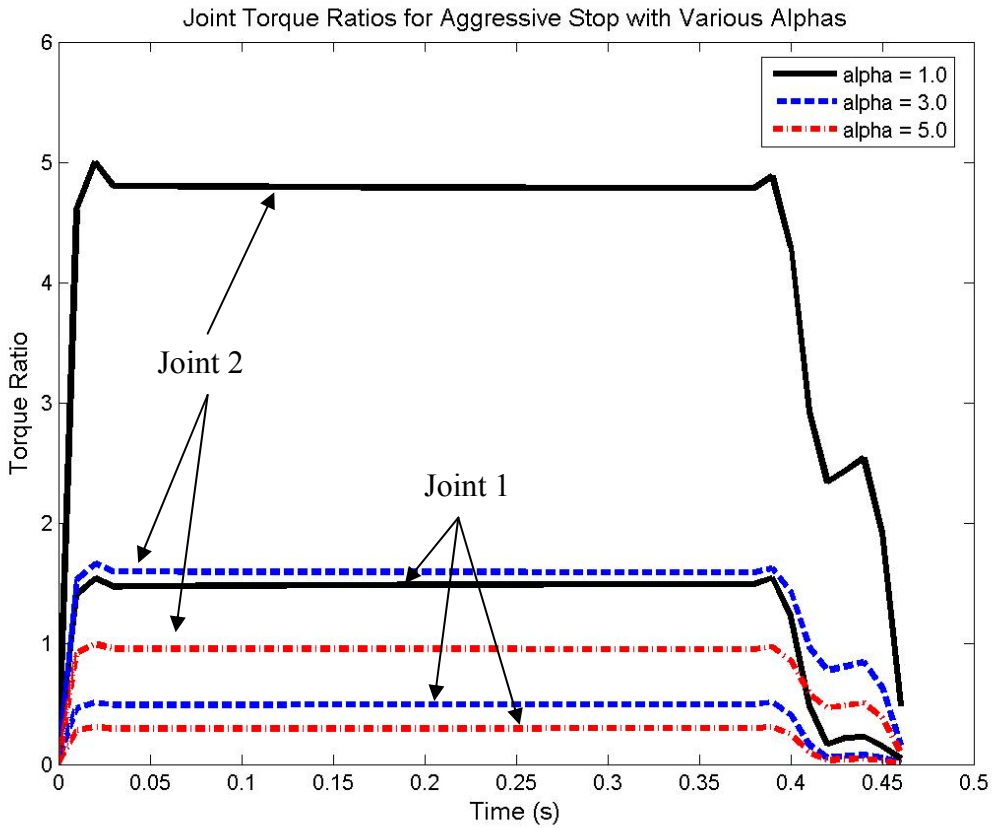

Table 3.16: Maximum torque ratios during aggressive stopping scheme

Alpha	Joint	Maximum Torque Ratio Value
1.0	1	1.5506
	2	5.0049
3.0	1	0.5169
	2	1.6683
5.0	1	0.3101
	2	1.0010

Here, an "aggressive" stop is defined by the acceptable stopping torque to be five times the nominal torque value used during standard operation of the manipulator. This should be considered to be the maximum acceptable torque under normal conditions, although if the designer deems it to be acceptable, higher values could be used at the corresponding higher risk of failure. Again, as with the torque ratio values for the control scheme with alpha equal to three, it can be seen that this criteria would generate unacceptable conditions if the actuators were unable to exceed the standard values of either the nominal torque, or three times the nominal torque.

3.3.2.2 Kinetic Energy

Figure 3.9: Kinetic energy during different stopping trajectories

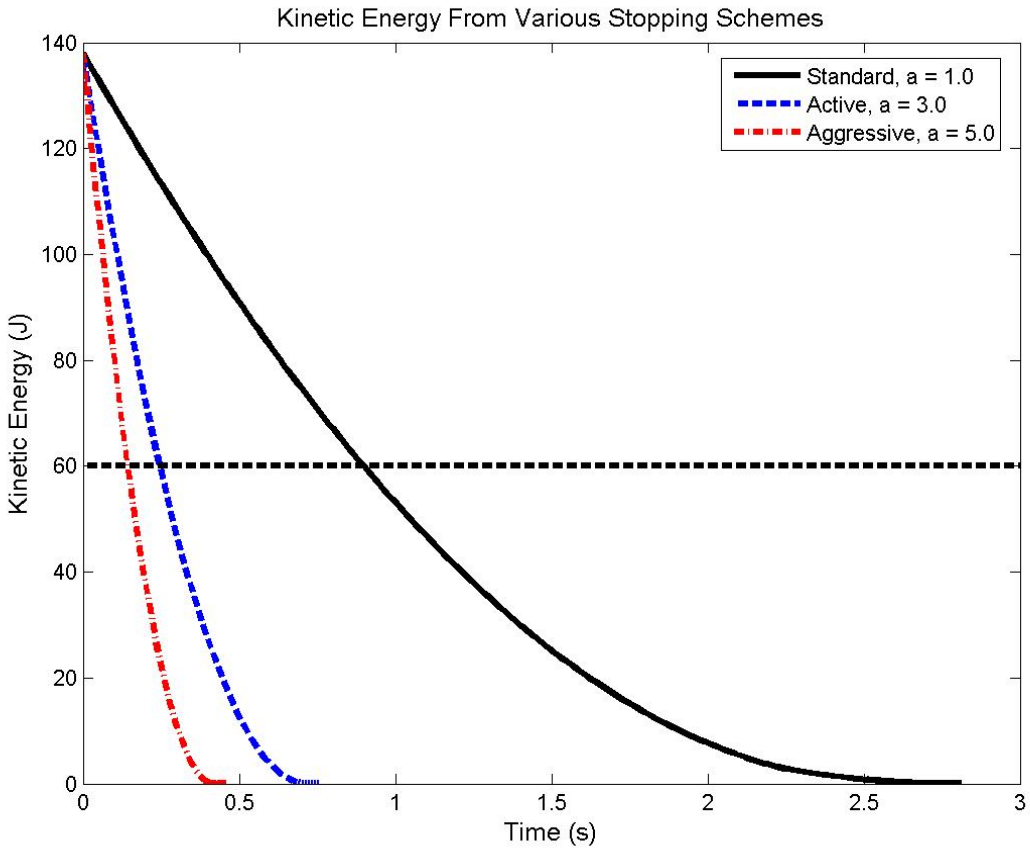

Table 3.17: Time to "safe" kinetic energy in system

Stopping Scheme	Time to 60 J KE in system (sec)
Standard ($\alpha = 1$)	0.91
Active ($\alpha = 3$)	0.26
Aggressive ($\alpha = 5$)	0.16

As can be seen in the Figure 3.9, the total energy in the system decreases much more rapidly in both the active and aggressive stopping schemes. In both of these cases, the total energy in the system falls below 60 J within .5 seconds of the stopping motion being initiated by the operator, a threshold which isn't reached by the standard stop until nearly twice as long into the trajectory. If the task requirements allow for a certain minimum amount of energy to be transferred to the environment without causing damage this provides a baseline time that the operator can be sure that the energy in the system will be below that minimum. Here, it can be seen that if a maximum of 60J can be absorbed in a collision without damaging the manipulator or environment, there will be a .5 second window in which potential danger can occur. Once this .5 sec passes, the operator can know with some degree of certainty that no damage can be done from a collision. As with the previous criterion, because this is starting from the maximum allowable kinetic energy state this represents the worst case scenario. In most normal operations of this manipulator, it is unlikely that the initial kinetic energy would be this great, so the length of time spent in a "dangerous" energy state would be reduced even further.

3.3.2.3 Energy Distribution

Figure 3.10: Kinetic energy partition values for different stopping trajectories

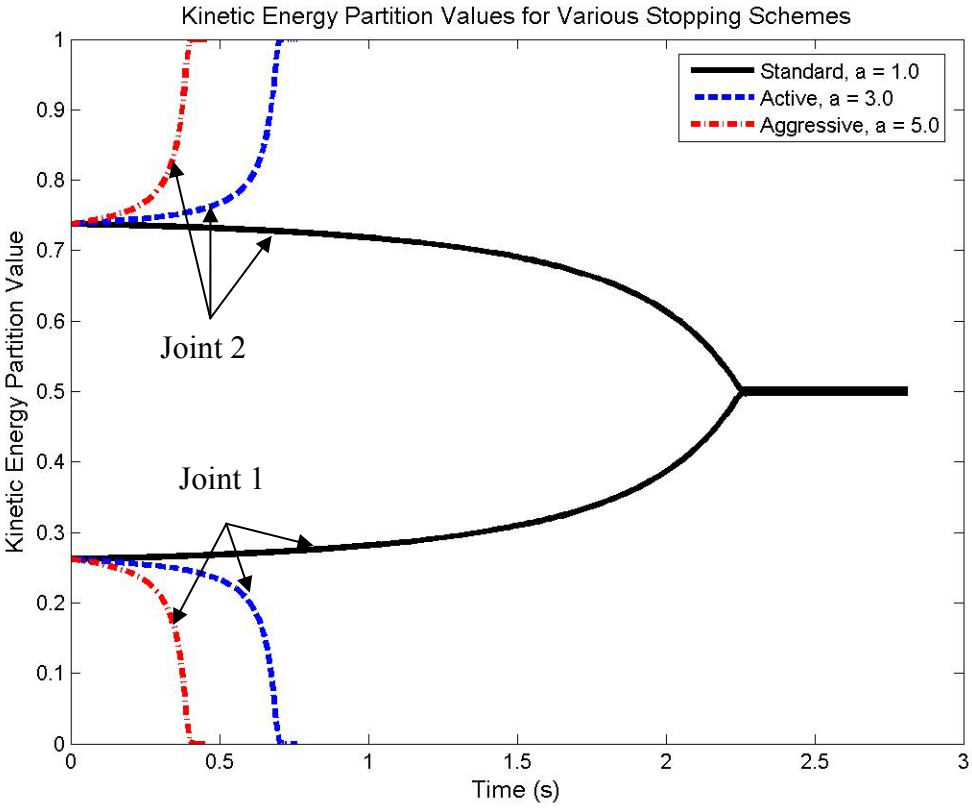

Once the total energy in the system is examined, it's important for the operator to determine how the energy is distributed throughout the system. Not only does the energy in the system represent a potential for damage to the environment in a collision, but because stopping control schemes naturally lead to condition where the actuators operating at extreme conditions. When the actuators are operating near their allowable limits, additional failures are possible, so once the total energy in the system approaches a point that would cause a failure in any individual actuator, it becomes necessary to monitor whether that energy is concentrated in sensitive actuators, particularly actuators

closer to the end-effector, which tend to be smaller and have less capacity to dissipate energy.

In this case study, it can be seen that there is a distinctly different shape between the partition values of the standard stop compared to the active and aggressive stops. This is not entirely unexpected, as operating at greater extremes can mean that joints will be able to cease motions at different periods in the trajectory, so that if joint 1 is able to decelerate to zero before joint two or vice versa, the partition values will be entirely different. While it may be alarming to the operator to see the partition values go to the extreme values of zero and one, this only occurs as the total energy in the system goes to zero, and so should be disregarded as an issue. For this manipulator and control scheme, however, it can be seen that at the highest energy levels (corresponding to the initial states of the manipulator), the energy is relatively evenly distributed with a little over a 70% of the energy in the manipulator being located in the second joint. This is within reason for a simple system, although ideally, the manipulator's energy would be more concentrated in the larger and more powerful first joint. If the total energy in the system were much larger due either to higher inertias in the links or actuators or greater initial velocities, this could be hazardous, as the weaker second joint is dissipating most of the energy in the system.

For this particular example, the problem could be alleviated in a couple different ways. First, the second actuator can be changed out for a larger model. This will actually make the numbers seem even more skewed since more powerful actuators weigh more, thereby increasing the inertia of the second joint relative to the first joint, resulting in more energy being concentrated in joint two assuming similar velocities.

Second, the gear ratio of the second joint can be lowered. This will affect the partition values in a couple ways. An actuator with a smaller reduction ratio tends to be heavier, so weight will be increased in the second joint, which will increase the joint's local inertia, but lower the inertia at the joint level due to the small gear ratio, and redistribute more energy to the stronger first joint which is presumably much farther away from its operating limits. The other benefit comes because the inertia of the motor is reflected through the gear train at a rate of the reduction ratio squared. Therefore, even though the actuator inertia tends to be fairly small at the point of the actuator, lowering the gear ratio can lead to significantly less inertia being focused into lower joints. In this case study, reducing the gear train reduction of the second joint from 10 to 1 could improve the energy distribution throughout the system by vastly reducing this squared multiplier. However, this is a tradeoff, as the higher torques and higher prime mover mass seen at the joint will allow for lesser performance from the actuator in terms of being able to decelerate the joint more quickly. Finally, the configuration of the manipulator can be altered by the designer by adjusting the link lengths or axis offsets and/or orientations. This is a little more difficult since this must occur at the design phase rather than be done by the operator and any adjustments to the system configuration will affect the entirety of the criteria so that the total effects of the configuration change might not be the result that the designer is attempting to achieve.

3.3.2.4 Weighted Kinetic Energy Distribution

Figure 3.11: Weighted kinetic energy partition values for different stopping schemes

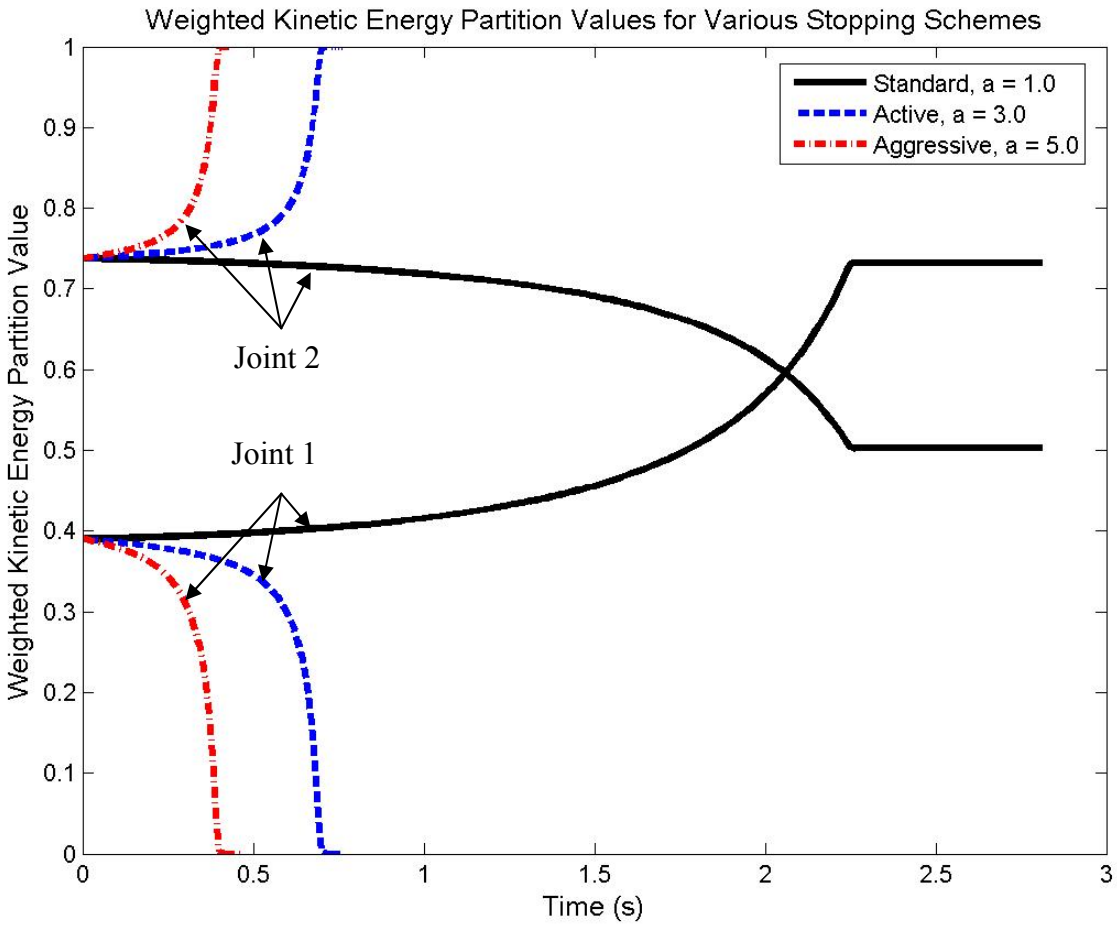

Weighting the values of the kinetic energy partition values allows the operator to gain a little more insight into the energy distribution of the system. As can be seen here and was described in the initial introduction of the criteria, the sum of the individual values for the joints for this criterion do not have to add up to one. Also, this represents merely the percentage of the maximum partition value that is represented in the current energy state at any specific time. Even though the value for joint 1 is higher in the

standard stop near the end of the trajectory, the fact that the maximum percentage of energy that can be stored in the first joint is roughly 70% of the maximum that can be stored in the second joint, this does not represent a situation that should concern the operator. In general, data from the KEPV criteria should be cross-examined with it, and the total energy present in the system. While it is desirous in general to keep energy distributions balanced towards the more powerful actuators in the system, it is often the case, as shown here, that either the total energy in the system will make the energy distribution concerns fairly negligent, or the weighting of the partition values will cause potential false alarms in terms of joints approaching their partition value limits.

3.3.3 System Level Criteria

Having examined the actuator level criteria values to determine the maximum acceptable performance, it is useful to investigate the potential performance gains from using the different allowable values of alpha as a failure point. Often, there is no simple rule to say that one value of alpha should be used over another, but instead, it is up to the designer and operator to evaluate the options and tradeoffs and decide upon an acceptable value to represent safe operation during stopping while maximizing performance.

3.3.3.1 Total Distance Traveled

Figure 3.12: EEF distance traveled over different stopping trajectories

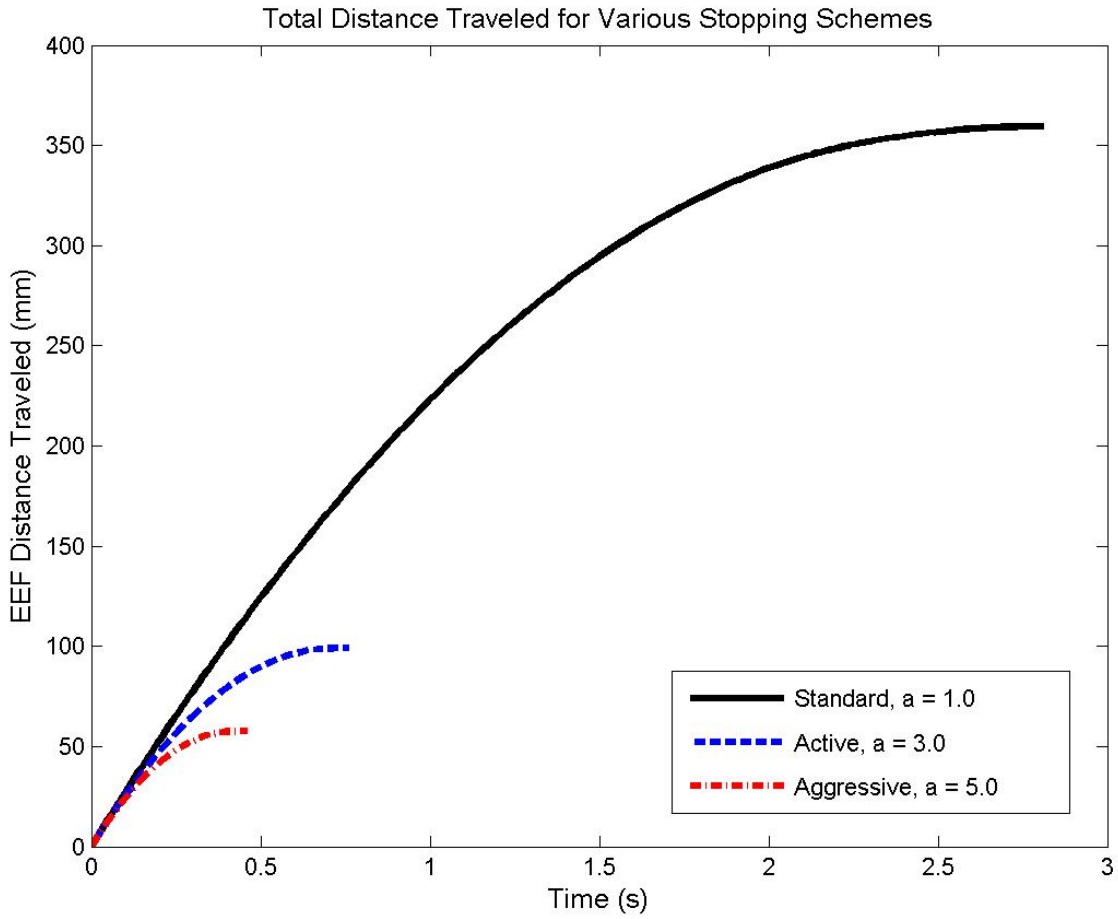

Table 3.18 Total distance traveled over different stopping trajectories:

Stopping Control Scheme	Total Distance Traveled (mm)
Standard (α = 1)	359.5
Active (α = 3)	99.1
Aggressive (α = 5)	57.6

The first criterion for assessing the safety of a stopping trajectory is the distance traveled by the end-effector. Shown in the above figure is a plot of the distance traveled over time. As can be seen, there are large gains to be made by increasing the acceptable torque during a stopping procedure. This gain can be seen to be roughly proportional to the alpha value, with the distance traveled for alpha equal to three being roughly one fourth of the distance traveled with the nominal value for alpha, as shown in the table. Similarly, the distance traveled for alpha equal to five is roughly one sixth of the distance traveled with the nominal value. This will vary depending on the initial state and configuration of the manipulator, but it provides a simple example of the potential benefits to be gained from using greater acceptable torque values.

By using this simple "worst-case" scenario of an initial state with all joints moving at maximum velocity in the same direction, it is possible to generate a type of upper limit on the distance traveled during a stopping motion. Therefore, it can be assumed that for this manipulator these values can provide a reasonable estimate of the maximum distance that the end-effector will travel once a stopping command is received by the actuators. With this upper limit, the operator can determine whether the safety requirements are being met by the manipulator or if a more aggressive stopping control scheme needs to be implemented. In this example, if the manipulator's task requirements called for the maximum stopping distance to be less than 70 mm, the manipulator could be considered unsuitable for the task, and so a different manipulator would have to be chosen or the designer would have to evaluate a different manipulator configuration or adjust the actuators or gear ratios of the joints in order to satisfy the task requirements.

3.3.3.2 Directional Distance Traveled

Figure 3.13: Directional distance traveled over different stopping trajectories

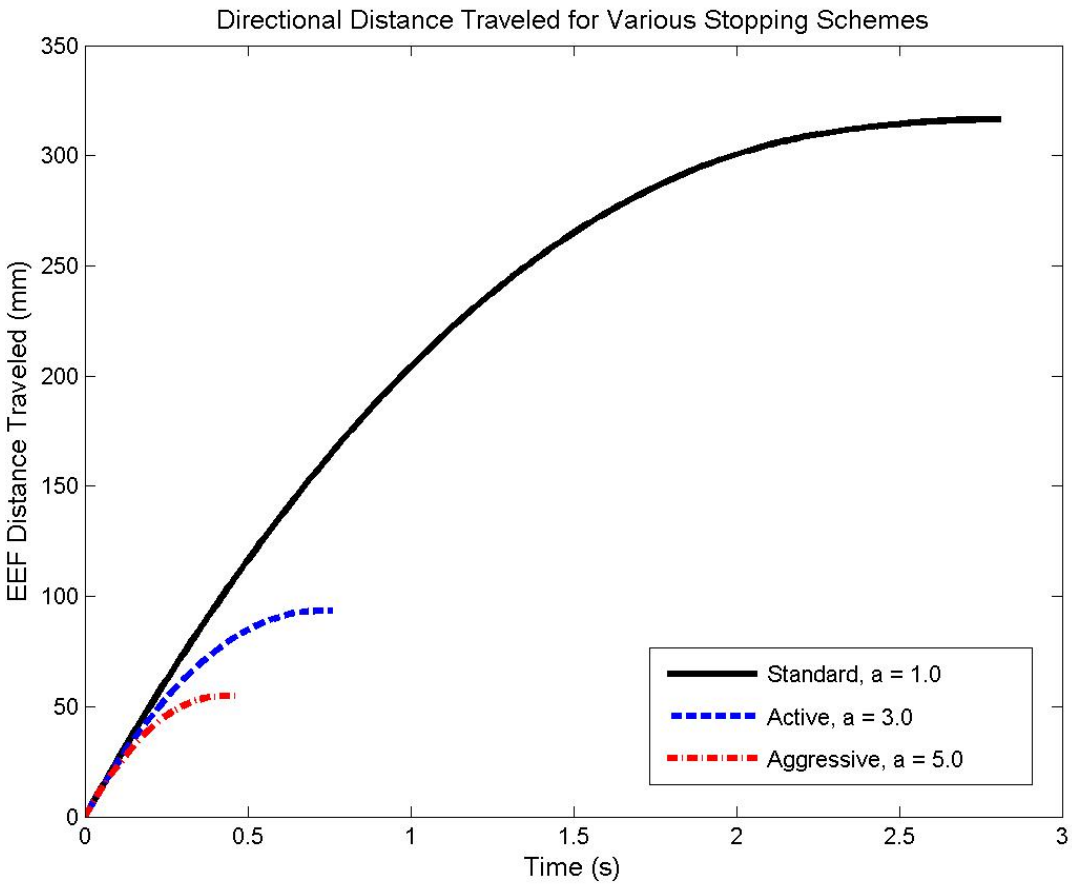

Table 3.19: Distance traveled in *u*-direction over different stopping trajectories

Stopping Control Scheme	Distance Traveled in *u*-direction (mm)
Standard (α = 1)	316.4
Active (α = 3)	93.5
Aggressive (α = 5)	54.9

Usually for safety applications, however, it is less important that the end-effector not move at all, and more important that the end-effector not move in a specific direction, either toward a location where humans are, or else towards the object that the manipulator is currently being used to work on. In this example, the direction designated as the "dangerous" direction, as designated by the vector,

$$\hat{u} = \begin{bmatrix} 1 \\ 0 \\ 0 \end{bmatrix}$$

In the equation for the criteria. This is again, completely arbitrary and chosen simply because it represents a direction the manipulator is moving in during the stopping trajectory. If the direction were chosen in the negative x or positive y directions, this criterion would be trivial in this case because no motion occurs in that direction. However, if the joint velocities were simply reversed, this triviality would reverse itself. Also of note is that the vector chosen is a unit vector. This is recommended to provide for a reasonable comparison between the two previous criteria.

3.3.3.3 Distance From Given Trajectory

Figure 3.14: Distance traveled from initial trajectory over different stopping trajectories

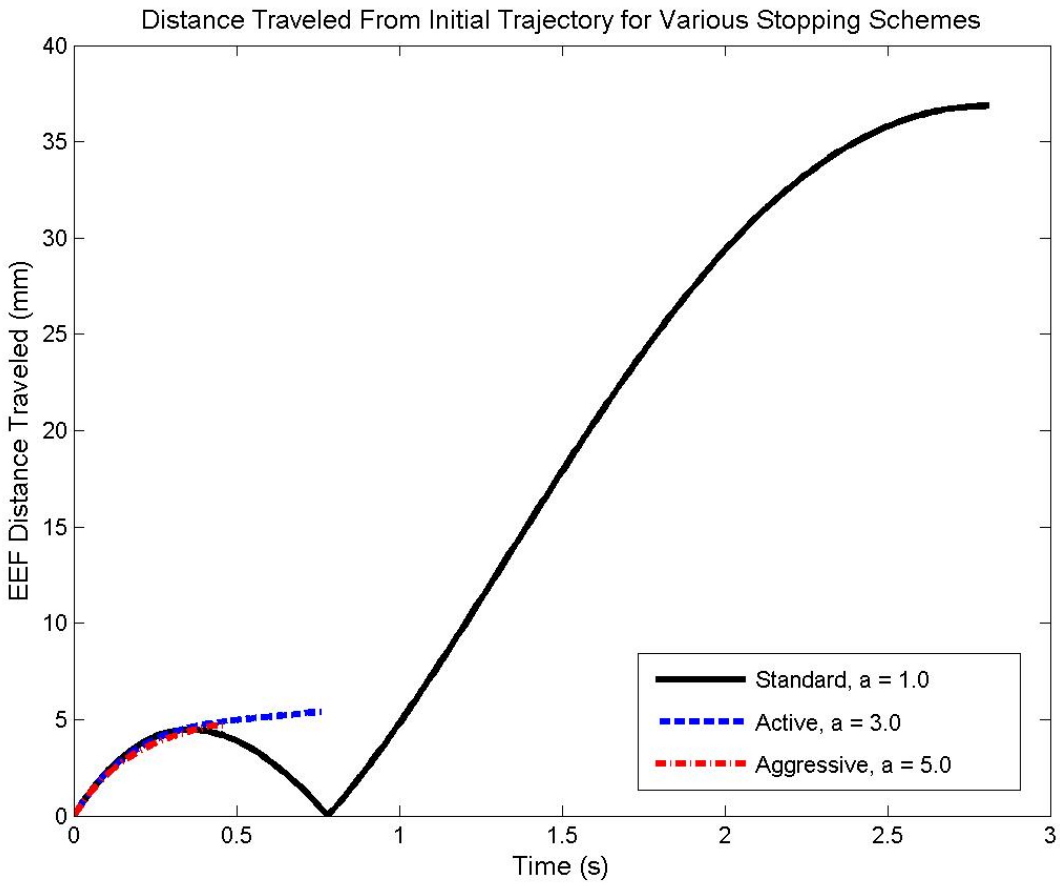

Table 3.20: Distance traveled from initial trajectory over different stopping schemes

Stopping Control Scheme	Distance Traveled off initial trajectory (mm)
Standard (α = 1)	36.8
Active (α = 3)	5.4
Aggressive (α = 5)	4.7

This criterion, perhaps more than any other is most dependent on the initial state of the manipulator so while examining extreme cases for the joint velocities can be useful in the sense of giving an estimate of the criterion's maximum value for the manipulator's configuration, the operator and designer should be careful to note that this will vary wildly depending not only on the configuration of the manipulator, but also the path chosen.

Still, in this configuration, it can be seen that there is a significant departure from the initial trajectory. Depending on the application, this may be considered a potential safety issue. While a 36.8 mm departure from the trajectory may be acceptable for a welding application in which the only potential issues are damage to the part(s) being welded. However, if the robot were being used in a rehab application, this departure from the desired trajectory could be sufficient to either cause discomfort to the individual in the sense of wrenching the body part being exercised out of its comfort zone, or else cause harm by actually impacting the subject. If it is the latter, care should be taken to monitor the potential for clamping and velocity of the manipulator. As described previously, these have been shown to be the greatest indicators of potential injury in the case of impact. For reference, a plot of the actual trajectories followed by the EEF during the stopping motion is provided below in Figure 3.15.

Figure 3.15: X-Y path of manipulator during stopping trajectories

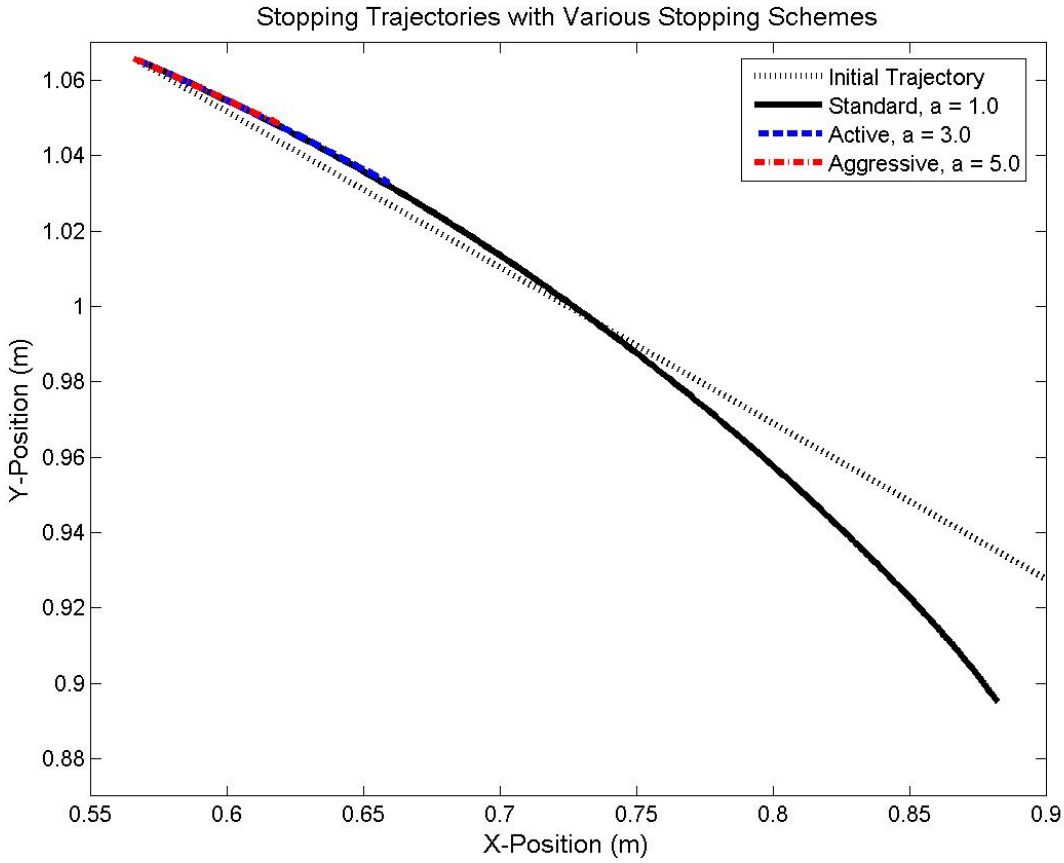

3.3.3.4 End-Effector Velocity

Figure 3.16: End-effector velocity over different stopping trajectories

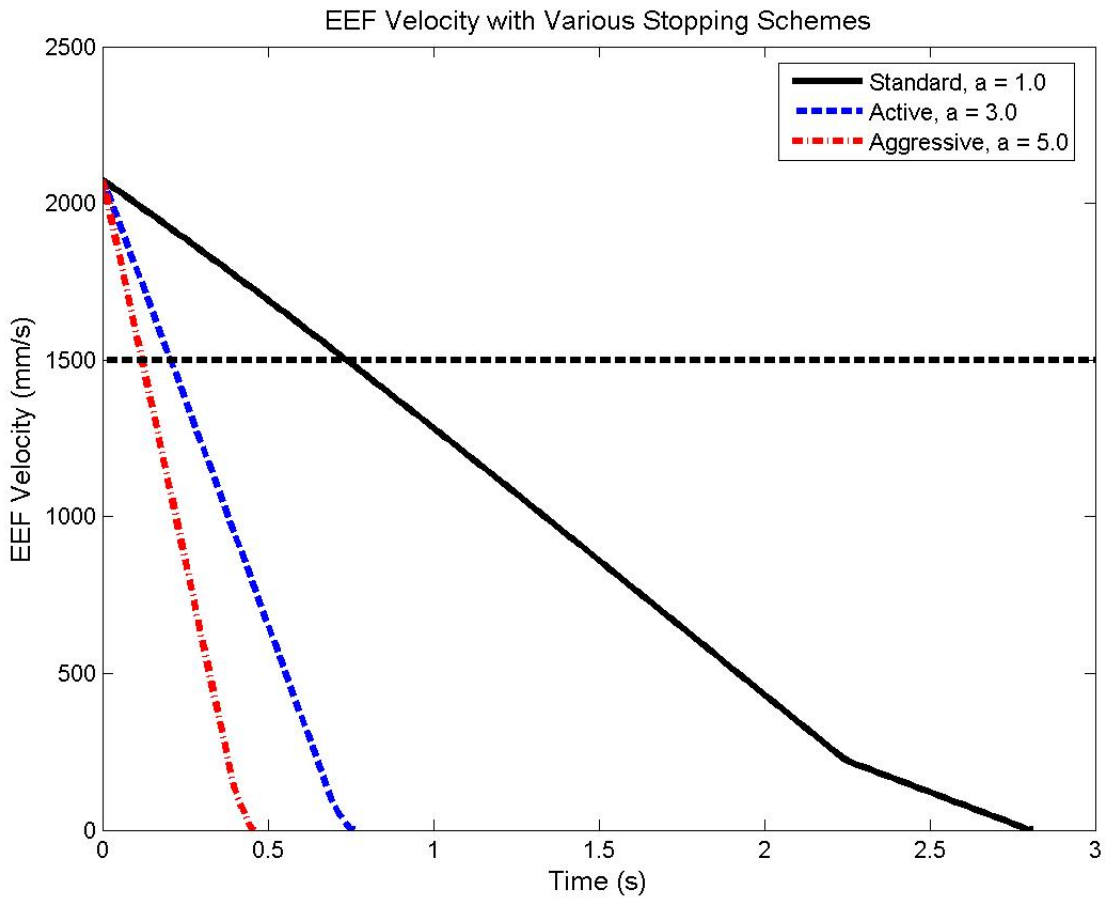

Table 3.21: Time to "safe" velocity for different stopping trajectories

Stopping Control Scheme	Time to reach 1.5 m/s (sec)
Standard (α = 1)	0.75
Active (α = 3)	0.22
Aggressive (α = 5)	0.13

After examining the distance traveled during the stopping trajectory, another important criterion to examine to measure the overall safety is the end-effector velocity of the manipulator. As described in the previous section, this is important because previous work has shown that the velocity at point of impact is the greatest determinant of injury severity during impact with a human in a collision. In this sense, it is useful for the operator to determine beforehand a cutoff "safe" velocity, below which a collision would cause either negligible or else non-catastrophic harm, depending on the application and the safety requirements. For this application, the arbitrary value of 1.5 m/s is chosen.

In order to measure the safety, the time to reach this speed is calculated for each of the stopping schemes. Again, large gains can be seen from utilizing the capabilities of the actuators beyond the nominal torque with a 70% reduction in the time to a safe velocity occurring when a "active" stopping scheme is used and over an 80% reduction from the aggressive stopping scheme. Since the initial joint velocities being used here are a maximum and both in the same direction the end-effector velocity contributions from each joint will be additive, and so performance in normal applications should be considered to be better than that measured here.

The other point of interest in Figure 3.16 can be seen with the slight job in the velocity curve near the end of the trajectory. This discontinuity is a result of the first joint completing its motion, with the final section of the trajectory representing the motion of the second joint alone. This discontinuity represents a pitfall of using differential analysis on these criteria, so it is largely avoided.

3.3.3.5 Directional End-Effector Velocity

Figure 3.17: Directional end-effector velocity over different stopping trajectories

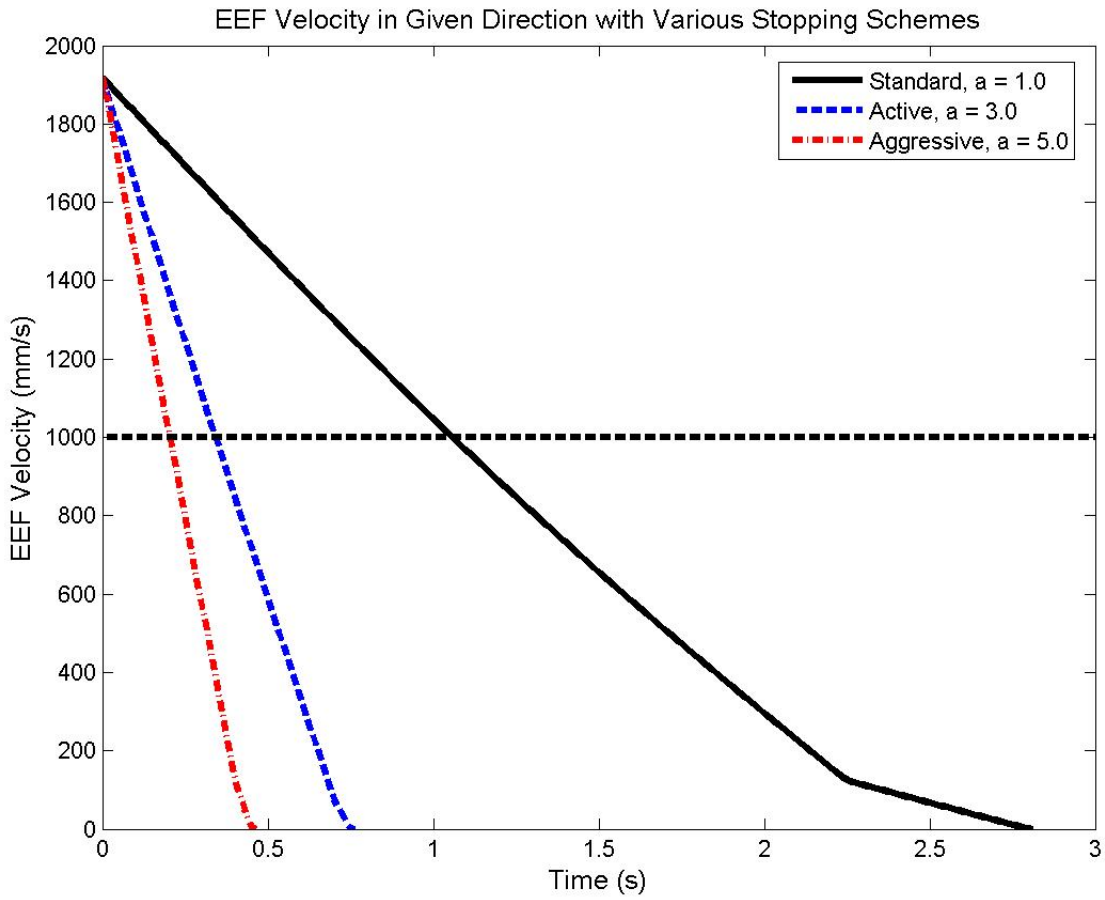

Table 3.22: Time to reach 1 m/s in *u*-direction for different stopping trajectories

Stopping Control Scheme	Time to reach 1 m/s in *u*-direction(sec)
Standard (α = 1)	1.07
Active (α = 3)	0.36
Aggressive (α = 5)	0.22

In order to gain more insight into the safety situation using the velocity information, the directional information can be used as well. By adding the directional information, depending upon the nature of the potential safety hazard, the operator can maintain stricter velocity limits to assert that the manipulator is in a "safe" state. In particular, if the potential hazard comes from the potential to impact a human, this can be important since the most potential for an injury from a collision between a manipulator and a human stems from motion in the normal direction to the subject. However, depending on the tooling located at the end effector, there may be as much potential damage regardless of whether the robot is moving normal to the subject, or transverse along the subject. For example, a tool designed to cut would either result in a deeper puncture wound, or a longer, but shallower slicing wound, depending on the motion of the manipulator at contact with the human subject.

3.4 CONCLUSIONS

In this chapter, two sets of criteria were presented. First, a set of system level criteria to measure the safety of a manipulator's stopping motion was presented to provide a framework to assess how safely a manipulator is able to halt itself. Next, a set of joint level criteria to assess the degree to which the prime movers are performing to their limits was established to allow the operator to assess whether any joint is near an unexpected failure.

Finally, a 2DOF case study was presented in order to demonstrate the use of the criteria and explain the physical meanings and real life analogues.

CHAPTER 4

Effect of Actuator Parameters on Stopping Criteria

For the manipulator designer, it is often desirable to be able to estimate the effects that the actuator parameters will have upon the stopping performance of the manipulator. Therefore, some knowledge of the relationship between parameters such as the nominal torque values and the gear reduction ratios and the ability of the manipulator to safely stop can be of great use to the designer. This provides for simpler calculations rather than requiring the designer to run complete simulations of the system's dynamics in order to determine whether the manipulator meets task specifications. Thus, the designer is able to start with a simple set of task requirements, and from these, choose appropriate actuators and gear reductions to satisfy them. For the most part, however, these remain as mathematical estimates, with the actual values largely dependent on the exact control scheme used to generate the joint trajectories. Particularly as control strategies are implemented in order to optimize trajectories according to the safety criteria presented, these estimates may prove to be worse than the actual performance achieved by the system. However, this will be counterbalanced by the fact that stopping constraints will not allow the manipulator to perform at peak end-effector decelerations over the course of the trajectory. As seen in the previous section with the discontinuous end-effector velocity curve, as each joint decelerates to zero, it is no longer able to effect the deceleration of the end-effector, resulting in the manipulator not being able to sustain the maximum end-effector acceleration over the course of the trajectory.

These estimates can also be of use to the operator when task requirements change and it must be determined whether the manipulator can meet these new requirements. As robotic systems become more and more modular this kind of reusability will become of

greater importance, making it important for quick estimates to be determined of manipulator capabilities. While any manipulator in a structured, industrial environment should still undergo full testing and re-certification when the task requirements change, manipulators deployed in field uses with lesser certification requirements may be able to use a simpler method of estimation in order to save the operator time and effort

4.1 END-EFFECTOR SAFETY CRITERIA

As described in the previous chapter, there are five criteria that are directly related to the position and velocity of the end-effector during the stopping trajectory. These criteria are Total Distance, Directed Distance, End-Effector Velocity, Directed End-Effector Velocity and Distance from Trajectory. All of these are dependent mainly upon the manipulator's capacity to decelerate the end-effector. Therefore, in order to estimate a manipulator's performance in these criteria, its capacity to decelerate must be known given the actuator parameters.

4.1.1 Acceleration Estimation

In order to estimate the end-effector acceleration capacities given the actuator parameters, work done by Rios is implemented. The full derivation of the equations can be found in his work, but the final equation derived relating actuator parameters to the acceleration capacity of the end-effector is as follows in Eq. 4.1 and 4.2.

$$a_i^{eff} = \frac{\tau_i^M L_i}{\bar{g}_i \sum_{j=1}^{N} \left\{ {}^{a}I_{ij}^{*} + {}^{l}I_{ij}^{*} \right\}} \tag{4.1}$$

$$a_i^{manip} = \sum_{i=1}^{N} a_i^{eff} \tag{4.2}$$

Where, a_i^{eff} is the effective contribution to the acceleration capacity of each actuator and a_i^{manip} is the actual acceleration capacity of the actuator in end-effector

space. Because the stopping controls are only being applied for limited times, however, this allows for an additional modification of Eq. 4.1 as seen in Eq. 4.3.

$$a_i^{eff} = \frac{\alpha_i \tau_i^M L_i}{\bar{g}_i \sum_{j=1}^{N} \left\{ {}^{a}I_{ij}^{*} + {}^{l}I_{ij}^{*} \right\}} \tag{4.3}$$

The α coefficient in Eq. 4.3 accounts for the additional torque capacity usable due to the low duty cycle and duration of stopping control. This accounts for the designer's intent that the manipulator may use more than the nominal torque during a stopping motion, and should be chosen appropriately to avoid damage to the actuators during this motion. This coefficient should always be greater than or equal to one, but typically ranges between three and five, although the actual choice is up to the discretion of the manipulator designer.

The actuator parameters easily controlled by the designer that the end-effector acceleration is dependent on are the motor torque, τ^M, and the gear reduction ratio, $\bar{g}$. The designer also has a limited ability to control the actuator inertia without altering the manipulator configuration because of the differences in actuator and gear train weights. Typically, more powerful actuators and larger gear trains will have greater masses, resulting in higher inertias, although there can be a tradeoff with cost as well. More expensive actuators will generally have much better power/weight ratios, so the designer can weigh this as a design factor as well.

However, an additional factor that must be considered when choosing actuators and gear reduction ratios is the fixed torque requirements. All manipulators will require a minimum amount of torque to support the weight of the links and payload, so factoring in the need to generate torque above this minimum threshold, the designer may consider the product of the gear ratio and the prime mover torque to be relatively constant. Therefore,

special attention should be paid by the operator the gear ratio's effect on the system inertia. The prime mover inertia is amplified into joint space by the square of the reduction ratio, so this will have a great effect in general upon the system responsiveness since the acceleration capacity is inversely related to the inertia of the system. In general, the designer should pay special attention to the inertia in designing the system in order to assure that the acceleration response will be adequate for safety measures.

4.1.2 Estimating Velocity Criteria

Knowing the acceleration capacity of the manipulator is only the first part of the criteria analysis, however. Once the designer is able to estimate the maximum deceleration capacity of the manipulator, some simple calculations are required to convert this acceleration into useful safety criteria estimations.

First, some assumptions are required. Because it is desired to look at worst-case performance, the manipulator's initial end-effector speed will be assumed to be some manipulator dependent maximum operating speed. This is intended to closely simulate operating conditions in application environments, where the maximum end-effector speed is often specified.

The second assumption will be a constant acceleration at the maximum capacity. This will obviously be a somewhat more ideal situation than will actually occur, since this requires an immediate impulse in the acceleration that is unable to be achieved in actual operating conditions. More likely, either a control scheme such as the trapezoidal or polynomial motion plans will be implied, meaning that the actuators will take slightly longer to reach the maximum acceleration. Still, these effects should be fairly small, and the estimate will still be valid.

The final assumption is that each of the joints is able to use its acceleration capacity to decelerate the end-effector, resulting in the maximum acceleration. As shown in Eq. 4.2, the acceleration capacity is a sum of the effective accelerations of each of the actuators, if any actuator is not actively working to decelerate the end-effector, the possible acceleration will be less. This situation may occur if one or more of the actuators start at rest or at a very low speed, as most control schemes will disregard an actuator from control once it is at rest.

Using these assumptions, it is easily shown with a simple integration that the end-effector velocity at any point during the stopping motion can be simply estimated as in Eq. 4.4.

$$\|\dot{x}\| = \|\dot{x}_i\| - a_i^{manip} t \tag{4.4}$$

a_i^{manip} is defined as in equation 4.2. This can be further expanded upon if the designer wishes to estimate the time to reach a "safe" end-effector velocity by substituting for this velocity and solving for the time as in Eq. 4.5.

$$t_{safe} = \frac{\dot{x}_i - \dot{x}_{safe}}{a_i^{manip}} \tag{4.5}$$

Because it is so dependent on the actual state of the manipulator, there is no reliable way to estimate the directional velocity criterion, short of running actual simulations. Insight into estimating the criterion's potential values can be gained by examining the previous analysis. These estimates can be seen as fairly definitive worst-case estimates for directional velocity criterion values, because the direction is unaccounted for, so all motion is inherently assumed to be in the direction in which motion is trying to be prevented. In the real world, this is never the case, as the manipulator will most likely only rarely be moving in the exact direction, and as seen

with the 2 DOF case study, the process of stopping the manipulator often leads to direction changes, and the end-effector not following a set linear trajectory, making it highly unlikely that the directional velocity value could ever even be equivalent to this estimate. Therefore, the same estimate should be used for the directional velocity criteria, with the designer and/or operator assuming that the actual performance will be much better than this estimate, regardless of the actual direction in which motion is to be prevented.

4.1.3 Estimating Position Criteria

Similar to the velocity estimation, knowing the velocity and acceleration of the end-effector allows the operator to get a viable estimate for the distance traveled by the end-effector during the stopping trajectory. Again, with a simple integration from equation 4.4, equation 4.5 shows the position of the manipulator.

$$x = x_i + \dot{x}_i t - a_i^{manip} t^2 \tag{4.5}$$

Since the actual, Cartesian position is largely irrelevant in safety terms, the differential can be calculated simply as in equation 4.6.

$$d = \|\dot{x}_i\| t - a_i^{manip} t^2 \tag{4.6}$$

Using Eq. 4.4, the designer is able to obtain an estimate of the time it takes the end-effector to reach either a zero velocity or the designated "safe" velocity. Substituting for this time gives Eq. 4.7.

$$d_{safe} = \|\dot{x}_i\| \left(\frac{\|\dot{x}_i\| - \|\dot{x}_{safe}\|}{a_i^{manip}} \right) - \frac{\left(\|\dot{x}_i\| - \|\dot{x}_{safe}\|\right)^2}{a_i^{manip}} \tag{4.7}$$

In Eq. 4.7, if the designer wishes to estimate the total distance traveled during the stopping motion, a value of zero should be used for the safe velocity. Otherwise, the designer can determine how far the end-effector travels until it reaches a "safe" velocity,

designating two separate concentric spheres of differing "danger". Within the smaller sphere, the end-effector is traveling at an unsafe speed during the stopping motion. Within the larger sphere, the end-effector is still moving, but at a velocity that would be considered nonlethal should a collision occur.

As with the velocity criteria estimation, the directional criteria are largely neglected here because of its high dependence on the actual state of the manipulator. Similarly, though, the estimate of the distance traveled without directional information can be used as a worst case scenario for the directional distance if the designer or operator wishes to obtain a rough estimate.

Finally, the trajectory distance criteria is so coupled with the initial state of the manipulator at the time the stopping command is received that it is impractical to estimate it at all. Depending on the manipulator state and stopping control scheme used, the end-effector may follow the given trajectory extremely closely, or may veer wildly. This makes it impractical to estimate without a full simulation. If the designer wishes to take this criteria into account during the design process, a more thorough simulation should be run, allowing directional estimates to be obtained since the trajectory estimates are largely useless without any directional estimates of the stopping motion.

Now that each of the end-effector state criteria can be estimated as a function of the motor torque and the gear reduction ratio, the designer is able to take the task requirements and use them to determine a valid actuator and gearing combination to satisfy the requirements.

4.2 JOINT-LEVEL CRITERIA

Also of importance to the designer and operator is how the actuator parameters relate to the internal energy distributions and torque capacity of the manipulators.

Evaluating these estimates are a little more opaque to the designer and a little less controllable since most control schemes will result in the actuators performing at near their maximum capacity. While this may limit the insight gained from examining this relationship, it can still be useful to the designer in order to determine the full state of the actuator.

Table 4.1: Effective actuator output properties for high gear train reduction ratio (i.e. $\bar{g} \ll 1$) [Benedict and Tesar, 1978]

Input Parameter	Relation	Effective Output Property
Inertia I^M	$I^* = \frac{I^M}{\bar{g}^2}$	• Increased inertial content of actuator with potential for high impact loads. • Leads to a slower and less responsive system.
Speed ω^M	$\omega^* = \bar{g}\omega^M$	• Decreased speed capacity of actuator. • Leads to a slower system.
Torque τ^M	$\tau^* = \frac{\tau^M}{\bar{g}}$	• Increased torque capacity of actuator. • Leads to a system with higher load capacity and responsiveness.
Stiffness K^M	$K^* = \frac{K^M}{\bar{g}^2}$	• Increased stiffness of actuator. • Leads to more accurate system that can handle a higher load capacity
Damping ζ^M	$\zeta^* = \frac{\zeta^M}{\bar{g}^2}$	• Increased damping of actuator. • Leads to a non-linear system behavior with lower resolution, speed and responsiveness.

Table 4.1 contains some examples of how an actuator's properties are mapped into joint space from motor space through the gear train. Of importance to the designer for joint level safety criteria is the mapping of the motor torques and inertias relative to the gear ratios.

4.2.1 Torque Ratios

For the operator, a manipulator operating at the peak responsiveness capacities determined in Section 4.1 means that one or more joints are operating at near the torque operating limits. This is due to the close relationship between an actuator's acceleration and torque capacities. When simple motion plans are being used, however, it may be of use to examine how the actuator's torque ratio criteria values change if the motion plan parameters (i.e. maximum joint accelerations/velocities) are kept constant with a changing gear ratio.

Adding the gear reduction ratio into the equation for the torque ratio criterion gives Eq. 4.8.

$$\text{TRT} = \left[\frac{\bar{g}\tau_k}{\alpha\tau_{k,nom}}\right]_{max/average} \tag{4.8}$$

Assuming that the motion plan and actuators are the same, τ_k and $\tau_{k,nom}$ will be constant because the required joint torques will be the same to produce the same acceleration, and the nominal torque will be the same as long as the same actuators are being used. As can be seen here, though, as the gear ratio rises, the torque ratio will decrease ($\bar{g}$ is the inverse of the gear ratio). This is represented physically in the sense that larger gear ratios result in a larger mechanical advantage, allowing the motor torque to be felt at a greater effect at the joint space.

In order to demonstrate these effects, the 2 DOF manipulator used for the case study in the previous chapter was examined using various gear ratios for each joint to show the effects of altering the gear ratio. Because the gear ratio is a discrete variable, a set of five gear ratios was chosen for each joint. Joint 1 gear ratios were chosen to be [10, 20, 30, 40, 50], and joint 2 gear ratios were chosen to be [5, 10, 15, 20, 25]. All

combinations of these ratios were evaluated, and the surface plots comparing the torque ratios for actuators 1 and 2 are shown in Figures 4.1 and 4.2, respectively.

Figure 4.1: Surface plot of torque ratios for joint 1 by varying gear ratio.

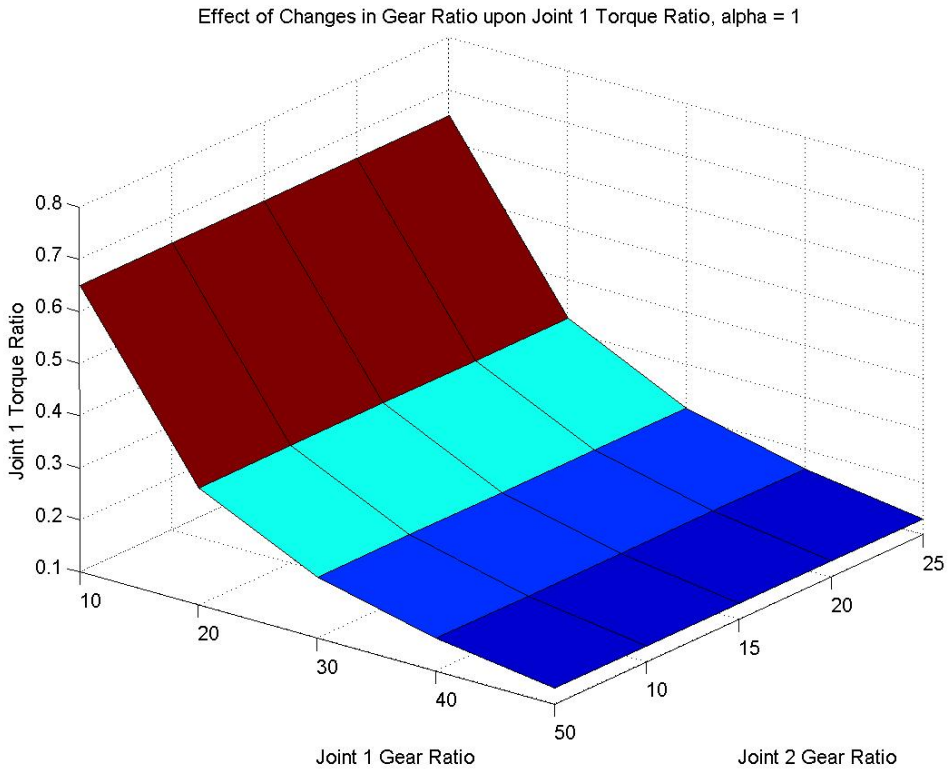

Figure 4.2: Surface plot of torque ratios for joint 1 by varying gear ratio.

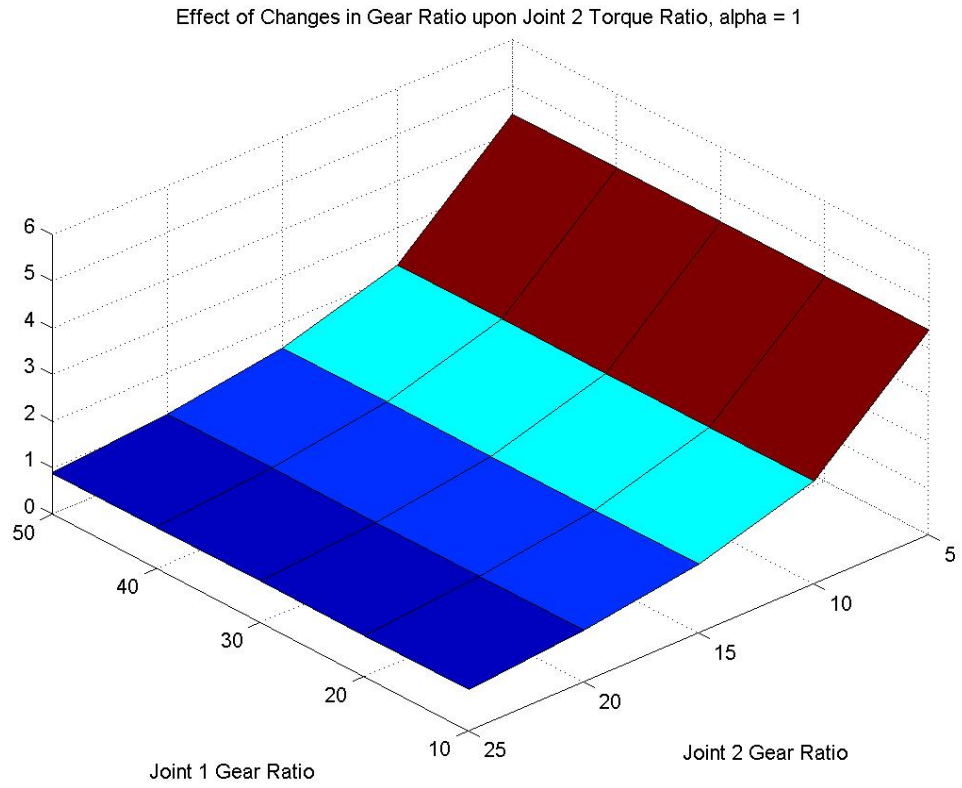

These plots were generated using the standard stopping control scheme described in previous chapters (i.e. $\alpha = 1$), but since this represents a simple coefficient, the only difference between plots for various alphas would be to adjust the scaling of the z-axis. As can be seen from the plots, the two torque ratios are largely independent of the opposite joint's gear ratio. This is because the control scheme involved a simple deceleration of each joint independently. If an optimization scheme were used to minimize distance traveled or some other criteria, some coupling of the torque ratios would be inevitable.

It is also clear from these plots that as the gear ratio lessens (larger reduction ratios), the actuators quickly descend into unsafe operation territory. The lesser

mechanical advantage associated with a smaller gear ratio results in a lower capacity for the actuator to decelerate the joint. Since this control scheme is previously set to have the second joint operating at near its torque capacity, reducing the effective torque capacity in joint space quickly forces the actuator beyond its capacity.

However, with the first joint, even at the smallest gear ratio, the actuator still stays within torque limits, indicating that, at least for this initial configuration and state, the designer would have a large range of choices for the gear ratio in the first joint. By selecting a smaller gear ratio the designer may increase the speed capacity of the joint and also decrease the amplification of the motor inertia into joint space, resulting in less kinetic energy being present in the system.

4.2.2 Kinetic Energy

As with any mechanical property, transmission through a gear train will either amplify or lessen its value. With the torque capacity, a larger mechanical advantage results in greater torque capacity at the joint in a linear relationship. Inertia behaves inversely. From Table 4.1, it can be seen that mapping the inertia from the motor level to the joint level is amplified by the square of gear reduction ratio. Especially with large gear ratios or actuators, this can lead to a huge energy amplification at the end-effector, which may result in increasing the energy to an unacceptably dangerous level.

The exact relationship between the criteria and the gear ratio for the kinetic energy is a little more opaque, however. Since the links and end-effector load are not massless, their contributions must be taken into account as well. This final inertia is represented in Eq. 4.9.

$$I^* = \bar{G}^T \left[{}^M I^* \right] \bar{G} + {}^L I^* \tag{4.9}$$

Where $\bar{G}$ is a vector of the gear ratios and is equal to the inverse of the mechanical gains, $\bar{g}$. The inertia due to the end-effector load is included in the link term for the link inertia. Substituting this into the equation for the kinetic energy criteria gives Eq. 4.10.

$$TKE = \frac{1}{2}\dot{\varphi}^T[\bar{G}^T\left[{}^M I^*\right]\bar{G} + {}^L I^*]\dot{\varphi} \tag{4.10}$$

Since the link inertia is largely fixed given the configuration, the designer has a limited control over this criterion. To give an example of the variance that can be obtained by varying the gear ratios, the 2 DOF case study is used again. Figure 4.3 shows the differences in the maximum kinetic energy over the same range of five discretized gear ratios for each joint.

Figure 4.3 Maximum kinetic energy over various gear ratios

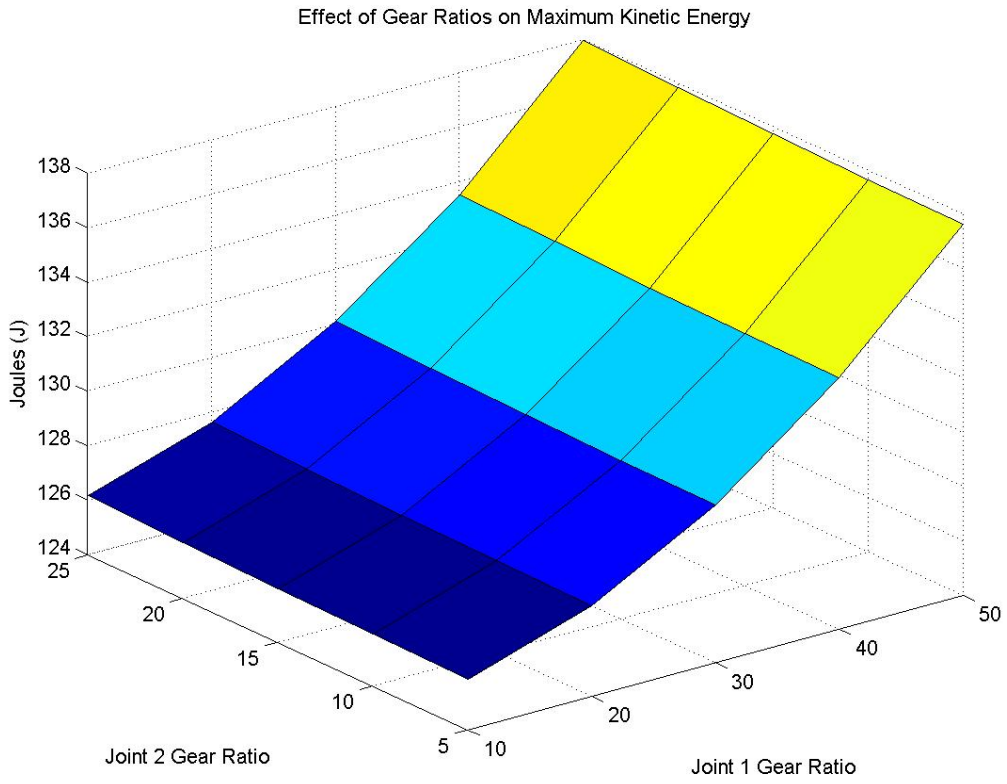

As can be seen in the plot, the total kinetic energy will increase as either gear ratio increases. A greater effect is seen from joint one due to not only the greater difference between the discrete values, but also the fact that the motor inertia in the first actuator is an order of magnitude greater than the motor inertia in the second actuator.

This detrimental behavior is in direct opposition to the potential gains achieved by the increased torque capacity at the joint level from a greater gear ratio. Therefore, it is up to the designer to examine and balance the different objectives and determine the optimal configuration of actuator parameters to satisfy the task requirements.

In terms of comparison, however, this configuration is an extreme case, given the large difference in the prime mover inertia compared to the link inertias and the relatively small gear reduction ratios. More commonly, the prime mover inertias will dominate the link inertias, and this effect will be even more pronounced.

4.2.3 Kinetic Energy Distribution

Even less clear to the designer is how the distribution of energy within the system will be affected by varying the gear ratios. This energy distribution is reflected by the kinetic energy partition value and weighted kinetic energy partition value criteria. In the most basic sense, this can be approximated in the sense that a larger gear ratio means that more of an actuator's inertia is amplified, so that joints with larger gear ratios will tend to have a greater inertia, so that if one joint's gear ratio increases while all other are held constant, this will tend to shift more of the energy into this joint. Depending on the relative inertias and gear ratios of the different prime movers in the system this effect may be more or less pronounced. However, in general due to the large gear reduction ratios typically found in systems, especially at the shoulder joints, this should not be considered a trivial concern by the designer.

Once again, to display the effects of gear ratio changes upon the kinetic energy partition values, the 2DOF manipulator is used as an example. Figures 4.4 and 4.5 respectively show the effect of varying gear ratios upon the average kinetic energy partition values during the stopping trajectory.

Figure 4.4: Effect of gear ratios upon average joint 1 kinetic energy partition value

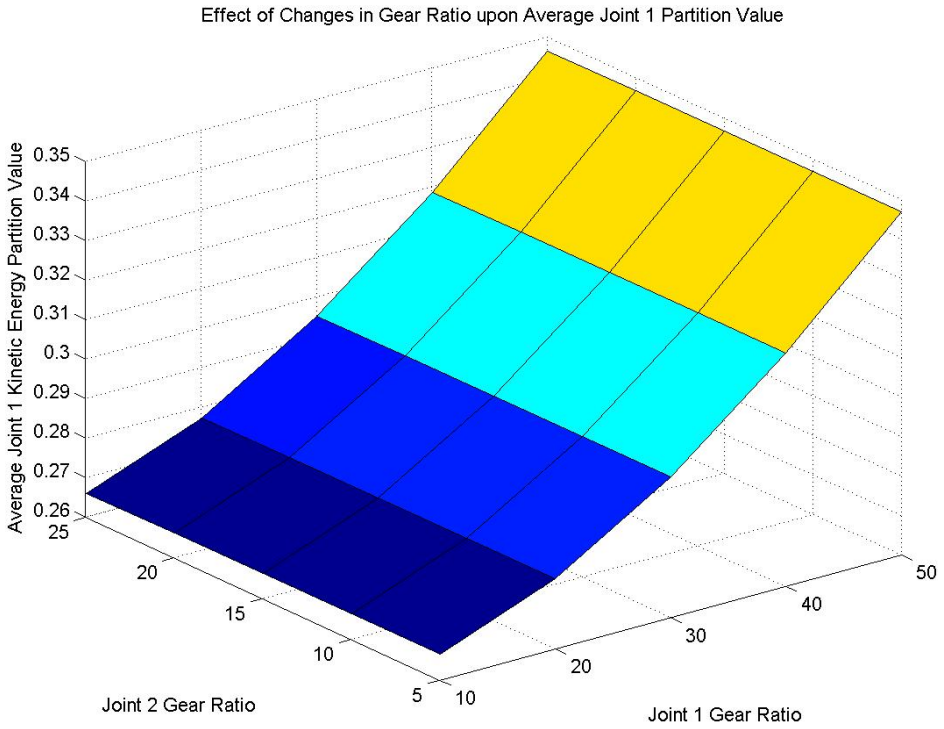

Figure 4.5: Effect of gear ratios upon average joint 2 kinetic energy partition value

As seen in the plots, the total gear ratios are largely decoupled from the opposite joint's partition value for this system. Changes in the gear ratio for joint 1 have very little affect on the average partition value for joint 2 and vice versa. The relatively small range in values for each plot is representative of the bounded nature of the criterion. Still, large changes in the gear ratio here only affect the partition value by a maximum of nearly .1, meaning that the difference in energy distribution is roughly 10% of the total energy in the system. For systems with higher gear ratios, and greater prime mover inertias relative to the link inertias, this will represent far more than 10% of the total energy. Also, since the criterion constraints require the partition values to sum to one, the inverse nature of these plots should be expected.

4.3 CONCLUSIONS

This chapter presented a simple framework for the manipulator designer to follow in order to estimate the safety criteria in the system to task safety parameters. Methods of mapping both the gear reduction ratio of the actuator and the nominal torque of the prime mover to the distance that will be traveled in a stopping event and the inertia present in the manipulator allow for the estimation of not only the potential for a collision, but also the severity of a collision.

Next, a discussion of how the actuator parameters affect the torque ratios and energy distributions was presented. This mainly focused on the gear reduction ratio and the relative inertias of the system. By monitoring the relative inertias during the design process the designer can gain an understanding of how the energy will be distributed during operation of the manipulator.

CHAPTER 5

Application to Industrial Environments

In order to gauge the applicability and usability of the framework described in Chapter 3 to a standard industrial implementation of a manipulator arm, an analysis of a full 6DOF PUMA-type manipulator is presented in this chapter. This includes an examination of the effects that the initial configuration, the operating speed, the inertial load at the end point, and different stopping control types has upon the ability of the manipulator to stop itself safely.

5.1 SYSTEM DESCRIPTION

Figure 5.1: 6DOF Puma-type Arm

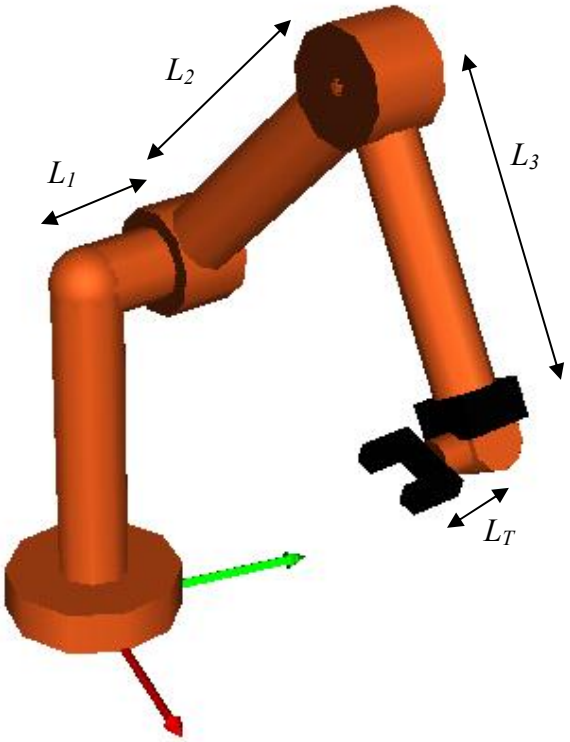

The manipulator upon which this case study was based was a 6DOF Puma-style arm, shown in Figure 5.1. This manipulator geometry is based on the classic Unimation Puma-arm, although this specific manipulator setup is discussed more thoroughly in Tesar and Rios [28]. A full table of the standard Denavit-Hartenberg parameters for this manipulator is included in Appendix A.

The actuator parameter values used for this manipulator are chosen based on values from a separate work by Rios evaluating a similar manipulator [29]. This solution was chosen to ensure that the manipulator has a sufficient ability to account for gravity torques during normal operation of this manipulator and to allow for an acceptable acceleration capability. The gear trains of each actuator weigh 1.1 kg and have a rotary inertia of 7.9×10^{-2} kgm^2.

Table 5.1: Relevant Actuator Parameter Values

Actuator Parameter	Axis 1	Axis 2	Axis 3	Axis 4	Axis 5	Axis 6
Nominal Motor Torque (N-m)	3.85	3.85	3.85	2.51	2.51	2.51
Weight (kg)	1	1	1	0.68	0.68	0.68
Rotor Inertia (kg m^2)	6.57×10^{-4}	6.57×10^{-4}	6.57×10^{-4}	3.12×10^{-4}	3.12×10^{-4}	3.12×10^{-4}
Gear Ratio	75	75	75	75	75	5

In order to develop a full dynamics model of the manipulator, the inertial properties of the links must be known as well. While a standard PUMA arm tends to have complicated link inertias, in this analysis, each link was assumed to be a simple hollow cylinder to calculate these parameters in the absence of a real-life manipulator. These parameters are shown below in Table 5.2.

Table 5.2: Link Inertial Parameters

Link	Mass (kg)	Inertia (kg-m^2)	CG Location (m)
2	1.8	($9.0x10^{-3}$,$9.0x10^{-3}$,$1.3x10^{-2}$)	(0,0,$6.3x10^{-2}$)
3	5.1	($8.7x10^{-2}$, $8.7x10^{-2}$, $3.8x10^{-2}$)	(0, 0, $2.0x10^{-1}$)
4	4.4	($6.1x10^{-2}$, $6.1x10^{-2}$, $3.3x10^{-2}$)	(0, 0, $1.8x10^{-1}$)
5	0.1	($4.5x10^{-4}$, $4.5x10^{-4}$, $7.5x10^{-4}$)	(0, 0, 0)
6	0.9	($4.1x10^{-3}$, $4.1x10^{-3}$, $6.7x10^{-3}$)	0, 0, $5.0x10^{-5}$)

With the system fully defined, the effects of the variable operating conditions upon the stopping performance of the manipulator will now be investigated.

5.2 EFFECT OF OPERATING CONDITIONS ON PERFORMANCE

Throughout the course of normal operation of a manipulator, the parameters under which the system is operating may vary wildly. For example, the effective inertia of a system operating near the edge of its work space may vary wildly from the effective inertia of a manipulator operating near its base. If a manipulator is used in pick and place tasks, depending on the relative inertia of the object being carried, this will have a large impact not only upon the energy contained within the system, but also upon the ability of actuators to extract energy from the system given the redistribution of inertia towards the end of the manipulator.

These effects are significant enough that it is useful for the operator to be aware of how they influence the system's safety, and what the effect will be to the performance of the system over the course of a stopping motion. To that end, four different, commonly adjusted operating parameters are shown here.

First, the effect of the initial configuration of the manipulator is shown, with the performance of a manipulator extended near the edge of its workspace compared to that of a manipulator contorted to operate near its base and that of a manipulator operating outside of its general X-Y plane.

Next, the effect of different Cartesian operating speeds is investigated. ANSI safety standards specify that a manipulator operate at no greater than 250 mm/s while a human is within the manipulator workspace [3] while the research done by Haddadin et al [19] indicates that speeds below 2 m/s may be sufficient to prevent injury. The effect of operating at both a high and low speed according to the safety criteria presented here is investigated.

Next, in order to address the specific case of pick and place operation and also that of tasks which require a heavy or high inertia tool, the effects of operating the manipulator with and without a high inertial load at the end of the manipulator is shown.

Finally, different strategies from decelerating the manipulator are examined. Three different strategies are presented: the ramped trapezoidal acceleration motion plan as shown in Chapter 3, a constant acceleration motion plan for simplicity and ease of calculation, and a torque-based viscous braking strategy to generate decelerating torques based on the individual joint speeds.

5.2.1 Manipulator Configuration

As described, the effect of three different initial configurations representing the extremes of the possible manipulator configurations. These three configurations are shown in Figure 5.2. The twisted configuration represents a situation in which the manipulator is tightly coiled about itself, operating near manipulator base. The velocity at the start of the stopping motion is in the Cartesian direction, {1, -1, 0}.

Figure 5.2: Initial Manipulator Configurations

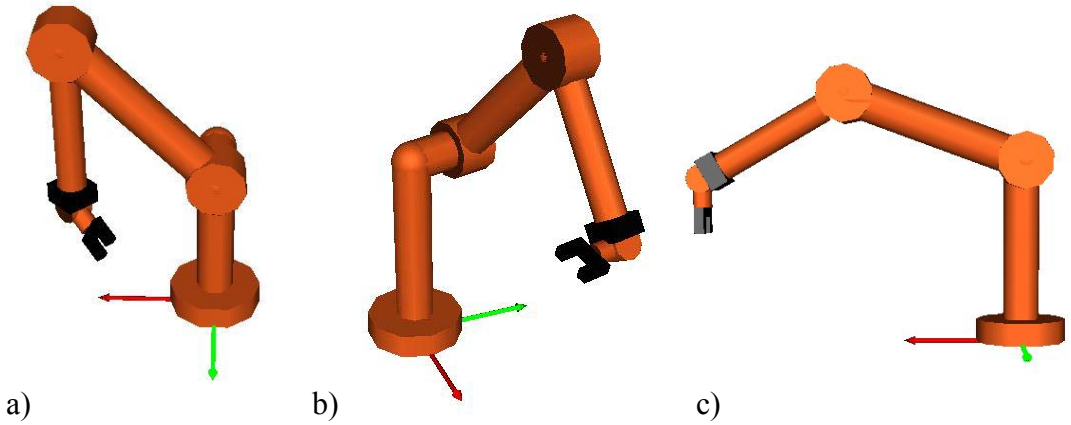

a) b) c)

Table 5.3: Joint Values of Initial Configurations of Manipulator

Configuration	Joint 1	Joint 2	Joint 3	Joint 4	Joint 5	Joint 6	Velocity
Twisted	0	-45	45	-135	-60	-90	{-1,0,-1}
Out of Plane	15	-45	15	90	-90	-45	{1,-1,0}
Extended	0	-20	-40	0	60	0	{1,0,-.5}

The next configuration corresponds to a manipulator roughly in the middle of its workspace, but oriented and moving orthogonally to the standard XY plane of the manipulator that corresponds to a zero value for the first joint. This could be indicative of any task requiring motion through multiple axes in the workspace.

The final configuration is when the robot is extended near the edge of its workspace, representing a task where the entirety of the manipulator's workspace is used. For industrial applications, it is often more likely humans will not be near the manipulator base but instead operating around the periphery of the workspace, so this case may be of special interest.

For each of these simulations, an initial speed of 500 mm/sec in the direction specified by the velocity in the table was used. No additional inertial load was applied to the end-effector. Additionally, a ramped acceleration motion plan in joint space was used to generate the trajectory.

Figure 5.3 shows a plot of the distance traveled for the different initial configurations. As can be seen, the total displacements of the end-effector are very small, but there is a significant difference between the performance of the manipulator in the extended configuration and the other two configurations, indicating that the configuration of the manipulator has a potentially large effect upon the safety performance of the manipulator. For a higher speed or inertial load, this difference may have been of greater effect.

Figure 5.3: Distance traveled for different initial configurations

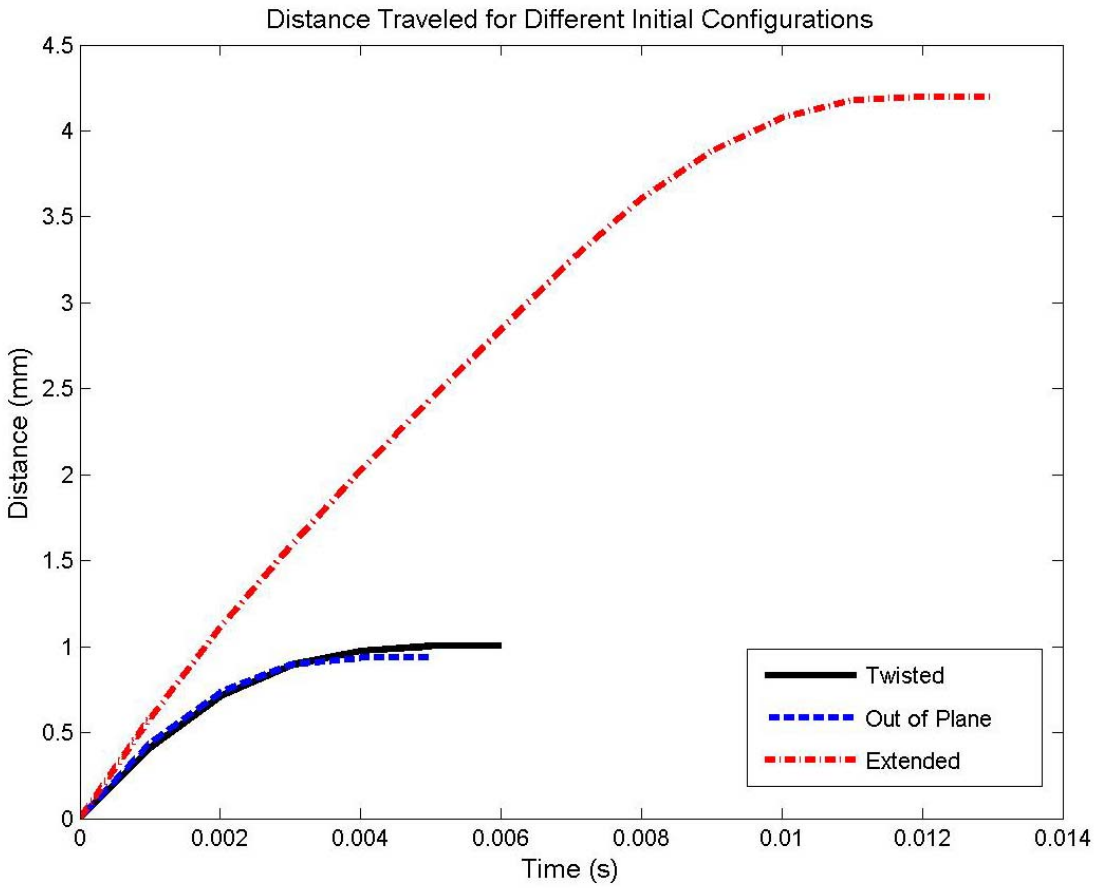

Shown in Table 5.4 are the values for selected other criteria over the course of the stopping trajectory. The direction used to calculate the directional distance criteria is the initial direction of the manipulator, and the trajectory calculations are based off of the initial trajectory of the end-effector. In order to quantify the speed and energy criteria, a "safe" velocity and kinetic energy were defined as 25 mm/s and 25 J, respectively. The time it took the manipulator to satisfy these "safe" values was then determined.

Table 5.4: Selected Safety Criteria Values for Different Configurations

Configuration	Total Distance (mm)	Directional Distance (mm)	Trajectory Distance (mm)	Time to "Safe" Velocity (s)	Time to "Safe" Kinetic Energy (s)
Twisted	1.0036	0.9949	0.1316	0.006	0.002
Out of Plane	0.9343	0.9341	0.0219	0.005	0.001
Extended	4.198	2.7955	3.1318	0.013	0.002

In order to provide a point of comparison, the "Out of Plane" configuration was established as a baseline, and the relative magnitudes of the values were then calculated and presented in Table 5.5.

Table 5.5: Relative Magnitudes of Selected Safety Criteria

Configuration	Total Distance (mm)	Directional Distance (mm)	Trajectory Distance (mm)	Time to "Safe" Velocity (s)	Time to "Safe" Kinetic Energy (s)
Twisted	1.07	1.07	6.01	1.20	2.00
Out of Plane	1.00	1.00	1.00	1.00	1.00
Extended	4.49	2.99	143.00	2.60	2.00

As can be seen in Table 5.5, the configuration may have a profound difference on the degree to which the manipulator is able to satisfy the safety criteria. In the "Extended" configuration, significantly worse performance was exhibited in all of the distance criteria, indicating that the potentially large impact that simply the manipulator's configuration at the moment a stopping event is initiated can have upon the safety of the ensuing trajectory. The large relative magnitudes of the trajectory distance value should be considered anomalous, given the extremely small value for the system for the "Out of Plane" configuration.

In order to gauge the level to which the joints are performing at their capacity, Table 5.6 shows the maximum values of the torque ratios for each joint over the trajectory. These were calculated for a stopping coefficient of one, so that the listed values correspond to the multiplier beyond which the actuator's nominal torque is required. Therefore, while values below five may be preferable, it is possible that any value up to ten may be acceptable to the operator if potential damage to the prime mover is considered an acceptable side effect of the stopping motion.

Table 5.6: Maximum Joint Torque Ratios

Configuration	Joint 1	Joint 2	Joint 3	Joint 4	Joint 5	Joint 6
Twisted	2.28	**14.33**	9.71	4.01	3.65	3.29
Out of Plane	7.15	2.01	2.80	1.87	1.29	1.01
Extended	0.17	7.01	5.79	0.00	2.53	0.00

Of key interest in Table 5.6 is the value of the maximum joint torque ratio for joint 2 in the "Twisted" configuration. This far exceeds even the maximum stopping coefficient value of ten prescribed previously in Chapter 3. Because of this value, the operator could not confidently apply this trajectory to a real system with the given parameters and expect the system to handle it without error. This means that either the operator must adopt less aggressive motion parameters such as acceleration limits to the trajectory generation scheme over the entirety of the workspace, resulting in lesser performance elsewhere, or else the motion parameters must be adjusted depending on the manipulator configuration, resulting in an added complexity to the trajectory generator.

As with the safety criteria, it is useful to determine how the configuration affects the torque requirements of a stopping trajectory. Table 5.7 contains the relative magnitudes of the maximum torque ratios for each joint, again using the "Out of Plane" configuration as a baseline.

Table 5.7: Relative Magnitudes of Maximum Torque Ratios

Configuration	Joint 1	Joint 2	Joint 3	Joint 4	Joint 5	Joint 6
Twisted	0.32	7.13	3.47	2.14	2.83	3.26
Out of Plane	1.00	1.00	1.00	1.00	1.00	1.00
Extended	0.02	3.49	2.07	0.00	1.96	0.00

As can be seen from the wildly divergent values, there is a fairly large effect that the configuration can have on each individual joint's torque load. This comes from the translation of the end-effector velocity to the joint velocities through the manipulator G-functions being dependent upon the joint positions, which are different for each configuration. The largest effects can be seen in the first three joints, which generally are used to locate the end-effector's position in PUMA-style geometry. The results from Table 5.7 indicate to the operator that monitoring one potential "problem" joint may not be sufficient to ensure the lack of hardware failures. The relative magnitudes indicate that, depending upon the configuration, both joints 1 and 2 are potentially the closest joint to failure, with joint 1 potentially failing in the "Out of Plane" configuration and joint 2 potentially failing in the "Twisted" configuration. In different configurations not shown here, a different joint may be the closest to a potential failure, so the entirety of the system state needs to be monitored.

5.2.2 Inertial Effects

One of the key values of a manipulator's is the ability to fit different tools at the end-effector in order to accomplish a given task. Often, these tools are bulky and heavy, creating loads that must be accounted for during safety criteria calculations.

In order to assess the effects of inertial loads at the end-effector, a steel bar measuring 50x500x50 mm was assumed to be in the manipulator's grasp. This set up is shown in Figure 5.4 in the "twisted" configuration. The bar of these dimensions weighed 9.8 kg with the inertias {0.2065, 0.0041, 0.2065} kg-m^2 about the primary axes. This is compared to the 23.94 kg total weight of the manipulator. The inertia compares to the 3.69 kgm^2 inertia of the first actuator seen at the joint level and the 0.0078 kgm^2 inertia of the actuator at joint 6 seen at the input level.

Figure 5.4: Manipulator with High Inertial Load

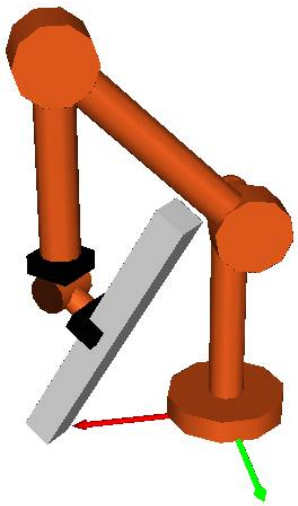

In order to maintain a valid comparison, the same motion parameters (maximum accelerations and velocities) were used to generate the stopping trajectory. Because of this, the same total distance will be traveled. In order to gauge the effect that the

additional inertia will have on the system, it is important to gauge the different levels of kinetic energy present during the stopping motion. This plot, including the values for each initial configuration is shown in Figure 5.5.

Figure 5.5: Kinetic Energy During Stopping Motion

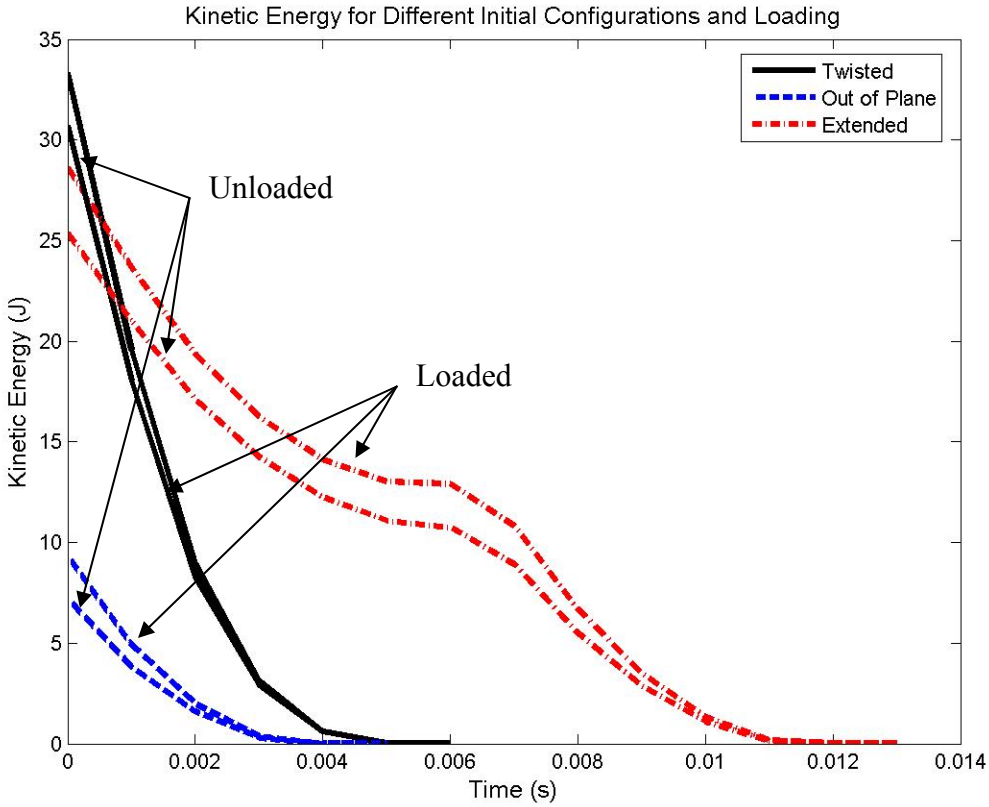

As further evidence of the dominant effect that the prime mover inertia has over all other inertias in the system, the presence of the inertial load at the end-effector has almost no effect on the safety criteria. Because a kinematic-based trajectory generation scheme is used, the distance traveled and velocity criteria remain the same, so the only effect seen in the safety criteria will be in the total kinetic energy of the manipulator. However, as seen in Figure 5.5, the load inertia is small for this system as the

amplification of the rotor inertias dominates all other inertias in the system, including that of the end-effector. While a greater effect would definitely be seen with a larger inertial load at the end-effector, the issues of payload capacity and a manipulator's ability to adequately control the load during normal operation within the nominal torque limits becomes a limiting factor.

Where the difference can be seen between the two loading situations is in the torque loading on the individual joints. The maximum torque ratios for the inertially loaded manipulator in each of the three configurations are shown in Table 5.8.

Table 5.8: Maximum Torque Ratios for High Inertia Load

Configuration	Joint 1	Joint 2	Joint 3	Joint 4	Joint 5	Joint 6
Twisted	1.72	15.36	11.33	4.04	4.08	11.60
Out of Plane	9.05	2.63	3.52	1.79	1.86	3.54
Extended	0.43	8.83	6.96	0.00	2.91	0.00

Compared with Table 5.6, where only joint 2 was operating outside of the loosest torque limits, the addition of a greater inertial load at the end-effector causes joints 2, 3, and 6 to require torques which are unacceptable to safe operation of the manipulator. Thus, even if the operator has taken care to adjust the motion parameters of a trajectory generator to ensure that all actuators will be operating within torque limits, the addition of an end-effector load may push one or more actuators outside those limits. In order to determine how the inertial load affects the torque ratios, the relative magnitudes of the torque ratios compared to the unloaded state is shown in Table 5.9. The values are normalized to the unloaded torques so that a value of one refers to the maximum torque

ratio refers to an equal maximum torque ratio to the unloaded trajectory for the given configuration found in Table 5.6.

Table 5.9: Relative Magnitudes of Maximum Torque Ratios

Configuration	Joint 1	Joint 2	Joint 3	Joint 4	Joint 5	Joint 6
Twisted	0.75	1.07	1.17	1.01	1.12	3.53
Out of Plane	1.27	1.31	1.26	0.96	1.44	3.50
Extended	2.53	1.26	1.20	0.00	1.15	0.00

The greatest effect is unsurprisingly seen at the sixth joint, which saw its inertia effectively tripled by adding the tool inertia to the rotor and link inertia of the system. This results in required torques of roughly three times greater than that of the unloaded situation. Small multipliers are also seen at joints 2 and 3 that can be at least partially attributed to the fact that with the PUMA manipulator geometry, these joints are oriented perpendicular to the gravity load, requiring these two joints to support the majority of the additional weight from the end-effector load.

5.2.3 Effects of Operating Speed

The Cartesian operating speed of the end-effector is one of the most important parameters for determining safety historically. It remains the sole parameter specified in the RIA safety standard for industrial manipulators that can allow for a human to enter the workspace safely when it is below a specific value. For the current standard, this speed is designated as 250 mm/s.

In order to assess the effects of the speed, simulations were run at two different speeds: 500 mm/s as used in simulations in the previous sections, and 2000 mm/s as described in Haddadin's work as the point of saturation for potential human injury. In

Figure 5.6 the total distance traveled for the two different operating speeds in the different manipulator configurations is shown.

Figure 5.6: Total Distance Traveled at Different Operating Speeds

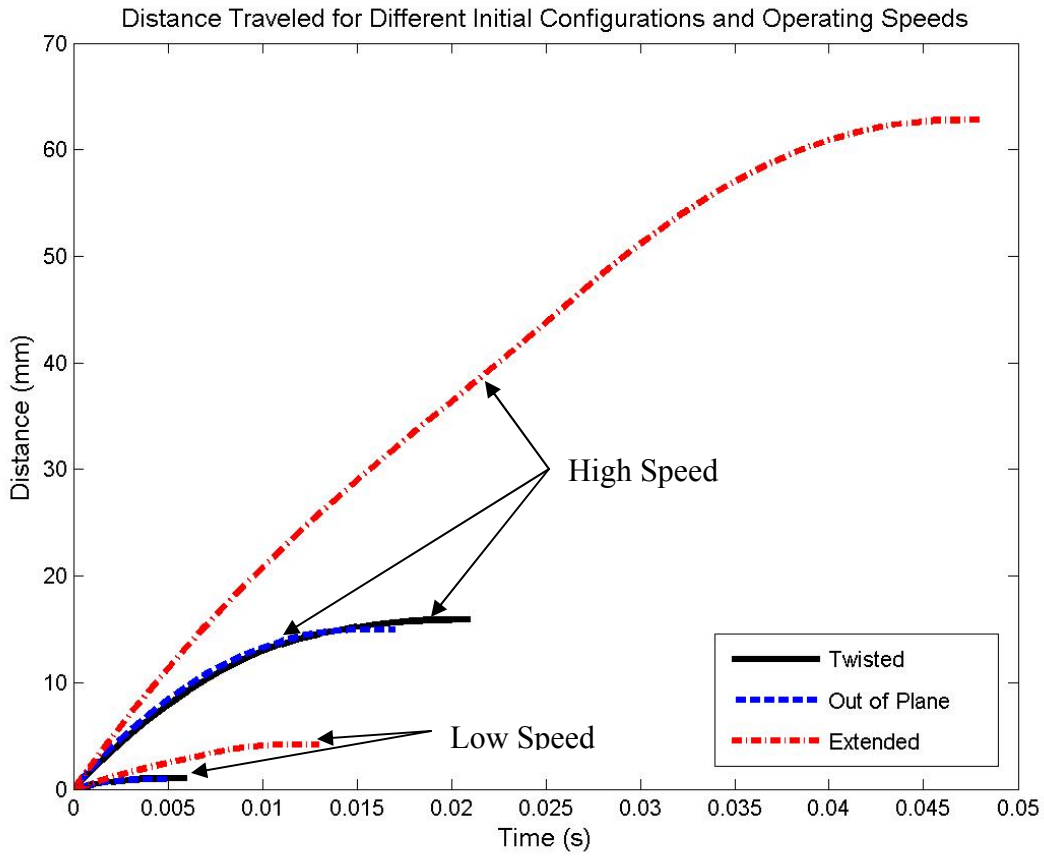

As can be seen in Figure 5.6, the operating speed of the manipulator has an extremely large effect on the distance traveled by the end-effector during the stopping trajectory. This is especially pronounced for a kinematic trajectory generation scheme like the one used here since the actuator accelerations are specified so the larger joint velocities will still be decreasing at roughly the same acceleration regardless of their initial speeds.

The other key criterion that will be greatly affected by the increase in the initial velocity will be the kinetic energy of the manipulator. This is due to the relationship between the kinetic energy and the velocity being the square of the velocity. Since the other key component of the manipulator energy is the inertia, plots of the energy over the course of the trajectory for the various values of the velocity presented in this section and the inertia from Section 5.2.2 are shown in Figures 5.7, 5.8, and 5.9.

Figure 5.7: Kinetic Energy Plots for Twisted Configuration

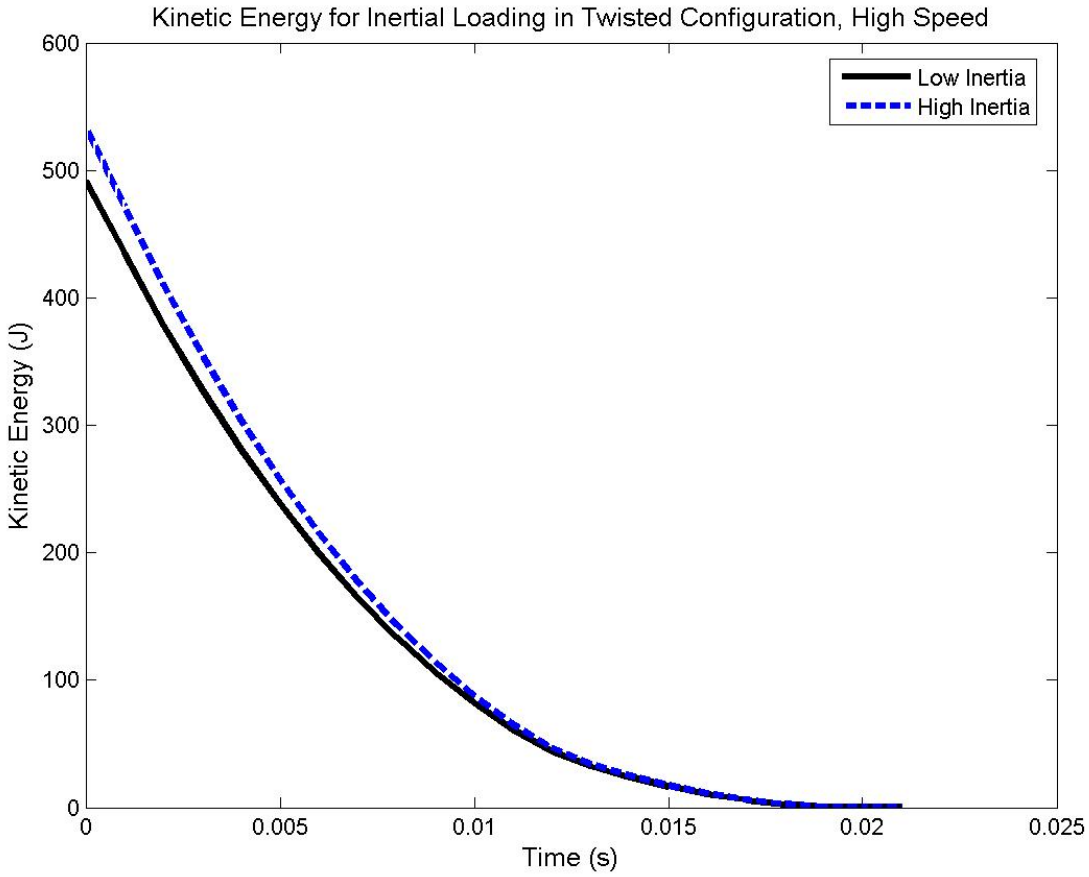

Figure 5.8: Kinetic Energy Plots for Out of Plane Configuration

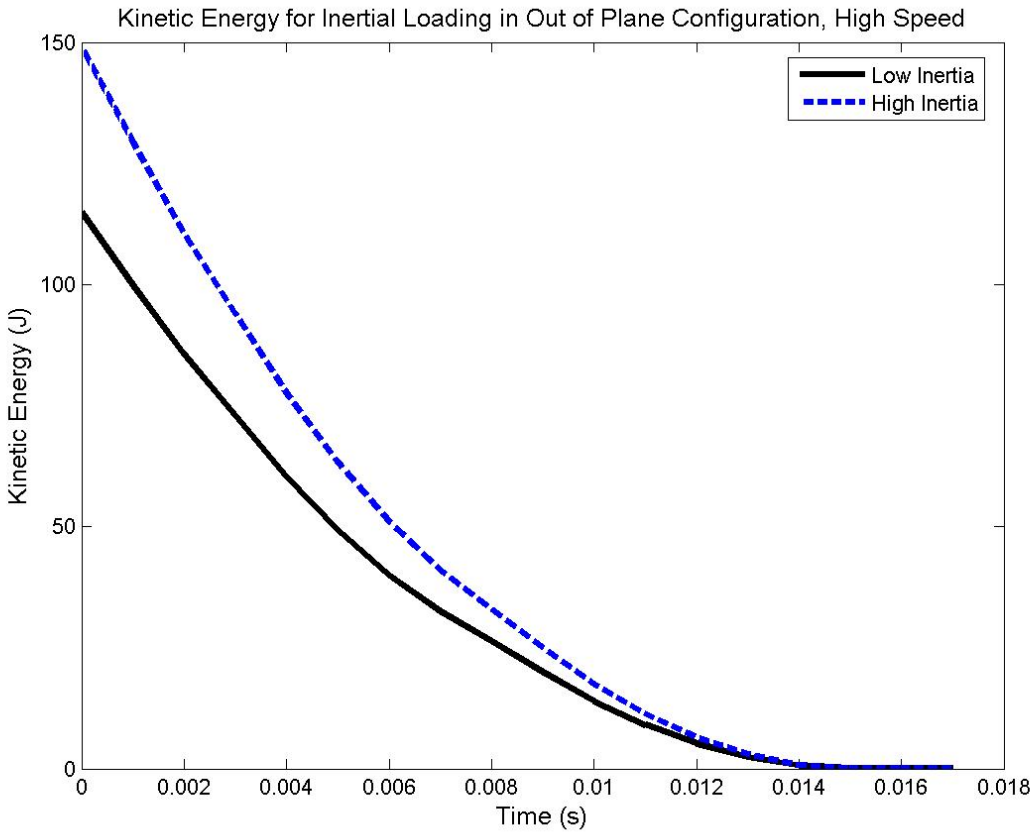

Figure 5.9: Kinetic Energy Plots for Extended Configuration

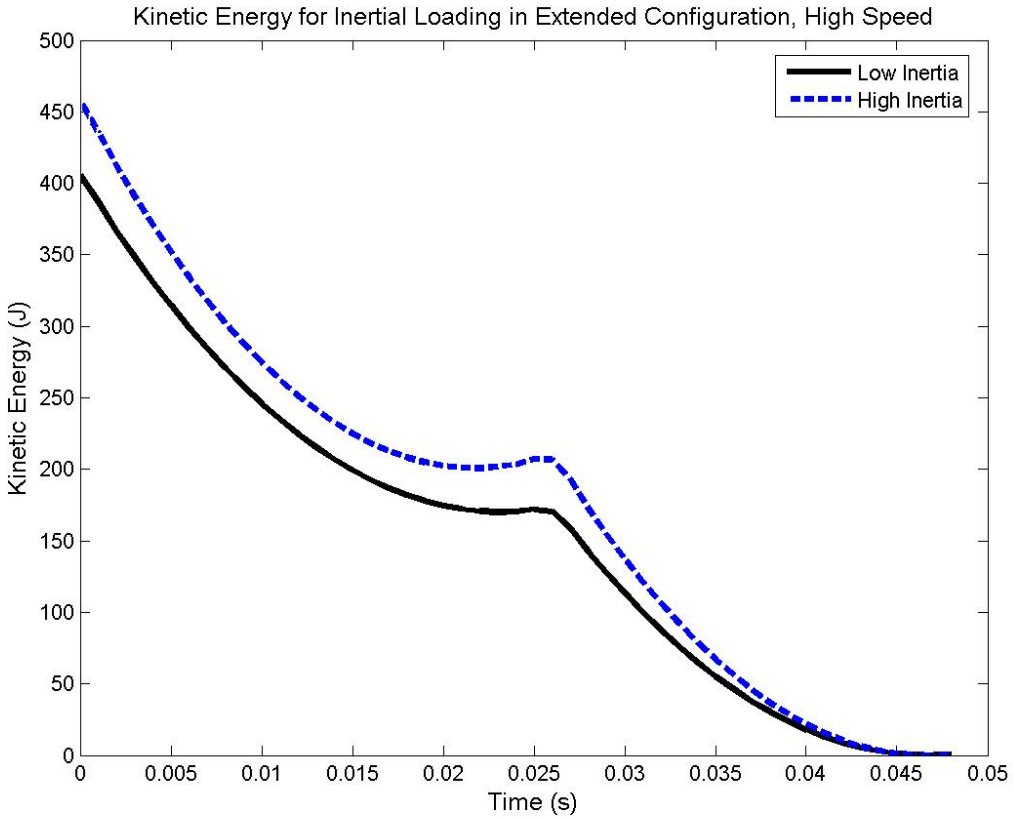

As seen in the figures, the speed has a much greater impact on the energy in the system than the inertia here. Since there isn't a clear mapping between the magnitude of the changes in the inertia and speed, this remains a somewhat qualitative assessment, but of the criteria presented thus far, the speed remains the biggest determinant of the safety of the system. Table 5.10 shows the values of the other safety criteria.

Table 5.10: Selected Safety Criteria Values for High Operating Speeds

Configuration	Total Distance (mm)	Directional Distance (mm)	Trajectory Distance (mm)	Time to "Safe" Velocity (s)	Time to "Safe" Kinetic Energy (s)
Twisted	15.89	15.69	2.56	0.02	0.02
Out of Plane	14.96	14.95	0.55	0.02	0.01
Extended	62.78	37.27	50.52	0.05	0.04

These values are clearly worse than those shown in Table 5.4, but the relative magnitudes shown in Table 5.11 illustrate the extremely large effect that the greater operating speed has upon the ability of the manipulator to halt itself safely. The criteria magnitudes are normalized to the values from Table 5.4 for each configuration.

Table 5.11: Relative Magnitudes of Safety Criteria for High Operating Speeds

Configuration	Total Distance (mm)	Directional Distance (mm)	Trajectory Distance (mm)	Time to "Safe" Velocity (s)	Time to "Safe" Kinetic Energy (s)
Twisted	15.84	15.77	19.49	3.50	7.50
Out of Plane	16.02	16.01	25.10	3.40	10.00
Extended	14.96	13.33	16.13	3.69	20.00

As can be seen in Table 5.11, there are extremely large multipliers for every single criterion, with only the time to "safe" velocity representing a multiplier roughly equal to the four times multiplier between the two operating speeds used in this analysis. This represents by far the biggest effect of the three operating conditions previously described, so in terms of improving the operational safety of the manipulator, the greatest effect can be achieved from lowering the operating speed.

As with the previous comparisons, examining the torques required to generate the trajectories is important. The maximum torque ratios for each joint are presented in Table 5.12.

Table 5.12: Maximum Torque Ratios for High Initial Speeds

Configuration	Joint 1	Joint 2	Joint 3	Joint 4	Joint 5	Joint 6
Twisted	2.35	14.35	9.57	4.04	3.69	3.43
Out of Plane	7.57	6.39	4.55	2.32	1.28	1.70
Extended	0.23	7.45	5.91	0.00	2.57	0.00

As opposed to the high inertia load, a high speed stopping operation may be handled by the given motion parameters without exceeding acceptable torque limits. This indicates that if the manipulator's inertial loads are well-known by the operator and do not change over the course of the task, a kinematic trajectory generator may be applied without worries of exceeding torque limits. To show the relative effect of the initial speed on torque loads, the relative magnitudes are shown in Table 5.13. These values are normalized to the low speed values from Table 5.4.

Table 5.13: Relative Magnitudes of Torque Ratios for High Initial Speeds

Configuration	Joint 1	Joint 2	Joint 3	Joint 4	Joint 5	Joint 6
Twisted	1.03	1.00	0.99	1.01	1.01	1.04
Out of Plane	1.06	3.18	1.63	1.24	0.99	1.68
Extended	1.35	1.06	1.02	0.00	1.02	0.00

Table 5.13 shows the relatively small effect that the higher speed has on the torque required. Since the greatest determinant of the joint torque is the acceleration of

the actuator, a kinematic control scheme will generally have similar torque requirements regardless of the starting speed. The one exception to this rule is in the "Out of Plane" configuration with joint 2, which most likely can be attributed to this specific configuration. If a manipulator approaches near a singularity during the stopping trajectory, anomalous torques such as this may be produced.

While the 2 m/s operating speed used in this analysis represented the safe threshold for HIC impact found by Haddadin et al [19], it may represent greater operating speed than that commonly found in industry. Particularly since the large effects of the operating speed are shown in this report, 1 m/s may represent a more commonly used operating speed. This will still have a large, effect on the safety criteria compared to a low speed operation, as demonstrated by much larger effect that speed has on the safety criteria than any of the previously discussed operating parameters, but the effects observed will be less pronounced than at the threshold speed of 2 m/s.

5.2.4 Effects of Stopping Control Schemes

For every previous simulation in this report, and trapezoidal ramped acceleration trajectory generator was used to create stopping trajectories. The advantages of this motion planning algorithm are discussed in Chapter 1, but the main advantage is the reduction of shocks to the system imposed by non-zero initial and final accelerations. The two alternate stopping trajectory generators presented in this discussion both involve non-zero initial accelerations, making them potentially less desirable.

First, a simple constant acceleration algorithm was used to generate trajectories. This involves simply choosing a maximum acceleration for each joint and maintaining it over the course of the trajectory until the joint speed is equal to zero. This was chosen for the ease of calculation.

The final trajectory generation scheme is a torque-based algorithm based upon the concept of viscous braking. A torque is calculated by multiplying a constant chosen by the operator with the individual joint speeds. This torque is then generated by the actuator in order to decelerate the system in addition to the fixed torques from the gravity, velocity, and external loads to the system. This is shown for any joint *i* in Eq. 5.1.

$$\tau_i = -K_i\dot{\varphi}_i + \tau_f \tag{5.1}$$

This system has the advantage of ensuring that the manipulator will not breach any torque limits of any individual actuator since the torque is being commanded, but adds in the added complexity of not being able to determine any of the location-based criteria without employing an accurate dynamics model. Either a fixed value for the braking constant can be chosen no matter what the speed of the individual joints, or the braking constant values can be determined at the onset of the stopping trajectory by dividing the torque limit by the initial joint velocity for each actuator.

While the two kinematics-based criteria generate roughly similar performance, the viscous braking method diverges greatly from those methods. As an example of the different relative performances, Figures 5.10 and 5.11 show the different performances for the manipulator in the extended position for a low speed and high speed parameters, respectively.

Figure 5.10: Comparison of Stopping Controls for Extended, Low Speed Configuration

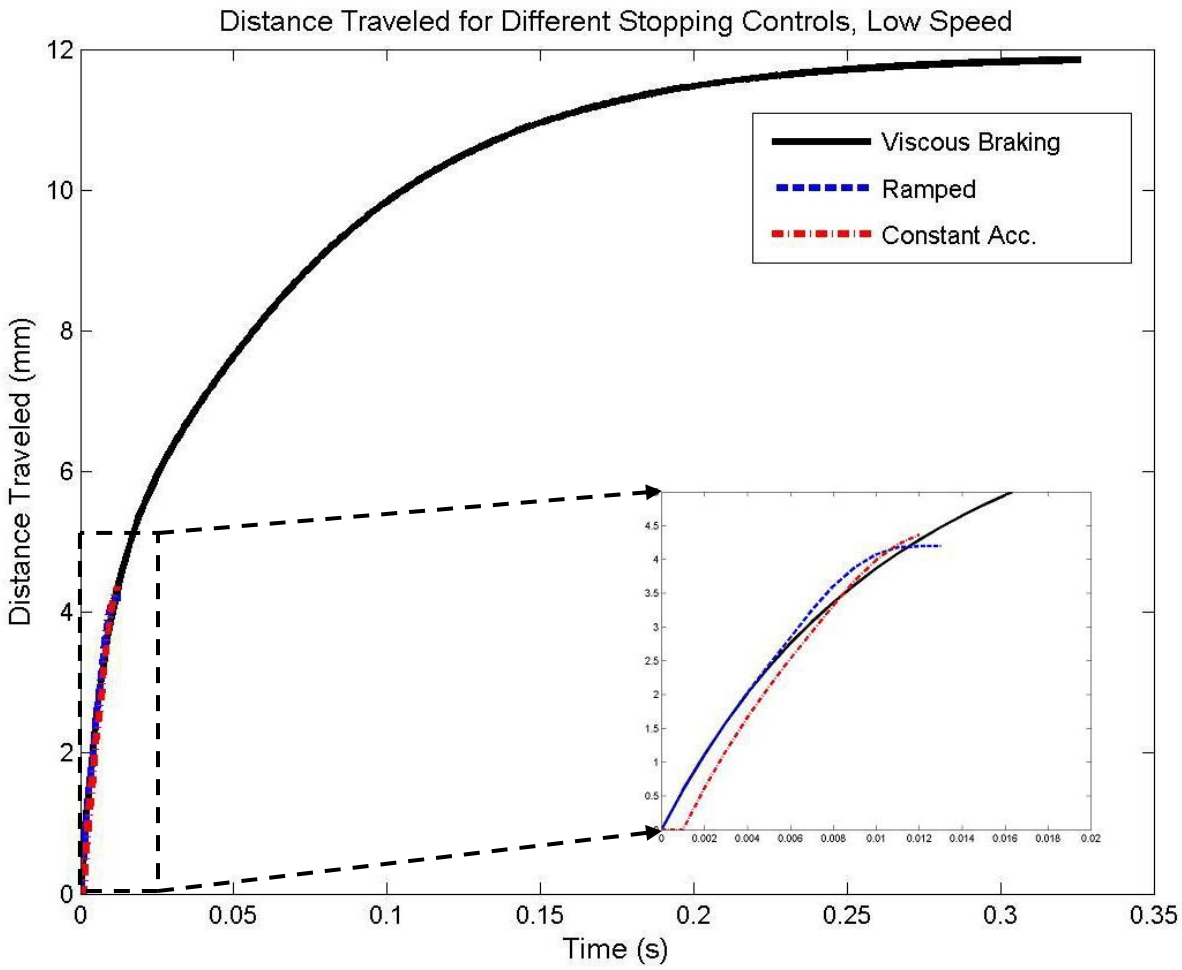

Figure 5.11: Comparison of Stopping Controls for Extended, High Speed Configuration

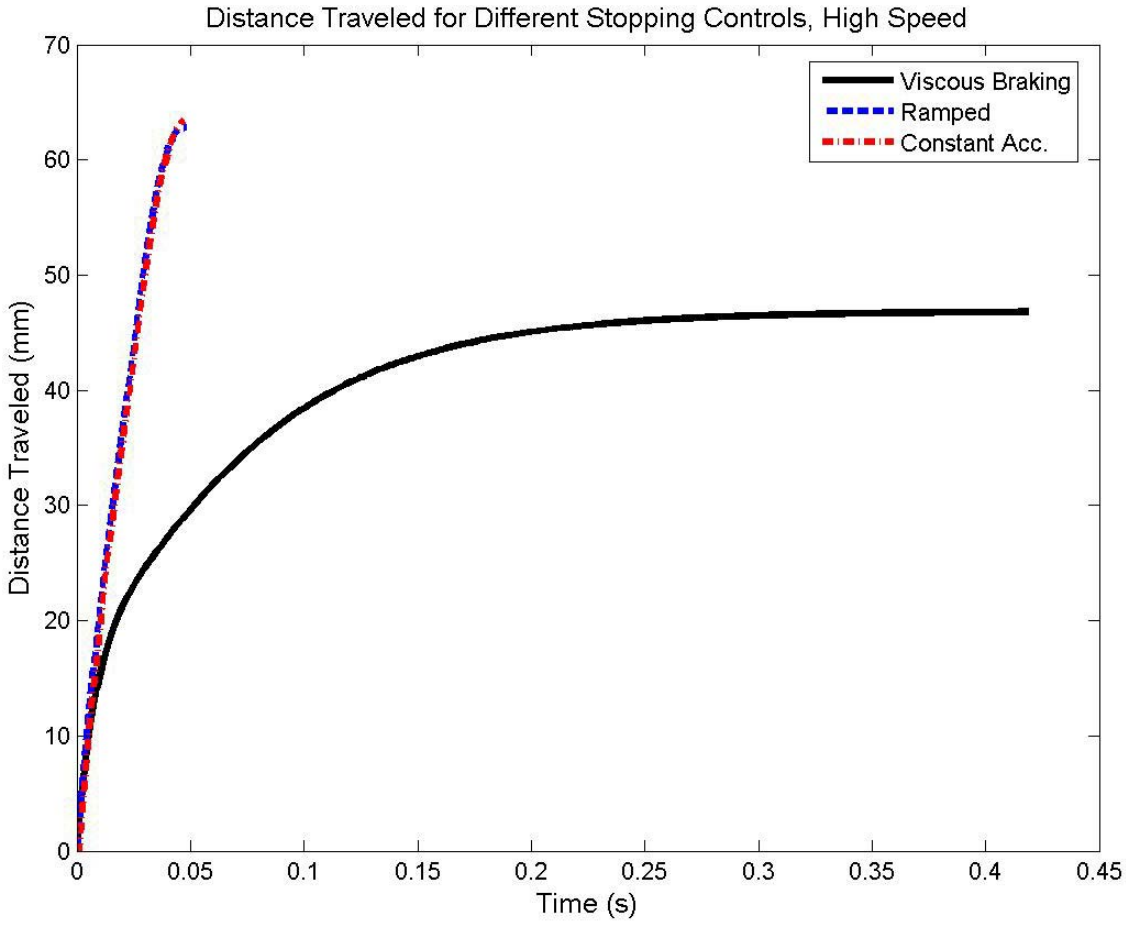

As can be seen in the figures, depending on the initial speed of the end-effector, the stopping control scheme that best satisfies the criteria may vary. In general, the torque-based scheme will do best at avoiding actuator torque limits and maximizing the performance with low inertias and high speeds. In this situation a maximal amount of the torque is able to decelerate the system. However, if a task requires a specific safety

criteria requirement such as distance traveled, it will be more difficult to ensure that this requirement will be satisfied. Table 5.14 shows the values of the safety criteria for the low operating speed in the different initial configurations for the torque-based control scheme.

Table 5.14: Selected Safety Criteria Values for Viscous Braking

Configuration	Total Distance (mm)	Directional Distance (mm)	Trajectory Distance (mm)	Time to "Safe" Velocity (s)	Time to "Safe" Kinetic Energy (s)
Twisted	23.86	19.1	14.25	0.12	0.005
Out of Plane	5.04	4.6	1.98	0.04	0.001
Extended	11.85	5.8	10.32	0.13	0.002

These values confirm what was seen in Figure 5.10; the torque-based control scheme performs significantly worse under low operating speeds. Table 5.15 shows the relative magnitude of this control scheme compared to the ramped acceleration values from Table 5.4.

Table 5.15: Relative Magnitudes of Safety Criteria for Viscous Braking

Configuration	Total Distance (mm)	Directional Distance (mm)	Trajectory Distance (mm)	Time to "Safe" Velocity (s)	Time to "Safe" Kinetic Energy (s)
Twisted	23.78	19.20	108.31	19.17	2.50
Out of Plane	5.40	4.92	90.23	8.60	1.00
Extended	2.82	2.07	3.30	10.00	1.00

Based on the values from Table 5.15, the choice of the control scheme used to generate the stopping trajectory of the manipulator is possibly the most important of the parameters discussed in this chapter. The values for every safety criterion are significantly greater under the torque-based control scheme, at least at low operating

speeds. Based on Figure 5.11, however, it appears that the torque-based braking scheme may provide improved performance at high operating speeds for the manipulator. Table 5.16 shows the relative magnitudes of the safety criteria for the high operating speed condition. Because the greater operation speed is being used, the values are normalized to the standard values for the ramped acceleration at a high operating speed from Table 5.10.

Table 5.16: Relative Magnitudes of Safety Criteria for Viscous Braking, High Operating Speed

Configuration	Total Distance (mm)	Directional Distance (mm)	Trajectory Distance (mm)	Time to "Safe" Velocity (s)	Time to "Safe" Kinetic Energy (s)
Twisted	5.93	4.11	26.80	9.62	4.40
Out of Plane	1.36	1.25	14.88	5.76	0.90
Extended	0.75	0.56	0.83	4.58	0.43

Examining the values from Table 5.16 shows that the safety performance of the manipulator using a torque-based control scheme is highly dependent upon the configuration of the manipulator. While the manipulator's performance remains significantly worse for the "Twisted" configuration, it is only slightly worse for the "Out of Plane" configuration and shows a significant improvement in every criteria but the velocity in the "Extended" configuration.

It is important to note, however, that the trajectories generated by the ramped acceleration kinematic algorithm required torques in some actuators that were outside of the actuator limits. As with the previous examples, Table 5.17 shows the maximum torque ratios for the high operating speed case.

Table 5.17: Maximum Torque Ratios for Viscous Braking, High Operating Speed

Configuration	Joint 1	Joint 2	Joint 3	Joint 4	Joint 5	Joint 6
Twisted	0.77	7.38	2.31	3.20	0.81	2.14
Out of Plane	9.74	1.21	1.25	3.48	0.80	0.30
Extended	0.25	9.29	8.11	0.03	1.97	0.16

Table 5.17 clearly shows that all torque values from the torque-based stopping trajectory are within limits, meaning that the system will theoretically be able to generate the trajectories, as opposed to the "Twisted" configuration trajectory with the ramped acceleration trajectory generator. Operating in torque space gives the added benefit of being able to more easily control to allow the manipulator to operate within actuator torque limits. However, this comes at the cost of a lesser ability to specify the desired safety parameters such as velocity and distance traveled, which occur in kinematic space. The relative magnitudes of the maximum torque ratios for the viscous braking scheme compared to the torque ratios from the kinematic control scheme are shown in Table 5.18. The values are normalized to the torque ratios in Table 5.12.

Table 5.18: Relative Magnitudes of Maximum Torque Ratios for Viscous Braking

Configuration	Joint 1	Joint 2	Joint 3	Joint 4	Joint 5	Joint 6
Twisted	0.33	0.51	0.24	0.79	0.22	0.62
Out of Plane	1.29	0.19	0.27	1.50	0.63	0.18
Extended	1.09	1.25	1.37	0.00	0.77	0.00

Somewhat unsurprisingly, in the configuration where multiple actuators are operating at greater torques with the viscous braking scheme, the performance is improved, indicating that a more aggressive torque-based trajectory generator that introduces a greater shock into the system may be able to improve some of the safety criteria at the added risk of damaging the manipulator.

Now that every case has been examined and simulated, the values of the safety criteria for all three stopping trajectory generators and every inertial load, speed condition and configuration described in previously in this chapter are shown in Table 5.19. The corresponding maximum torque ratios for each joint and each trajectory generated are shown in Table 5.20. To provide a point of comparison for how each individual case performs relative to a baseline, Table 5.21 shows the relative magnitude of the safety criteria for each of the cases. These values have been normalized to the unloaded manipulator operating at a low speed in the "Out of Plane" configuration using the ramped acceleration trapezoidal trajectory generation scheme.

Table 5.19: Safety Criteria for Different Stopping Scenarios

Control	Configuration	Inertia	Speed (mm/s)	TDT (mm)	dDST (mm)	TRJ (mm)	VEL (sec)	EKE (sec)
Viscous Braking	Twisted	Low	500	23.86	19.10	14.25	0.115	0.005
			2000	94.30	64.50	68.75	0.202	0.066
		High	500	27.87	21.80	17.38	0.168	0.007
			2000	106.53	68.90	81.21	0.231	0.076
	Out of Plane	Low	500	5.04	4.60	1.98	0.043	0.001
			2000	20.38	18.70	8.18	0.098	0.009
		High	500	6.74	6.10	2.95	0.060	0.001
			200	27.31	24.20	12.17	0.130	0.013
	Extended	Low	500	11.85	5.80	10.32	0.130	0.002
			2000	46.80	20.90	41.87	0.220	0.017
		High	500	13.37	6.80	11.53	0.152	0.002
			2000	52.29	23.90	46.49	0.266	0.020
Constant Acceleration	Twisted	Low	500	1.18	1.16	0.22	0.006	0.002
			2000	16.74	16.49	2.91	0.021	0.015
		High	500	1.18	1.16	0.22	0.006	0.002
			2000	16.74	16.49	2.91	0.021	0.016
	Out of Plane	Low	500	1.10	1.10	0.03	0.005	0.001
			2000	15.98	15.97	0.54	0.016	0.010
		High	500	1.10	1.10	0.03	0.005	0.001
			2000	15.98	15.97	0.54	0.016	0.010
	Extended	Low	500	4.37	3.09	3.09	0.013	0.002
			2000	63.37	38.22	50.55	0.048	0.040
		High	500	4.37	3.09	3.09	0.013	0.002
			2000	63.37	38.22	50.55	0.048	0.041
Ramped Acceleration	Twisted	Low	500	1.00	0.99	0.13	0.006	0.002
			2000	15.89	15.69	2.56	0.021	0.015
		High	500	1.00	0.99	0.13	0.006	0.002
			2000	15.89	15.69	2.56	0.021	0.016
	Out of Plane	Low	500	0.93	0.93	0.02	0.005	0.001
			2000	14.96	14.95	0.55	0.017	0.010
		High	500	0.93	0.93	0.02	0.005	0.001
			2000	14.96	14.95	0.55	0.017	0.011
	Extended	Low	500	4.20	2.80	3.13	0.013	0.002
			2000	62.78	37.27	50.52	0.048	0.040
		High	500	4.20	2.80	3.13	0.013	0.002
			2000	62.78	37.27	50.52	0.048	0.041

Table 5.20: Maximum Torque Ratios for Different Stopping Scenarios

Control	Configuration	Inertia	Speed (mm/s)	J1	J2	J3	J4	J5	J6
Viscous Braking	Twisted	Low	500	0.22	1.92	0.57	0.86	0.20	0.55
			2000	0.77	7.38	2.31	3.20	0.81	2.14
		High	500	0.2	1.98	0.54	0.86	0.14	1.05
			2000	0.69	7.51	2.22	3.20	0.67	4.04
	Out of Plane	Low	500	2.45	0.46	0.26	0.87	0.20	0.07
			2000	9.74	1.21	1.25	3.48	0.80	0.30
		High	500	2.45	0.58	0.22	0.85	0.11	0.14
			200	9.67	1.33	1.26	3.49	0.55	0.55
	Extended	Low	500	0.06	2.57	1.94	0.01	0.49	0.04
			2000	0.25	9.29	8.11	0.03	1.97	0.16
		High	500	0.09	0.03	1.87	0.01	0.58	0.09
			2000	0.37	9.40	8.21	0.01	2.35	0.37
Constant Acceleration	Twisted	Low	500	2.28	13.64	9.16	4.03	3.46	3.35
			2000	2.29	13.90	9.25	3.94	3.62	3.37
		High	500	1.70	14.63	10.84	4.06	3.85	11.8
			2000	1.72	14.97	10.75	3.97	3.97	11.8
	Out of Plane	Low	500	7.22	2.81	3.49	1.96	1.24	1.30
			2000	7.34	5.80	4.43	2.14	1.27	1.67
		High	500	9.05	3.52	4.27	2.22	1.95	4.57
			2000	9.19	7.04	5.47	2.42	2.08	5.88
	Extended	Low	500	0.17	6.75	5.62	0.00	2.46	0.00
			2000	0.24	6.97	5.61	0.00	2.46	0.00
		High	500	0.42	8.52	5.76	0.00	2.83	0.00
			2000	0.44	9.05	6.74	0.00	2.86	0.00
Ramped Acceleration	Twisted	Low	500	2.28	14.33	9.71	4.01	3.65	3.29
			2000	2.35	14.35	9.57	4.04	3.69	3.43
		High	500	1.72	15.36	11.33	4.04	4.08	11.6
			2000	1.78	15.43	11.05	4.07	4.06	12.0
	Out of Plane	Low	500	7.15	2.01	2.80	1.87	1.29	1.01
			2000	7.57	6.39	4.55	2.32	1.28	1.70
		High	500	9.05	2.63	3.52	1.79	1.86	3.54
			2000	9.47	7.76	5.60	2.62	2.19	5.99
	Extended	Low	500	0.17	7.01	5.79	0.00	2.53	0.00
			2000	0.23	7.45	5.91	0.00	2.57	0.00
		High	500	0.43	8.83	6.96	0.00	2.91	0.00
			2000	0.42	9.66	7.13	0.00	2.98	0.00

Table 5.21: Relative Magnitudes of Safety Criteria for Different Stopping Scenarios

Control	Configuration	Inertia	Speed (mm/s)	TDT (mm)	dDST (mm)	TRJ (mm)	VEL (sec)	EKE (sec)
Viscous Braking	Twisted	Low	500	25.54	20.45	650.82	23.00	5.00
			2000	100.93	69.05	3139.15	40.40	66.00
		High	500	29.83	23.34	793.51	33.60	7.00
			2000	114.02	73.76	3708.07	46.20	76.00
	Out of Plane	Low	500	5.40	4.92	90.23	8.60	1.00
			2000	21.82	20.02	373.58	19.60	9.00
		High	500	7.21	6.53	134.72	12.00	1.00
			200	29.23	25.91	555.61	26.00	13.00
	Extended	Low	500	12.68	6.21	471.32	26.00	2.00
			2000	50.09	22.37	1911.87	44.00	17.00
		High	500	14.31	7.28	526.27	30.40	2.00
			2000	55.96	25.59	2123.05	53.20	20.00
Constant Acceleration	Twisted	Low	500	1.26	1.24	9.99	1.20	2.00
			2000	17.92	17.65	132.71	4.20	15.00
		High	500	1.26	1.24	9.99	1.20	2.00
			2000	17.92	17.65	132.71	4.20	16.00
	Out of Plane	Low	500	1.18	1.18	1.32	1.00	1.00
			2000	17.11	17.10	24.82	3.20	10.00
		High	500	1.18	1.18	1.32	1.00	1.00
			2000	17.11	17.10	24.82	3.20	10.00
	Extended	Low	500	4.68	3.31	140.96	2.60	2.00
			2000	67.83	40.92	2307.99	9.60	40.00
		High	500	4.68	3.31	140.96	2.60	2.00
			2000	67.83	40.92	2307.99	9.60	41.00
Ramped Acceleration	Twisted	Low	500	1.07	1.07	6.01	1.20	2.00
			2000	17.01	16.79	117.11	4.20	15.00
		High	500	1.07	1.07	6.01	1.20	2.00
			2000	17.01	16.79	117.11	4.20	16.00
	Out of Plane	Low	500	1.00	1.00	1.00	1.00	1.00
			2000	16.02	16.01	25.10	3.40	10.00
		High	500	1.00	1.00	1.00	1.00	1.00
			2000	16.02	16.01	25.10	3.40	11.00
	Extended	Low	500	4.49	2.99	143.00	2.60	2.00
			2000	67.20	39.90	2307.07	9.60	40.00
		High	500	4.49	2.99	143.00	2.60	2.00
			2000	67.20	39.90	2307.07	9.60	41.00

5.3 OPERATIONAL RECOMMENDATIONS

Now that sufficient data has been gathered to make some early conclusions, the operator should consider some specific criteria to be more important depending upon the task that the manipulator will be performing. First and most important, it is necessary to ensure that actuator faults will not occur during the stopping trajectory of the manipulator. If an actuator fault were to occur during the stopping motion, unpredictable behavior will result in undesirable motion during a time when control of the manipulator is most critical. As can be seen in the analysis from Sections 5.2.1 and 5.2.2, both a change in configuration and a high inertial load can push the actuators past their torque limits. Therefore, if a kinematics-based controller is being used, the operator should take special care in the location of the manipulator within the workcell to ensure that the task does not involve moving through configurations where high torques would be required and that the motion parameters are sufficiently conservative that any additional end-effector load will not cause an actuator fault.

For tasks involving pHRI applications, the two most critical criteria are those that minimize the potential injury risk, specifically the kinetic energy and the end-effector velocity criteria. These have been previously in the literature to be the most critical parameters in terms of the potential head injury and fracture forces generated by a collision, so these should be of greatest importance for safety tasks involving human interaction with the manipulator. Additionally, as shown in Section 5.2.3, the operating speed of the manipulator has the greatest impact upon the manipulator's ability to stop itself safely, so this parameter should be adjusted to provide the greatest potential benefits towards making the manipulator safer for humans to interact with.

For tasks which require a specific path, such as cutting or seam welding, the operator should seek to minimize the trajectory distance criterion. In both of these tasks, there is a binary effect to being on the commanded trajectory versus traveling away from it. Moving off of the trajectory may result in damage to the manipulator tool or the part being operated upon, which may cause damaging effects elsewhere in the system for large parts.

At all times, the joint-level criteria such as the torque ratios should be monitored to indicate potential problems and sources of error within the system. This will ensure safe operation and fewer unexpected hardware failures.

5.4 CONCLUSIONS

In this chapter a 6DOF system was presented. Simulations of the stopping trajectories for a wide variety of states and configurations were developed in order to gauge the relative impacts of that these factors will have upon the manipulator's ability to stop itself safely.

Finally, a conclusive summary of the data was shown, along with a set of recommendations to the future manipulator operator and/or designer for the relative importance of the safety criteria given the manipulator task.

CHAPTER 6

Conclusion and Future Work

This report presented a new framework to be used to evaluate a manipulator's ability to halt itself safely and measure the system's capability to do so. This process relied on identifying the important operating parameters of manipulators, creating evaluator criteria based upon these parameters and determining how actuator parameters affect the ability of the manipulator to satisfy these criteria. The key to this report is developing a simple framework of physically significant criteria to allow the operator or system designer to determine how safely a manipulator is able to halt itself in the event that the system requires intervention to prevent a hazard. This allows the operator to simply assess the potential damages or injuries resulting from such an intervention and adjust the operating parameters to satisfy the task requirements. From the design side, the actuator parameters of motor torque and gear reduction ratio were examined in order to allow the designer to make design choices to ensure that the manipulator meets the task specifications. Furthermore, it was shown with a 6DOF industrial manipulator geometry example how different operation parameters will affect the ability of a manipulator to safely halt itself.

In the next section, a summary of the key work presented in each of the preceding chapters is presented. This includes the previous work done in the field of safety to both quantify and improve system safety, the evaluatory framework established in this work, and the relationship of actuator parameters to the performance capabilities of the system. The chapter concludes with a summary of the future work to be done to extend the research presented in this report.

6.1 RESEARCH SUMMARY

In each of the subsections below, a summary of one of the previous chapters from this work is presented. These are divided as follow: 1) Literature Review, 2) Safety Criteria Framework, 3) Effect of Actuator Parameters, and 4) Applications to Industrial Environments. In the section about the literature review, the major works previously done in the field of safety are presented and summarized. In the summary of the safety criteria framework, the criteria established in this work to evaluate manipulator safety and performance capacity are presented. The section on the effect of actuator parameters explains the results mapping the actuator parameters to the safety criteria performance. Finally, the section about applications to industrial environments presents a design case study involving a manipulator geometry commonly found in industry.

6.1.1 Previous Work

In this work, a framework for evaluating a specific portion of the manipulator's safety scheme is presented. While this has not been specifically addressed in the literature, there is a substantial set of work done to both evaluate the overall safety of the manipulator and methodologies to improve on different aspects of the manipulator safety. In a report evaluating the safety of a manipulator, it is important to examine the entirety of the strategies being used to improve manipulator safety. Chapter 2 presented and discussed four different approaches to evaluating and improving safety in manipulator systems. A summary of these works along with some examples in the literature is presented in Table 6.1.

Table 6.1: Summary of Safety Improvement Strategies

Safety Improvement Technique	Example technologies	Areas addressed
Improved Environmental Awareness	Vision systems [Cervera et al], improved sensor fusion [Jeong and Takahashi]	Early detection of hazards, obstacle avoidance
Improved Mechanical Safety	Hybrid actuators [Shin et al], selectively compliant joints [Rabindran], absorbent coverings [Ikuta et al]	Minimizing damage to environment, lowering injury potential
Determining injury potential from manipulators	Assessment of fracture forces, effect of manipulator collisions on HIC [Haddadin et al]	Standardization of injury ratings, generating useful information about injuries
Evaluation and optimal safe control	Optimal braking strategies , real-time safety monitoring, [Kulic and Croft, Haddadin et al, Jeong and Takahashi]	Improved safety during operation, faster hazard response

The work being done in environmental awareness includes two separate camera systems. The first camera system is a commercial product available intended to replace current safeguards preventing motion in manipulator workspaces such as light curtains and mechanical latches. This is a step forward, but of limited interest in the field of safety research since the functionality is identical to that of existing systems.

The second camera system uses a set of fixed fisheye cameras to provide real time information about the environment to the manipulator controller. This allows the manipulator to react and adapt to moving objects within the manipulator workspace, including humans. Cervera et al. were able to demonstrate the manipulator's ability to react to a human entering the workspace and respond to the presence. This work is of

greater interest to safe manipulation since there is a large body of work that has been done in the field of obstacle avoidance including establishing artificial potential fields and virtual force application that can be easily adapted to work with the information provided by these systems.

The second approach involves work being done to develop mechanically safer actuators and manipulators [Rabindran, Shin et al]. These include using inherently compliant pneumatic actuators combined with electric actuators to form a selectively compliant system along with the use of advanced gear trains and multiple actuators to remove disturbances from the system. Also, Ikuta et al's work investigates the effect of manipulator materials was estimated upon the safety of the manipulator's operation with the specific case of absorbent materials directly addressed.

The third approach encompasses the work being done to adapt current injury criteria used in automobile safety standards to manipulators [Haddadin et al]. This work examines the potential for injury in both unconstrained and constrained, or clamped, blunt impacts. These injury criteria include Head Impact Criterion (HIC), a metric based upon the resulting acceleration of the head after an impact to measure the lethality of a collision and the fracture force of the impact relative to the fracture force of the cranial and chest bones. Table 6.2 shows the fracture effects of manipulators in constrained impacts.

This work also shows the importance of the end-effector velocity. For unconstrained collisons, this is the most important criteria in terms of the potential HIC values. While this relies on empirical results since the HIC is measured as a function of the resulting head acceleration from an impact, establishing a relationship between HIC and the manipulator state is important for establishing future safety standards.

Table 6.2: Impact Forces with clamping at 2 m/s for different manipulators [Haddadin et al, 2008]

Robot	Contact Force (kN)	Maxilla Fracture?
LWRIII	0.6 @ 1 m/s	No
LWRIII	1.2 @ 2 m/s	Yes
KR3	2.2 @ 2 m/s	Yes
KR6 (Cat0 & 1)	5.1 @ 2 m/s	Yes
KR500 (Cat0 & 1)	23.6 @ 2m/s	Yes
Robot	Contact Force (kN)	Frontal Fracture?
LWRIII	3.5 @ 2 m/s	No
KR3	6.9 @ 2 m/s	Yes
KR6 (Cat0 & 1)	16.3 @ 2 m/s	Yes
KR500 (Cat0 & 1)	86.3 @ 2 m/s	Yes

The fourth approach involves evaluating the danger present in the standard operation of the manipulator and reactive control strategies. These include the Danger Criterion (DC) and Danger Index (DI) used by Kulic and Croft, and the danger-index used by Ikuta et al. In terms of the factors related to the manipulator control, all of these criteria depend mainly upon three factors: the distance between the manipulator and the obstacle, the velocity of the manipulator and the inertia of the manipulator, which directly maps to the kinetic energy present in the system.

The optimal braking strategy demonstrated by the Dynamic Acceleration Polytope (DAP) is one such reactive method from the literature. This algorithm involved the construction of a mapping between a hypercube in joint torque space bounded by the acceptable nominal joint torques and a polytope in joint acceleration space. This allowed the operator to choose an optimal braking acceleration at the bounds of the polytope, and then invert the mapping, shown in Eq. 6.1 to determine the joint torque required to achieve this acceleration.

$$\tilde{x}_p = J_P[T_\tau^{-1}M]^{-1}\hat{\tau} \tag{6.1}$$

In order to establish the base framework for the mapping of actuator parameter values to the safety performance of the manipulator, the relationship between actuator parameters and the output capabilities needs to be examined. This analytic mapping is presented in Section 2.2 of the work. Specifically, the relationship of the actuator nominal torque and the gear reduction ratios to the effective inertia of the manipulator allows for the determination of the not only the energy present in the system, but also the responsiveness of the end-effector. This mapping of the actuator parameters to the effective inertia of the system is shown in Eqs. 6.2 and 6.3.

$$I_{ii}^* = \sum_{j=i}^{N}\left\{ {}^{a}I_{ij}^* + {}^{l}I_{ij}^*\right\} \tag{6.2}$$

$${}^{a}I_{ij}^* = m_j^a({}^{a}J_T^{c_j})_i^T({}^{a}J_T^{c_j})_i + \bar{g}_j{}^2 I_j^M({}^{a}J_R^{c_j})_{z,i}{}^2 \tag{6.3}$$

In Eq. 6.3, ${}^{a}J_T^{c_j}$ and ${}^{a}J_R^{c_j}$ refer to the translational and rotational g-functions for the center of gravity of the *j*-th axis. To determine the responsiveness of the manipulator, however, the torque capabilities of each axis must also be taken into account. The equivalent mapping of the end-effector's acceleration capabilities is shown in Eq. 6.4

$$a_i \leq \sum_{i=1}^{N} \frac{\tau_i{}^{M}L_i}{\bar{g}_i \sum_{j=i}^{N}\left\{ {}^{a}I_{ij}^* + {}^{l}I_{ij}^*\right\}} \tag{6.4}$$

Chapter 4 later adapts this work to estimate the safety performance of a manipulator given the actuator parameters.

6.1.2 Safety Criteria

6.1.2.1 System Level Criteria

Based upon this previous research, this report develops a set of criteria in order to evaluate the ability of a manipulator to halt itself safely. This is done to specifically address the gap in the work discussed in the previous section, which largely neglects

evaluation of the halting motion and focuses instead upon only the period before the hazard response is initiated, operating on the assumption that the manipulator is able to halt itself safely once a hazard is detected. These criteria, presented in Section 3.1, assess both the likelihood of a collision between the manipulator and a hazard and the potential severity of a collision if it occurs. A full description of the criteria is presented in Section 3.1, but a short summary, along with a description of the physical meaning of each criterion is shown below in Table 6.3.

Table 6.3: System level Safety Criteria

Safety Criteria	Symbol	Description	Behavior
Total Distance Traveled (Section 3.1.1)	TDT	Total distance traveled by the manipulator after receiving the stop command	TDT→0, manipulator travels no distance TDT→∞, manipulator never fully stops
Directional Distance Traveled (Section 3.1.2)	dDST	Distance traveled by the manipulator in the specified direction	dDST→0, manipulator travels no distance in specified direction dDST→∞, manipulator continues to move in specified direction
End-Effector Kinetic Energy (Section 3.1.3)	EKE	Amount of kinetic energy present in the system at the end-effector	EKE→0, manipulator energy quickly dissipates EKE→*max*, manipulator stores a large amount of energy through motion
Stiffness (Section 3.1.4)	STF	Stiffness of the system at the end-effector	STF→0, manipulator is in a configuration such that forces will cause deflection of the EEF STF→*max*, manipulator responds rigidly to external forces

Safety Criteria	Symbol	Description	Behavior
End-Effector Velocity (Section 3.1.5)	VEL	Speed that the end-effector is moving at during the stopping trajectory.	VEL→0, manipulator quickly decelerates to zero speed VEL→∞, manipulator never fully stops
Directional End-Effector Velocity (Section 3.1.6)	dVEL	Speed that the end-effector is moving in a specified direction during the stopping trajectory	dVEL→0, manipulator quickly decelerates to zero speed in direction dVEL→∞, manipulator never fully stops moving in direction
Distance from set trajectory (Section 3.1.7)	TRJ	Distance that the end-effector travels from a set trajectory defined by the operator	TRJ→0, manipulator travels no distance away from trajectory TDT→∞, manipulator veers far away from trajectory

While the distance criteria are primarily concerned with determining the probability of a collision, the criteria measuring the system stiffness and energy address the concept of determining the severity of a collision, should one occur. The velocity-based criteria combine the two concerns, addressing the previous work by Haddadin which demonstrated that the velocity of the manipulator at the point of a collision tends to be the greatest determinant of the resulting HIC if the manipulator collides with a human in its workspace.

Additionally, the trajectory following criteria, TRJ, is formulated specifically to address certain applications where it is of primary importance to keep the manipulator on a set path, such as seam welding, where motion along the manipulator's given path may be acceptable, but motion outside of this path may result in severe damage to the

manipulator, the part being machined, or tooling attached to the manipulator. Another example of a task which may require the manipulator remain on a set trajectory would be a cutting, or sawing task. Motion transverse to the cutting path may result in warping of the blade, requiring not only replacement of the tool, but also damage to the part being cut. If this is part of a larger assembly, this may have more severe consequences as well.

6.1.2.2 Joint Level Capability Criteria

It is also vitally important for the manipulator and designer to know how close to the capacity the manipulator is operating during safety critical motions such as emergency stopping. As actuators operate closer to their limits, the possibility of a hardware failure or damage to the system becomes greater. If this happens it will lead to unpredictable behavior, which is inherently unsafe and therefore is not allowable in manipulator used in a safety-critical environment.

To this end, a set of criteria to determine the performance of the manipulator at the joint and actuator level relative to its capacity are presented in this work. This set of criteria allows the operator to not only determine whether to be concerned about potential faults, but also to assess the capability of the manipulator to improve upon its method of halting, whether through a more aggressive motion plan, an alternative torque algorithm, or improved control. This allows for a potential set of "stopping" test requirements similar to what is seen in the automobile industry currently. These criteria are presented fully in Section 3.2, but are summarized here in Table 6.4 along with descriptions of their physical meanings.

Table 6.4: Joint Level Capacity Criteria

Safety Criteria	Symbol	Description	Behavior
Torque Ratio (Section 3.2.1)	TRT	Degree to which the actuators are performing at their capacity	TRT→0, No actuator is near maxium capacity TRT→1, one or more actuators are approaching torque limits
Kinetic Energy Distribution (Section 3.2.2)	KED	The maximum concentration of the total kinetic energy in the system within any single joint	KED→*min*, energy is evenly distributed throughout the joints KED→1, energy is concentrated in one joint
Weighted Kinetic Energy Distribution (Section 3.2.3)	wKED	The concentration of total kinetic energy in the system weighted by the joint's maximum	wKED→*min*, energy is evenly distributed throughout the joints EKE→1, one or more joints have their maximum possible energy concentration
Joint Kinetic Energy (Section 3.2.4)	JKE	The total kinetic energy present in the joints of the manipulator	JKE→0, no kinetic energy is present in the manipulator joints JKE→*max*, the manipulator is near its maximum kinetic energy
Joint Potential Energy (Section 3.2.5)	JPE	Amount of potential energy stored with the joints of the system	JPE→0, joints contain no stored potential energy JPE→*max*, a large amount of potential energy is in the joints

Of perhaps the greatest importance in this set of criteria is the torque ratio criterion. This criterion requires the operator to specify a stopping coefficient, α, to

determine the magnitude to which the operator wishes to allow the actuators to exceed their nominal operating torque limits. This in particular distinguishes stopping motions from the standard operation of the manipulator. Because of the extremely low duty cycle and short duration of the stopping motion, it is possible to operate outside the standard torque limits of the actuators without overheating them or causing other mechanical faults. While a standard value of three to five for the stopping coefficient should be considered acceptable to the operator without fear of damaging the actuators, it may be considered that damage to the actuators is more desirable than the results of a collision. If this is determined to be the case, a value of up to ten may be chosen for the stopping coefficient.

Again, the importance of these criteria will vary according to the discretion of the operator, the manipulator design and the task given. By monitoring these criteria in addition to the safety criteria described in the previous section during a stopping motion, the operator is able to gain a full understanding of the system functionality within the context of safety and manipulator capabilities.

6.1.3 Safety Performance Estimation

In order to assist the manipulator designer in creating a system which satisfies the task requirements for safe manipulator operation, it is important to be able to estimate the effects of design decisions upon the stopping performance of the manipulator. This report addresses this problem in Chapter 4 using the mappings between the prime mover torques and gear reduction ratios to the system's effective inertia and responsiveness from Section 2.2.

In order to account for the differences in stopping motion compared to standard operation of the manipulator, the effective acceleration defined in Eq. 6.4 is first modified to the form of Eq. 6.5.

$$a_i^{eff} = \frac{\alpha_i \tau_i^M L_i}{\bar{g}_i \sum_{j=1}^{N} \left\{ {}^{a}I_{ij}^{*} + {}^{l}I_{ij}^{*} \right\}} \tag{6.5}$$

In this equation, α is defined as the stopping coefficient chosen by the operator to determine the excess capacity of the actuator that the operator wishes to be used. As described previously, due to the extremely low duty cycle of emergency stopping of the manipulator, the operator may deem it to be necessary to use between three and five and up to ten times the nominal torque of the manipulator in extreme cases. While this would be infeasible during normal operation due to the damage potentially done to the manipulators, the infrequent nature of the stopping methods enables this expansion of torque capacities. This stopping coefficient can be defined separately for all joints.

First, the velocity criteria are examined. This method uses an alternate formulation of the velocity criteria, namely, the time required to decelerate the manipulator to a safe end-effector speed. This is done by assuming that each of the actuators is able to contribute to decelerating the end-effector, in addition to the constant acceleration assumption. With the effective acceleration of the manipulator defined as in Eq. 6.5, it was shown that the velocity is described in Eq. 6.6 as in Section 4.1.2.

$$\|\dot{x}\| = \|\dot{x}_i\| - a_i^{manip} t \tag{6.6}$$

From Eq. 6.6, it can then be shown that the time to reach a safe velocity is easily solved for. This solution is presented in Eq. 6.7.

$$t_{safe} = \frac{\dot{x}_i - \dot{x}_{safe}}{a_i^{manip}} \tag{6.7}$$

This requires the determination of a safe velocity by the operator. This can be done either through analysis of the potential for injury such as the work done with HIC and fracture forces, or else by setting it as the standard low speed used in teach pendant operation currently, defined as 250 mm/s in the current ANSI/RIA safety standard. Since the acceleration in Eqs. 6.5 and 6.6 is defined as a function of the motor torques and gear ratios, the final equation represents a relationship between these base actuator parameters and the performance.

With the velocity determined, the distance criteria are examined. This is more straightforward since the distance traveled by the manipulator can be directly calculated given the assumptions and requires no additional analysis to provide a useful metric to the designer. This relationship, again in terms of the effective manipulator acceleration defined in Eq. 6.5, is shown in Eq. 6.8.

$$d = \|\dot{x}_i\| t - a_i^{manip} t^2 \tag{6.8}$$

As with the velocity criteria, the operator may wish to determine how far the manipulator travels until it reaches the designated safe speed in order to determine a radius of severe injury potential about the manipulator's end-effector. This distance is shown in Eq. 6.9.

$$d = \|\dot{x}_i\| \left(\frac{\|\dot{x}_i\| - \|\dot{x}_{safe}\|}{a_i^{manip}} \right) - \frac{\left(\|\dot{x}_i\| - \|\dot{x}_{safe}\|\right)^2}{a_i^{manip}} \tag{6.9}$$

Finally, the relationship between the joint level criteria and the actuator parameters needs to be examined, as done in Section 4.2. For the simple torque ratio it is straightforward to determine the mapping between the motor torque and torque ratio given that both parameters appear directly in the equation for the torque ratio, shown in Eq. 6.10.

$$\text{TRT} = \left[\frac{\bar{g}\tau_k}{\alpha\tau_{k,nom}}\right]_{max/average} \tag{6.10}$$

The mapping in general is fairly self-evident because as actuator parameters are adjusted, the operator will presumably update the control scheme to maximize the use of these parameters, resulting in a similar capability performance.

However, with the kinetic energy distribution criteria, the effects of differing the gear ratios on the individual joints will have an effect upon the energy distribution of the system since these gear ratios transmit the rotor inertia into joint space. In order to investigate this effect, an empirical study was done with a 2DOF manipulator by varying the torque ratios on the first and second joint and generating surface plots of the resulting average in Section 4.2.1. These results are shown in Figures 6.1 and 6.2.

Figure 6.1: Effect of Gear Ratios upon Average Joint 1 Kinetic Energy Partition Value

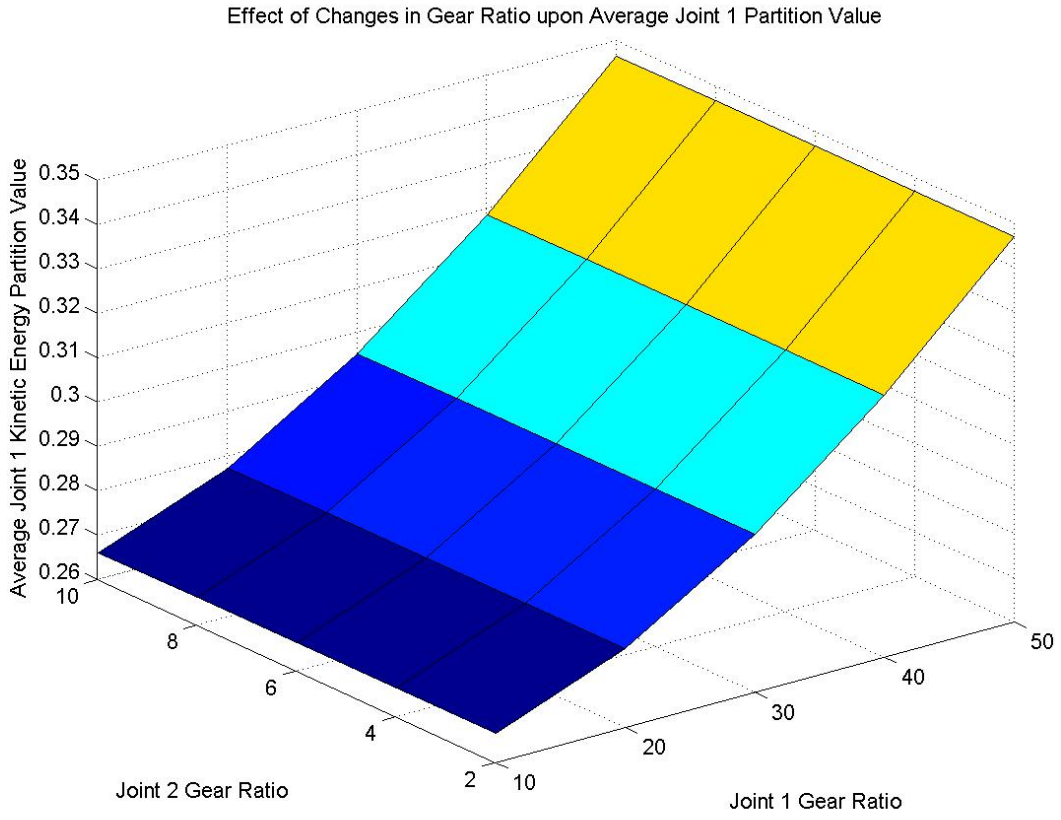

Figure 6.2: Effect of Gear Ratios upon Average Joint 2 Kinetic Energy Partition Value

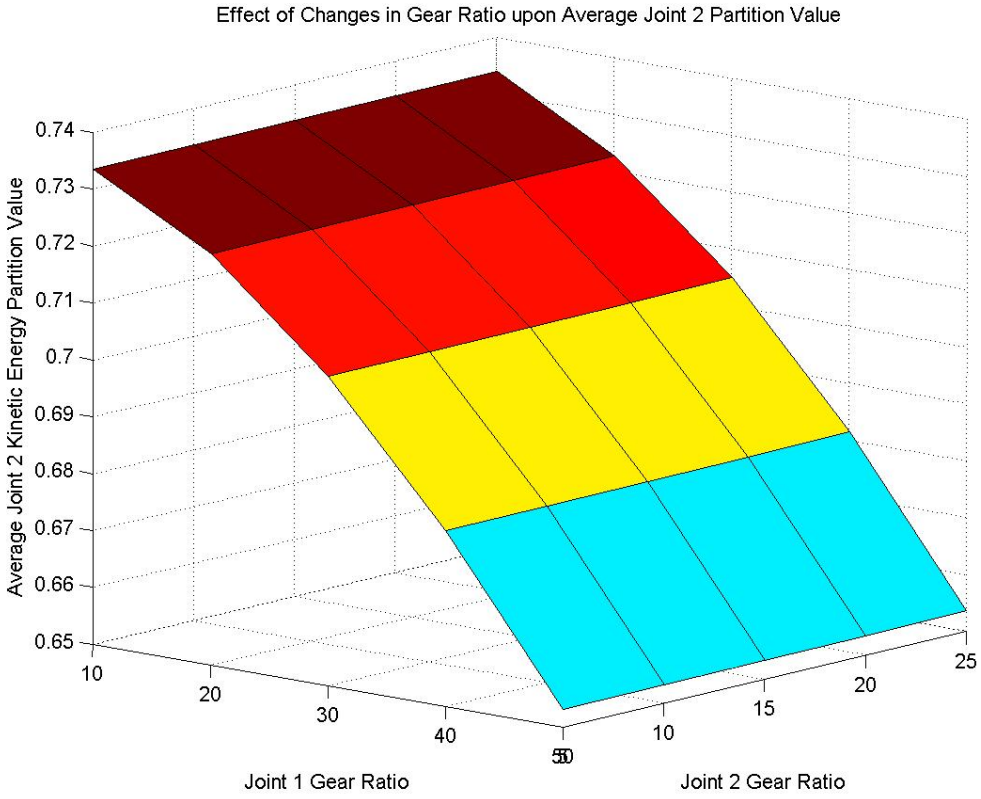

As can be seen from the two plots, the distribution values were largely decoupled in this study, but small effects upon the opposite joint's gear ratio can still be seen, even in a 2 DOF manipulator. This suggests that this is an effect that the designer should not want to neglect. Given that the large gear ratios typically found in real world manipulators will greatly amplify the actuator inertias relative to other inertia in the system, the effects of varying the gear ratio should be of concern to the designer.

6.1.4 Application to Industrial Environments

In order to demonstrate the effects that operating conditions will have upon a manipulator geometry commonly found in industry, a set of simulations for PUMA-style

manipulator, shown in Figure 6.3 were conducted in this report. This uses the framework presented in Chapter 3 to evaluate the relative effects of changes in the manipulator's configuration, end-effector load, operating speed and stopping control scheme upon the safety criteria developed. The full description of the manipulator, including actuator parameters and the inertial properties of the links can be found in Section 5.1.

Figure 6.3: 6-DOF PUMA-Type Arm

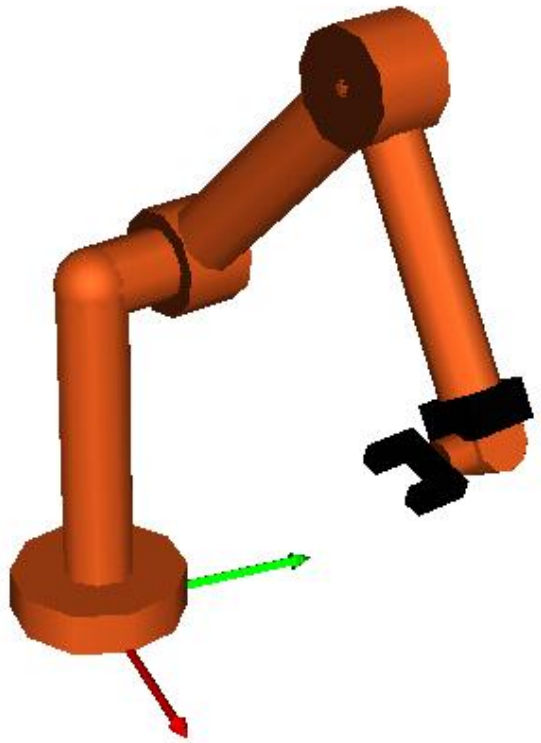

First, the effects of the initial configuration of the manipulator upon the safety criteria are evaluated. This is to determine the relative ability of the manipulator to safely halt itself throughout its workspace. Three different configurations were examined: a "Twisted" configuration in which the manipulator is oriented near its base, an "Out of Plane" configuration in which the manipulator is moving transverse to the standard plane

of motion, and an "Extended" configuration in which the manipulator is operating near the outer edges of its workspace. A more complete description and illustrations of these configurations is shown in Section 5.2.1. Figure 6.4 shows a plot of the distance traveled by the end-effector during the stopping motion for each configuration.

Figure 6.4: Distance Traveled in Various Initial Configurations

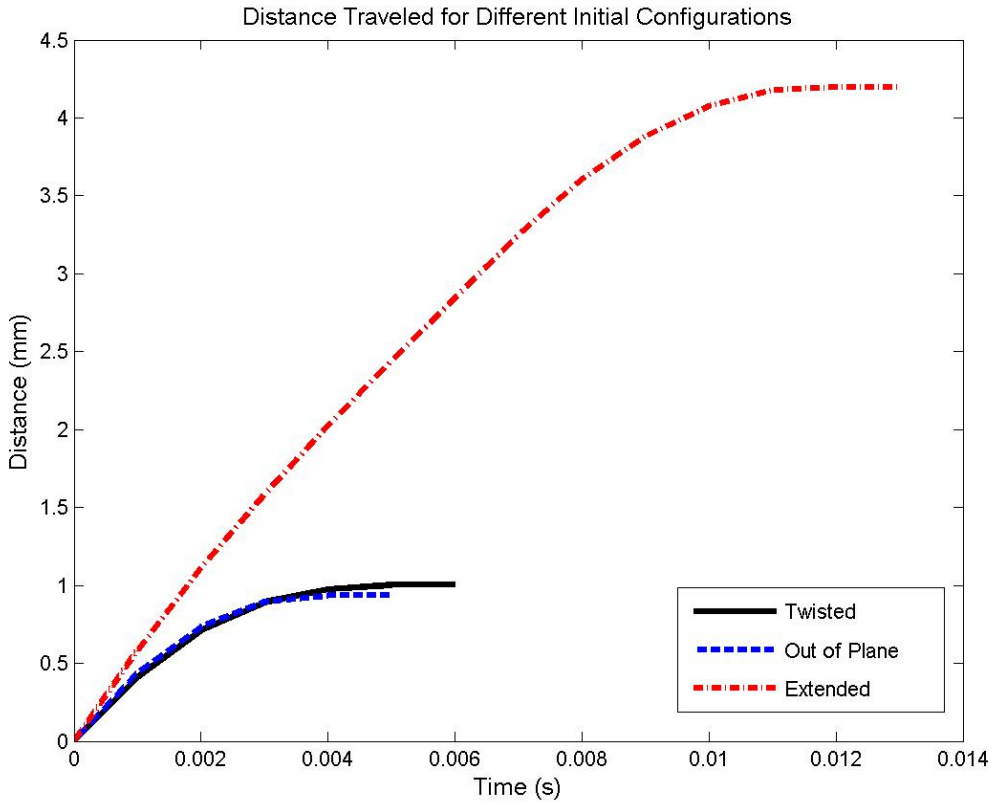

As can be seen in the plot, the initial configuration of the manipulator may have a potentially large effect upon the distance traveled by the end-effector. . In order to analytically compare the effects that the configuration has on the full set of the safety criteria, Tables 6.5 and 6.6 show the values of the safety criteria and their relative magnitudes for each configuration. The raw data used is also available in Section 5.2.1.

Table 6.5: Selected Safety Criteria Values for Different Configurations

Configuration	Total Distance (mm)	Directional Distance (mm)	Trajectory Distance (mm)	Time to "Safe" Velocity (s)	Time to "Safe" Kinetic Energy (s)
Twisted	1.0036	0.9949	0.1316	0.006	0.002
Out of Plane	0.9343	0.9341	0.0219	0.005	0.001
Extended	4.198	2.7955	3.1318	0.013	0.002

Table 6.6: Relative Magnitudes of Selected Safety Criteria for Different Configurations

Configuration	Total Distance (mm)	Directional Distance (mm)	Trajectory Distance (mm)	Time to "Safe" Velocity (s)	Time to "Safe" Kinetic Energy (s)
Twisted	1.07	1.07	6.01	1.20	2.00
Out of Plane	1.00	1.00	1.00	1.00	1.00
Extended	4.49	2.99	143.00	2.60	2.00

However, in order to determine the manipulator's ability to execute the trajectory, it is likewise important to monitor the maximum torque ratio of each actuator during the stopping trajectory. As can be seen from Table 6.7, when in the "Twisted" configuration, the torque required at actuator two far exceeds even the largest torque limits of the manipulator, meaning that the configuration of the manipulator has a large effect on the torque requirements for a stopping trajectory.

Table 6.7: Maximum Joint Torque Ratios for Different Configurations

Configuration	Joint 1	Joint 2	Joint 3	Joint 4	Joint 5	Joint 6
Twisted	2.28	**14.33**	9.71	4.01	3.65	3.29
Out of Plane	7.15	2.01	2.80	1.87	1.29	1.01
Extended	0.17	7.01	5.79	0.00	2.53	0.00

Next, the effects of the inertial loading at the end-effector are examined by adding a 500 mm long steel bar to the robot gripper. Because a kinematics-based motion plan is used, this shows no effect upon the motion criteria for a motion parameter plan, but demonstrated a slightly harmful effect to the kinetic energy stored in the manipulator during the trajectory. As described in Section 5.2.2, the relative inertia of the bar is still dwarfed by the inertia of the lower joint actuators due to the amplification effects of the gear train, so the total kinetic energy of the system is not greatly affected by the end-effector load.

However, because of the much smaller gear train of the sixth joint and its proximity to the added load, the inertial load of the steel bar significantly increases the required torque for the sixth actuator, more than tripling it for the two configurations which required acceleration of the sixth joint. Table 6.8 shows the relative magnitudes of the torque ratios for the loaded manipulator as compared to the unloaded case based on the data from Section 5.2.2. The slight increases in the torque requirements for joints 2 and 3 are also important to note. Because of this amplification, if the actuators are operating near their limits in an unloaded case, the addition of a load may push them beyond acceptable torque limits.

Table 6.8: Relative Magnitudes of Maximum Torque Ratios for Inertial Load

Configuration	Joint 1	Joint 2	Joint 3	Joint 4	Joint 5	Joint 6
Twisted	0.75	1.07	1.17	1.01	1.12	3.53
Out of Plane	1.27	1.31	1.26	0.96	1.44	3.50
Extended	2.53	1.26	1.20	0.00	1.15	0.00

Next, the effects of changes in the Cartesian operating speed are assessed. This is of special importance given that the main requirement under the current ANSI/RIA safety standard to operate a manipulator with a human inside the workspace is the limiting of a manipulator's operating speed to 250 mm/s. Additionally, work previously described in this chapter has demonstrated that speed may be the greatest determinant of injury in the case of a collision.

Simulations involving the manipulator at high speeds showed a marked worsening in all safety criteria. Much greater than the effect of the configuration or the effect of loading the manipulator, the speed has a pronounced effect upon the manipulator's ability to halt itself. Figure 6.5 shows a plot to compare performance of the manipulator at low speeds compared to that at high speeds.

Figure 6.5: Total Distance Traveled at Different Operating Speeds

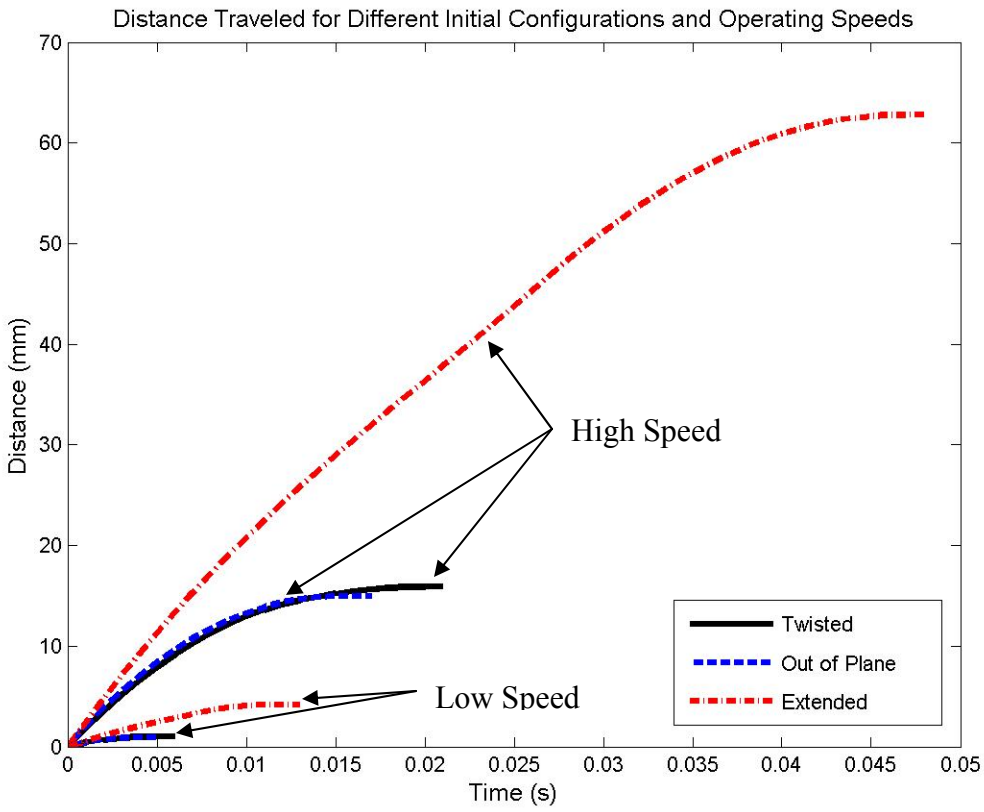

The numerical results of the safety criteria and their relative magnitudes of the safety criteria are presented in Tables 6.9 and 6.10. The values are normalized to the low speed performance for each configuration and show a clear worsening in safety performance, indicating that the operating speed is potentially the single greatest determinant of a manipulator's ability to halt itself in a safe manner. Thus, if the operator needs to quickly improve the safety of a system, the easiest way to accomplish this is by lowering the operating speed of the manipulator.

Table 6.9: Selected Safety Criteria Values for High Operating Speeds

Configuration	Total Distance (mm)	Directional Distance (mm)	Trajectory Distance (mm)	Time to "Safe" Velocity (s)	Time to "Safe" Kinetic Energy (s)
Twisted	15.89	15.69	2.56	0.02	0.02
Out of Plane	14.96	14.95	0.55	0.02	0.01
Extended	62.78	37.27	50.52	0.05	0.04

Table 6.10: Relative Magnitudes of Safety Criteria for High Operating Speeds

Configuration	Total Distance (mm)	Directional Distance (mm)	Trajectory Distance (mm)	Time to "Safe" Velocity (s)	Time to "Safe" Kinetic Energy (s)
Twisted	15.84	15.77	19.49	3.50	7.50
Out of Plane	16.02	16.01	25.10	3.40	10.00
Extended	14.96	13.33	16.13	3.69	20.00

Finally, the effects of using a torque-based control scheme to generate the stopping trajectory are examined. As shown in Figures 6.6 and 6.7, this offered potential gains and losses depending on the manipulator state. The advantages of using a viscous braking method were shown to be an assurance that torque limits will not be crossed and potentially enhanced performance in high speed operations. However, this comes at the cost of more unpredictable motion plan, and without an optimized system, worse performance. Table 6.11 shows the relative magnitudes of the safety criteria for the torque-based algorithm normalized to the kinematic-based algorithm. As can be seen in the values from the table, the performance is clearly worse, except in the "Extended" configuration, demonstrating the somewhat unpredictable nature of using an non-optimized torque-based algorithm.

Table 6.11: Relative Magnitudes of Safety Criteria for Viscous Braking

Configuration	Total Distance (mm)	Directional Distance (mm)	Trajectory Distance (mm)	Time to "Safe" Velocity (s)	Time to "Safe" Kinetic Energy (s)
Twisted	23.78	19.20	108.31	19.17	2.50
Out of Plane	5.40	4.92	90.23	8.60	1.00
Extended	2.82	2.07	3.30	10.00	1.00

Figure 6.6: Comparison of Stopping Controls for Extended, Low Speed Configuration

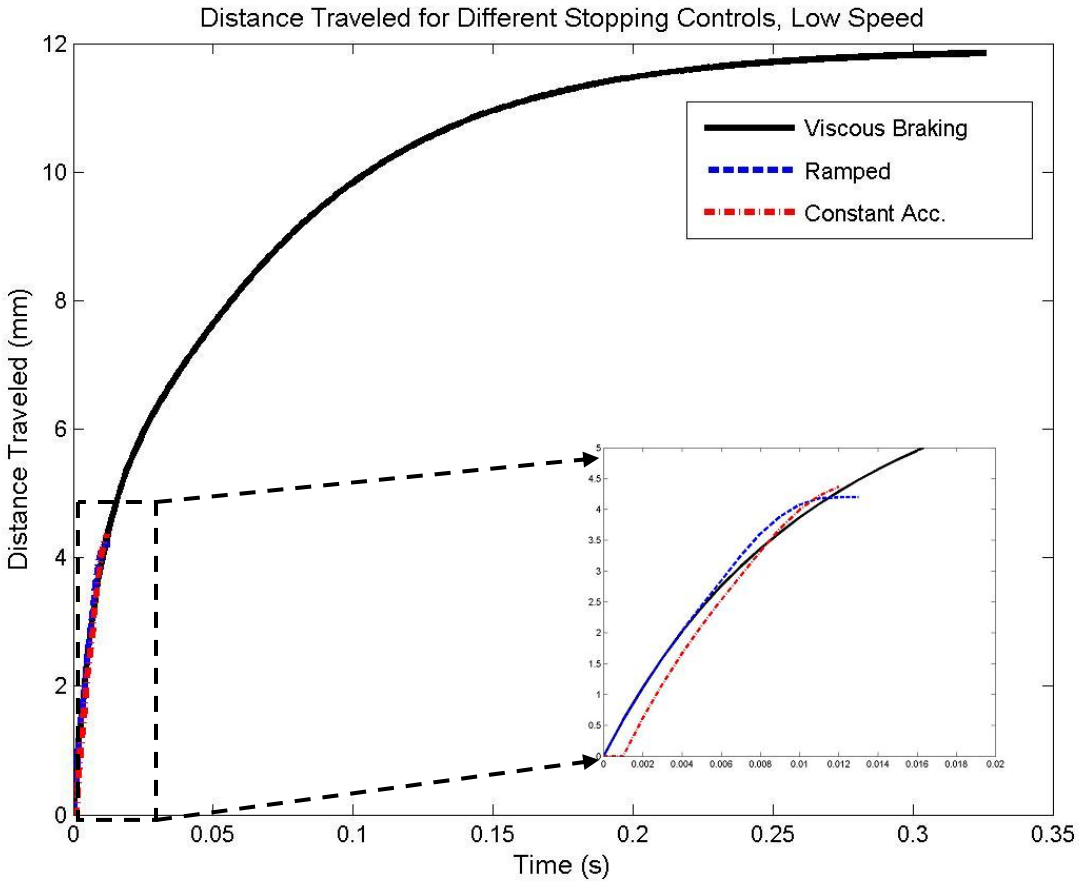

Figure 6.7: Comparison of Stopping Controls for Extended, High Speed Configuration

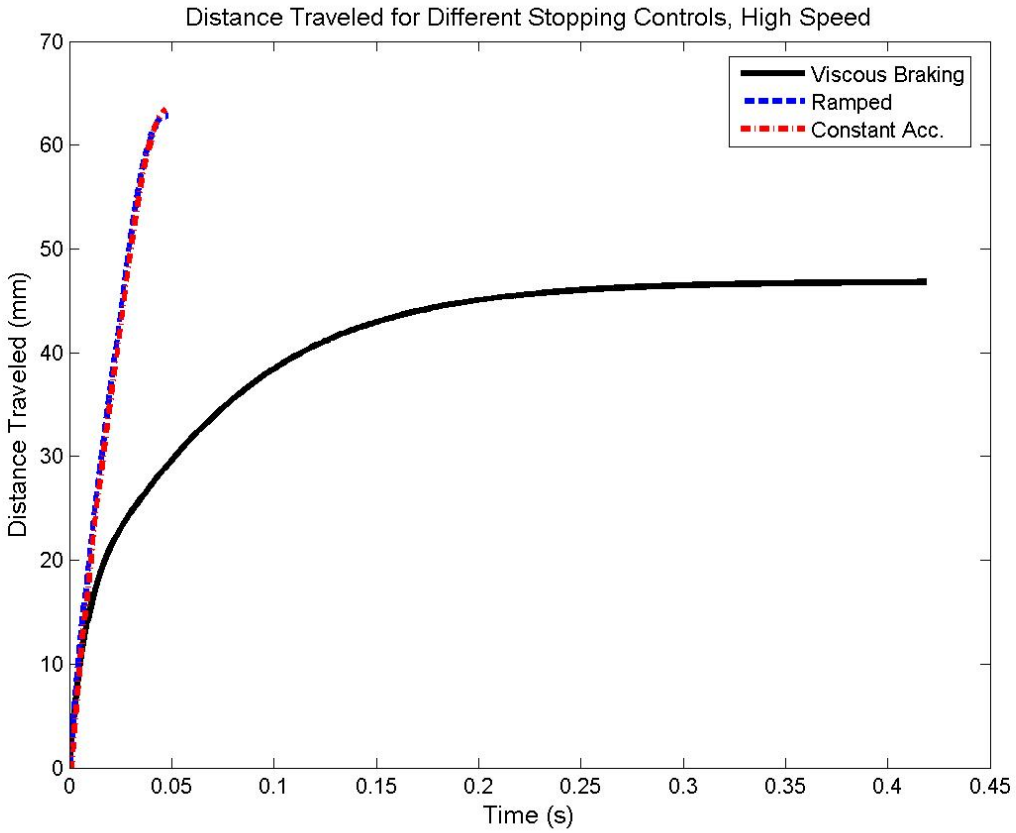

6.2 FUTURE WORK

The work in Chapters 3 and 4 outlines a framework for assessing the manipulator's safety but there remains a large body of work to be done in the application of this framework. A brief discussion of potential avenues for future work is presented here.

6.2.1 Injury Criteria

The current set of safety criteria includes no direct analogue in terms of the potential for human injury in the event of a collision. This would involve integrating and advancing the work done assessing manipulator collisions in terms of the fracture forces and HIC. Incorporating criteria involving a form of these metrics will allow for a greater physical meaning to the operator. It also allows the risk to be clearly laid out to potential recipients of medical care from manipulator based systems.

Bringing this degree of clarity to the safety evaluation is vitally important to removing manipulators from the highly constrained environment in which they currently operate and moving them into use by the common consumer. However, there still remains no consistent mapping of manipulator state at the point of impact to the commonly accepted injury metrics. These are determined through empirical testing which, while useful for assessing some of the maximum injury possibilities, does not allow for any degree of control optimization. When a method for determining these injury risks can be used in real time, these metrics will become much more useful and effective within the greater framework.

6.2.2 Decision Making

This report has mainly focused upon the development of an evaluation framework. In order to expand upon this work, the framework should be applied in a control scheme in order to optimize the manipulator's stopping motion according to some combination of the criteria. This expands the work from being a mere measurement of a system's safety into a methodology for actually improving the safety of a manipulation system.

There has been a large amount of work done in decision making strategies at the Robotics Research Group at the University of Texas-Austin in order to optimize the joint configuration in redundant manipulators [7, 30]. These include an adaptation of direct-search algorithm by Hooper and Tesar [31]. While the previous work adapted the optimization strategy for use in a highly constrained situation, the general algorithm remains expandable to be used in the highly unconstrained trajectory decision making problem as well.

A simpler expansion into the control problem would be an evaluation of the different stopping schemes according to the criteria presented here. These strategies include the DAP and those presented by Haddadin et al. This would allow for an objective measure of the efficacy of the various schemes, some of which are optimized according to the author's own metric. However, an independent framework to evaluate these halting methods would allow the operator a clear choice between stopping strategies in order to optimize according to the appropriate criteria given the manipulator task.

6.3 CONCLUSIONS

This report presented a framework for the evaluation of the safety of stopping trajectories in serial manipulators. First, an overview of joint motion control plans was discussed to provide a background for control strategies. Next, a summary of the previous work done in improving manipulator safety was presented. Based on this work, a set of criteria were developed in order to assess the motion of a manipulator during its halting trajectory. These were developed according to the safety concerns demonstrated previously. Another set of criteria in order measure the system's level of capacity to do work and measure the potential for failures at the joint and actuator level was developed

as well. As the research into mapping human injuries to manipulator parameters becomes more fully developed, these criteria could be added to. Finally, a methodology for mapping some of the safety criteria to the actuator parameters was provided in order to allow the designer to estimate the performance of a manipulator during the stopping motion without requiring assembly of the manipulator and performance tests. The methodology was then simulated over a full 6DOF industrial-type manipulator. As actuator design for low duty cycle, high demand stopping ($\alpha > 5$) improves, the potential to move past the values determined in Chapter 5 will expand greatly.

Finally, in this chapter the previous work was summarized and related to the work presented in this report. A set of possibilities for future work was presented as well. These include not only incorporating the injury metrics from the automobile industry into future development of safety criteria, but also the expansion of this work into the control field and optimal control. There already exists a set of stopping methodologies which could be empirically evaluated and compared using the framework presented here. Integrating this work into all of these avenues allows for exciting possibilities in the development of safe robotic systems in the future.

A. Denavit-Hartenberg Parameters for 6-DOF PUMA Arm

Link	a_{i-1} (m)	α_{i-1} (deg)	d_i (m)	Φ_i
1	0	0	0	Φ_1
2	0	-90	0.125	Φ_2
3	0.4	0	0	Φ_3
4	0	-90	0.35	Φ_4
5	0	90	0	Φ_5
6	0	-90	0.1	Φ_6

References

[1] "Robots: Nothing to lose but their chains." The Economist, Jun 19th, 2008.

[2] Krebs, H.I., Hogan, N., Aisen, M.L. Volpe B.T., "Robot-Aided Neurorehabilitation." IEEE Trans Rehabil Eng. March, 1998, Vol. 6, No. 1.

[3] RIA/ANSI 1999. "RIA/ANSI R15.06—1999 American National Standard for Industrial Robots and Robot Systems—Safety Requirements." American National Standards Institute, New York.

[4] Ikuta, K., Ishii, H/, and Nokata, M., "Safety Evaluation Method of Design and Control for Human-Care Robots." The International Journal of Robotics Research. May, 2003, Vol 22, No. 5.

[5] Zamojski, W., and Caban, D.. "Impact of Software Failures on the Reliability of a Man-Computer System." International Journal of Reliability, Quality and Safety Engineering. 2006, Vol. 13, No. 2.

[6] Shah, J.A, Saleh, J.H., and Hoffman, J.A. "Analytical basis for evaluating the effectiveness of a human-robot system." Reliability Engineering and System Safety. 2008, Vol. 93.

[7] Tisius, M. and Tesar, D., "An empirical approach to performance criteria and redundancy resolution." MS Thesis, the University of Texas at Austin

[8] Thomas, M. and Tesar, D. 1982 "Dynamic Modeling of Serial Manipulator Arms." *Journal of Dynamic Systems, Measurement, and Control* Vol 102, pp. 218-228.

[9] Hernandez, E. and Tesar, D. "Compliance Modeling for General Manipulator Structures." Ph.D. Dissertation, UT Austin, 1996

[10] Benedict, C. E. and Tesar, D., "Model Formulation of Complex Mechanisms with Multiple Inputs: Part 1 – Geometry, Part 2 – The Dynamic Model." *Journal of Mechanical Design*, 100:747-761, 1978.

[11] Rios, O. and Tesar, D., "Influence of actuator parameters on performance capabilities of serial robotic manipulator systems." 2008, Ph.D Dissertation.

[12] Rajan, Ratheesh. "Foundation Studies for an alternate approach to motion planning of dynamic systems", MS Thesis, 2001.

[13] March, P. and Tesar, D. "Criteria Based Motion Planning." MS Thesis, 2004.

[14] Bazaz, S. A., and Tondu, B. "3-Cubic Spline for On-line Cartesian space trajectory planning of an industrial manipulator." IEEE 5th Annual Workshop on Advanced Motion Control, 1998.

[15] Tesar, D. and Matthew, G., "The Dynamic Synthesis, Analysis and Design of Modeled Cam Systems." Lexington Books, D.C. Heath & Company, 1976.

[16] Asimov, Isaac, "Runaround." *Astounding Science Fiction*. March, 1942.

[17] Rabindran, D. and Tesar, D., "A Differential based parallel force/velocity actuation concept: theory and experiments." Ph.D. Dissertation.

[18] Shin, D., Sardeletti, I., and Khatib, O., "A hybrid actuation approach for human-friendly robot design." IEEE International Conference on Robotics and Automation, May 19-23, 2008

[19] Haddadin, S, Albu-Schaffer, A., and Hirzinger, G., "The role of robot mass and velocity in physical human-robot interaction – part I: Non-constrained blunt impacts." IEEE International Conference on Robotics and Automation, May 19-23, 2008

[20] Haddadin, S, Albu-Schaffer, A., and Hirzinger, G., "The role of robot mass and velocity in physical human-robot interaction – part II: Constrained blunt impacts." IEEE International Conference on Robotics and Automation, May 19-23, 2008

[21] Jeong, S. and Takahashi, T., "Impact force reduction of manipulators using a dynamic acceleration polytope and flexible collision detection sensor." Advanced Robotics, 2009, vol. 23, pp. 367-383.

[22] Kulic, D. and Croft, E., "Pre-collision safety strategies for human-robot interaction." Autonomous Robotics, 2007, Vol. 22, pp. 149-164.

[23] Haddadin, S., Albu-Schaffer, A., De Luca, A., and Hirzinger, G., "Collision Detection: A contribution to safe physical human-robot interaction." IEEE/RSJ International Conference on Intelligent Robots and Systems. 2008, Sept. 22-26.

[24] "Sensors, Robotics, Vision: 1st 3-D safe camera replaces light curtains, guarding." Control Engineering.

[25] Cervera, E., Garcia-Aracil, N., Martinez, E., Nomdedeu, L., Del Pobil, A.P., "Safety for a robot arm moving amidst humans by using panoramic vision." IEEE International Conference on Robotics and Automation, May 19-23, 2008

[26] Harden, T. and Tesar, D., "Minimum distance influence coefficients for obstacle avoidance in manipulator motion planning." Ph D. Dissertation.

[27] J. Versace, "A review of the severity index." Proc 15th Stapp Conference, vol. SAE paper, No. 710881, 1971.

[28] Rios, O., and Tesar, D., "Design Criteria for Serial Chain Mechanisms Based on Kinetic Energy Ratios." Journal of Mechanical Design, August, 2009, Vol. 131, No. 8

[29] Rios, O., and Tesar, D., "Effective Tool-Point Acceleration of Serial Chain Mechanisms Based on Geometric Transformations", Technical Report, 2008

[30] Pryor, M. and Tesar, D., 2002, "Task-Based Resource Allocation for Improving the Redundancy of Serial Manipulators", Ph.D. Dissertation, University of Texas at Austin.

[31] Hooper, R. and Tesar, D., "Multicriteria Inverse Kinematics for General Serial Robots", Ph.D. Dissertation, University of Texas at Austin.

Vita

Bryan Christopher Steinfeld was born in Fort Lauderdale, Florida, on November 26th, 1983. After graduating from Glencoe High School in Hillsboro, Oregon, he enrolled in Rice University in Houston, Texas. He received his Bachelor's of Science in Mechanical Engineering in May, 2006. He then enrolled in the graduate program at the University of Texas at Austin where he accepted a position as Graduate Research Assistant with the Robotics Research Group.

Permanent address: 3145 NW 132nd PL
Portland, OR 97229

This thesis was typed by the author.